UNIVERSIDAD POLITÉCNICA DE CATALUNYA

PONTIFICIA UNIVERSIDAD CATÓLICA DEL PERÚ

CENTRO TECNOLÓGICO DE TELECOMUNICACIONES DE CATALUNYA

Efficient Rectenna Design for Ambient Microwave Energy Recycling

por

Gianfranco Andía Vera

A thesis submitted in partial fulfillment for the
grado de Ingeniero

in the
Escola Técnica Superior d'Enginyeria de Telecomunicació de Barcelona
Departament de Teoria de Senyal i Comunicacions

July 2010

"Por nuestra ignorancia no sabemos las cosas necesarias; por el error las sabemos mal."

A.A.R.G.

UNIVERSIDAD POLITÉCNICA DE CATALUNYA
PONTIFICIA UNIVERSIDAD CATÓLICA DEL PERÚ
CENTRO TECNOLÓGICO DE TELECOMUNICACIONES DE CATALUNYA

Resumen

Escola Técnica Superior d'Enginyeria de Telecomunicació de Barcelona
Departament de Teoria de Senyal i Comunicacions

Grado de Ingeniero

por Gianfranco Andía Vera

El presente trabajo está basado en diseñar, medir y probar el desempeño de una antena y un circuito rectificador (RECTENA) optimizados para recibir señales de baja densidad de potencia. La rectena es usada para recolectar y re-usar energía proveniente de señales RF radiadas por sistemas de comunicación y broadcasting en la banda ISM centrada en 2.45GHz., Este trabajo usa métodos de simulación de Balance Harmónico y Momento Electromagnético de onda completa de Agilent ADS Advanced Design Software. En cuanto a las herramientas usadas: máquina pulidora LPKF para la fabricación de la antena, analizador vectorial de redes, analizador de espectro, generador de señal digital, multímetro y la cámara anecoica para las medición de desempeño de la rectena.

El trabajo fue motivado por dos tipos de aplicaciones: (1) Alimentación de sensores de baja potencia y (2) Reciclaje de energía RF, siendo consciente del consumo de energía y su efecto en el medio ambiente. El principal objetivo de este trabajo es valorar la rectificación a baja potencia.

Agradecimientos

A mi familia: a mis padres, por su incondicional apoyo, y a mis hermanos, por su experiencia e inquietud, ustedes son la razón y el motivo de intentar hacerlo todo bien. Gracias a los momentos que compartimos, los que, y tal vez sin valorarlos a su tiempo, hicieron, sin duda alguna, que todos estos años sean espléndidos. Muchas gracias, son una fuente inagotable de satisfacción.

A los amigos que gané en el transcurso de la carrera: Claudia, Alfredo, Gustavo, Alan y Lisset por escucharme, compartir experiencias e inspirar confianza; a los que me acompañaron desde antes: José Luis, Bera Lucía, Hugo Alexander; sin duda, de todos ellos y de nuestros problemas fue de lo que más aprendí.

De esta etapa Barcelona, una más de cambios, y creo que determinante para poder hacer esta valoración desde otra perspectiva, hay algunos nombres en especial que no quiero dejar de mencionar por su amistad, amabilidad y colaboracion. Al trabajo más importante de mi carrera le puse tantas ganas porque alguien tuvo mucha fé en mí, sus ganas de trabajar y sobre todo de ayudar, gracias a él la dificultad se hizo interesante y el trabajo resultó entretenido, no sólo en lo académico, sino también por el buen ambiente creado, gracias Apostolos, mi director de proyecto.

Este buen ambiente se debe también a las buenas personas que conocí en el CTTC, a David, por tu ayuda y por los buenos momentos que compartimos, las conversaciones, risas e historias hicieron que todo sea sencillo, a Selva, por su gran ayuda; a Ana, por el material brindado; gracias por su enorme simpatía

Debo agradecer también a mi director ponente Josep M. Torrents, por su gran amabilidad. en general, personas como las que menciono favorecerían cualquier escenario y harían del trabajo el mejor ambiente.

Gràcies!

Contents

List of Figures

List of Tables

A mis padres...

Chapter 1

Introduction

The combination of extremely low-power microprocessors, the realization of ubiquitous computing relies heavily on the miniaturization of computers and improvement of communication protocols and power supply technologies, increasingly affordable supercapacitors for energy storage and budding more energy efficient and monitor inventory has enabled a new generation of energy-recycling devices. Typically, wireless sensors are designed to observe environments in a more flexible way than wired ones can-tracking cattle in the middle of a field, generating early warnings of impending earthquakes, and assessing the structural health of bridges, for example. But sensor's power supply is the most confounding problem. In solving this problem, engineers dusted off a decades-old idea: radio-frequency energy recycling, be it from strategically placed transmitters or from the ambient energy emitted by cellphone towers and television stations. The concept was once dismissed as unfeasible because of the rapid dissipation of electromagnetic waves as they travel from their source . But even microwatts, if trickled into a battery or supercacitor, can be enough to power some sensors[1].

The use of batteries has two disadvantages: (1) the lifetime of the batteries is very limited even for low-power batteries, requiring impractical periodical battery replacement, (2) the use of commercial batteries usually overkills the power requirements for uW sensor nodes, adding size and weight while creating the problem of environmental pollution due to the deposition of these batteries, as well as increases significantly the cost overhead of disposable nodes; "being green" is becoming a big requirement in these days; new information and communication technology should be conscious of the energy consumption and effect to the natural environment; in this way solar cells, the most common energy-harvesting technique, cant't soak up photons from inside applications and will be major obstacles for the quick penetration of ubiquitous network services. A

[1]IEEE Spectrum 06.08, The magazine of the Technology insiders,page 13.

really emerging area is getting hybrid power supplies (solar cells, converting temperatura changes or mechanical movements into electrical energy and RF energy recycling) and might finally make the devices truly independent.

The technology for harvesting and recycling wireless power is essentially based on radio-frequency identification, or RFID, A transmitter sends a burst of radio-frequency energy that both carries information to a chip and can ve converted to dc electricity to power it. A tag consisting of an antenna a microchip responds by sending data about the object it is attached to. Turning those simple tags into fancier monitoring devices requires more power, so the RF energy would need to be captured and stored or transmitted continuously. A key development has been a steady growth in the distances over which the tags can communicate.

With significantly more flexible sensors installations come new applications. For example, using energy-recycling sensors to control thermostats in office buildings could improve the energy efficiency. To assess whether sensors in an office building could be powered ambiently.

A considerable amount of work has been done in the area of wireless powering, including inductive powering for short ranges, high power density directive powering in the microwave frequency range, as well as low-power near-field interrogation with RFID tags, and medium- and low-power density powering of low-power sensors. This is usually accomplished by receiving incident waves with an antenna and rectifying the received RF voltage (figure 2.2). An integrated antenna and rectifier is usually referred to as a rectenna.

This work focuses on low-power density incident; designing, measuring and testing an rectenna to harvest electric energy from the RF signals that have been radiated by communication and broadcasting systems at ISM band center in 2.45 GHz., The work contains methods to simulate circuits and antennas with Harmonic Balance and electromagnetic full-wave simulators respectively.

The work is motivated by two types of applications: (1)powering of low-power sensor networks and (2)RF energy recycling. Because of the low input power levels, a nonlinear decrease in efficiency is expected when compared to power-beaming applications. The goal of this work is to determine the usefulness of low-power rectification.

1.1 Overview

The issues related to low-power reception, rectification, and power management are addressed in this report as follows:

- Chapter 2 describes the state of the art in rectennas, discussing the electromagnetic environment; efficiency, a feasibility study of power scavenging from environmental RF signals made in Tokio and applications are presented
- Chapter 3 describes the design and results of simulations of an antenna center in 2.45 GHz. integrated with a rectifier circuit. Electromagnetic field simulations are coupled to nonlinear circuit simulations (both in Agilent ADS) to ensure optimal match between the antenna and rectifier. A brief background about simulation method used, microstrip antennas and rectifier circuits is presented. Based on a known range of input power levels, a rectifier diode is chosen from several candidates. An optimal antenna's performance is achieved in three designs reducing the size and increasing the bandwidth in each one. It shown plots of impedances, radiation patterns and efficiencies simulated
- Chapter 4 describes the fabrication process and measures of: two antennas (1) optimized size antenna and (2) optimized size and polarization bandwidth antenna, the rectifier circuit: also two sets,(1) one branch rectifier and (2) complete rectifier with two branches rectifiers, and the integrated rectenna, this is the optimal antenna with the rectifier circuit behind. The measurement setup on the anechoic chamber and general limitations are described. Measurements are compared to simulated results in plots.
- Chapter 5 presents a discussion on storage and management of the extracted dc power with two example applications.
- Chapter 6 presents the conclusions and future work.

Chapter 2

State Of The Art

2.1 History: Previous Power Transfer Technologies

Over 100 years ago, the concept of wireless power transmission began with the patented ideas and demonstrations by Tesla [1][2], he describes a "method for utilizing effects transmitted through natural media". In this patent, Tesla first describes several ways of transmitting electrical disturbances through the natural media: "One of these ways consists of producing by a suitable apparatus rays or radiations that is disturbances which are propagated in straight lines through space, directing them upon a receiving or recording apparatus at a distance, and thereby bringing the latter into action. This method has been brought particularly into prominence in recent years through investigations by Heinrich Hertz." Though described in somewhat confusing legal language, it is obvious that the disturbances in Tesla's patent are electromagnetic waves. Claim 11 of this patent specifies that the patented method of utilizing effects or disturbances transmitted through the natural media from a distant source, which consists in storing in a condenser electrical energy derived from an independent source, and using, for periods of time predetermined as to succession and duration, the accumulated energy so obtained to operate a receiving device. What is described above is wireless transmission of energy, storage of the energy in a capacitor and energy management over time.

Although Tesla was unsuccessful at implementing his wireless power transmission systems for commercial use, he did transmit power from his oscillators that operated up to 100 MV at 150 kHz. he failed because the transmitted power was diffused to all directions with 150 kHz radio waves whose wave length was 21 km.

To concentrate the transmitted power and to increase transmission efficiency, we have to use higher frequency than that used by Tesla. In 1930s, much progress in generating high-power microwaves, 1-10 GHz. radio waves, was achieved by invention of the magnetron

and the klystron. After World War II, high power and high efficiency microwave tubes were advanced by development of radar technology.

Based on the development of the microwave tubes during the World War II, rectification of microwave signals for supplying dc power through wireless transmission has been proposed and researched in the context of high power beaming since the 1950s by W. C. Brown who started the modern era of wireless power transmission with the advancement of high-power microwave tubes by Raytheon Company,[3]. By 1958, a 15-kW average power-band cross-field amplifying tube was developed that had a measured overall dc-to-RF efficiency of 81%. The first receiving device for efficient reception and rectification of microwave power emerged in the early 1960's.

Conceived at Raytheon, a rectifying antenna, or rectenna, was developed, consisting of a half-wave dipole antenna with a balanced bridge or single semiconductor diode placed above a reflecting plane. The output of the rectenna element is then connected to a resistive load. 2.45 GHz. emerged as the transmitting frequency of choice due to its advanced and efficient technology base, location at the center of an industrial, scientific, and medical (ISM) band, and its minimal attenuation through the atmosphere even in heavy rainstorms, then the conversion efficiency of the rectenna continued to increase from the 1960's through the 1970's a this frecuency. Based on the Brown's work, P. E. Glaser proposed a Solar Power Satellite (SPS) in 1968[4], development that was to profoundly affect the future direction of technology in this area. The SPS is a gigantic satellite designed as an electric power plant orbiting in the Geostationary Earth Orbit (GEO). This consists of mainly three segments; solar energy collector to convert the solar energy into DC (direct current) electricity, DC-to-microwave converter, and large antenna array to beam down the microwave power to the ground. This is expected to realize around 2030[5].

Conversion efficiency is determined by the amount of microwave power that is converted into dc power by a rectenna element, the greatest conversion efficiency ever recorded by a rectenna element occurred in 1977 by Brown in Raytheon Company using a GaAsPt Schottky barrier diode, a 90.6% conversion efficiency was recorded with an input microwave-power level of 8W. This rectenna element used aluminum bars to construct the dipole and transmission line, Later; a printed thin-film class of rectenna design was developed at 2.45 GHz. where conversion efficiencies of 85% were achieved.

Another important application for wireless power transmission is to identification tags. Invented in 1980, in recent years, there has been a trend to take RFID (Radio Frequency Identification) technology from labs to commercial applications. In this application, the system must maximize reading distance and robustness to collisions with cheap tag fabrication. Tags can be used to keep track on some retail products for inventory control,

automatic selling systems, intelligent systems at home, and so on. RF-ID is the first commercial wireless power transmission application system in the world

In the past few decades, a considerable amount of work has been done in the area of wireless powering, including inductive powering for short ranges, high power density directive powering in the microwave frequency range, as well as low-power near-field interrogation with RFID tags, and medium- and low-power density powering of low-power sensors.In microwave power transmission, the antennas have well-defined polarization, and high rectification efficiency is enabled by single frequency high microwave power densities incident on an array of antennas and rectifying circuits. Applications for this type of power transfer have been proposed for helicopter powering [3], solar-powered satellite-to-ground power transmission [4], inter-satellite power transmission [6] including utility power satellites, mechanical actuators for space-based telescopes [7], small dc motor driving [8] and short range wireless power transfer, e.g. between two parts of a satellite. Both linear [9], dual-linear [7] [10] and circular [11]polarization of the receiving antennas were used for demonstrations of efficiencies ranging from around 85-90% at lower microwave frequencies to around 60% at X-band and around 40% at Ka-band [12]. All this work is usually accomplished by using a rectenna which will be described below.

2.2 Recent Technologies of Rectenna

The word rectenna is composed of rectifying circuit and antenna. The rectenna and its word were invented by W. C. Brown in 1960's[3][13]. The rectenna can receive and rectify a microwave power to DC,is passive element with a rectifying diode, operated without any power source.

The antenna of rectenna can be any type such as dipole[3][13], Yagi-Uda antenna[14][15], microstrip antenna[16][10][17], monopole[18],coplanar patch[19], spiral antenna[20], or even parabolic antenna[21]. The rectenna can also take any type of rectifying circuit such as single shunt full-wave rectifier[22][10][17][23][18][24], full-wave bridge rectifier[3][15][25], or other hybrid rectifiers[16]. The circuit, especially diode, mainly determines the RF-DC conversion efficiency, rectennas with FET[19] or HEMT[20] appear in recent years. (the rectenna using the active devices is not passive element).The world record of the RF-DC conversion efficiency among developed rectennas is approximately 90% at 8W input of 2.45 GHz. microwave[3].

The RF-DC conversion efficiency of the rectenna with a diode depends on the microwave power input intensity and the optimum connected load (figure 2.1). When the power or

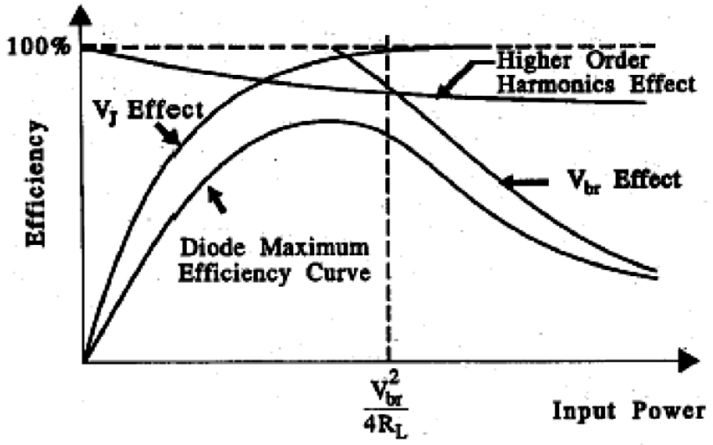

FIGURE 2.1: Typical characteristic of RF-DC conversion efficiency of rectenna

load is not matched the efficiency becomes quite low. The characteristic is determined by the characteristic of the diode. The diode has its own junction voltage and breakdown voltage, if the input voltage to the diode is lower than the junction voltage or is higher than the breakdown voltage, the diode does not show a rectifying characteristic. As a result, the RF-DC conversion efficiency drops with a lower or higher input than the optimum.

We have two approaches to increase the efficiency at the weak microwave power density input. One is to increase an antenna aperture as [24][21]. There are two problems for this approach. It makes sharp directivity and this is only applied for exclusive applications as SPS satellite experiment and not for low power applications like RF-ID or microwave energy recycling. The other approach is to develop a new rectifying circuit to increase the efficiency at a weak microwave input.

2.3 Wireless Powering for Low-Power Distributed Sensors

An overview of the field of wireless powering is presented with an emphasis on low-power applications where the powering range needs to exceed a few meters.

In the 2.5 section, a feasibility study and several rectenna elements and arrays examples are discussed in more detail: (1) Feasibility study for potential application of power scavenging (2) A 10 GHz. array for powering sensors in aircraft wings; (3) A single antenna in the 2.4 GHz. ISM band for low-power assisted-living sensors; and (4) A broadband array for power harvesting in the 2-18 GHz. frequency range.

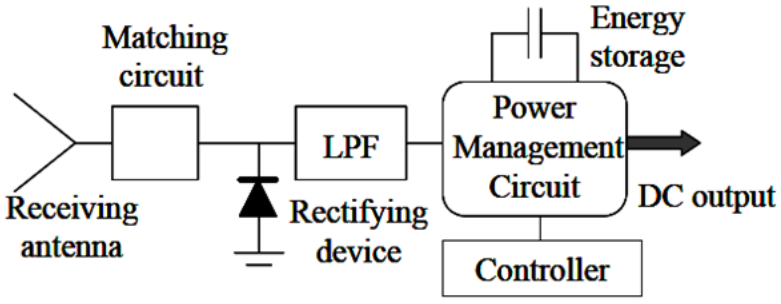

FIGURE 2.2: Schematic of a rectenna and associated power management circuit. The incident waves within a certain spectral range are received by the antenna, coupled to the rectifying device (diode in this case), and the low-pass filter (LPF) ensures that no RF is input to the power management circuit. A controller provides input to the power management circuit, which enables storage of the received energy over time, and delivery of DC power at the level and time when it is needed.

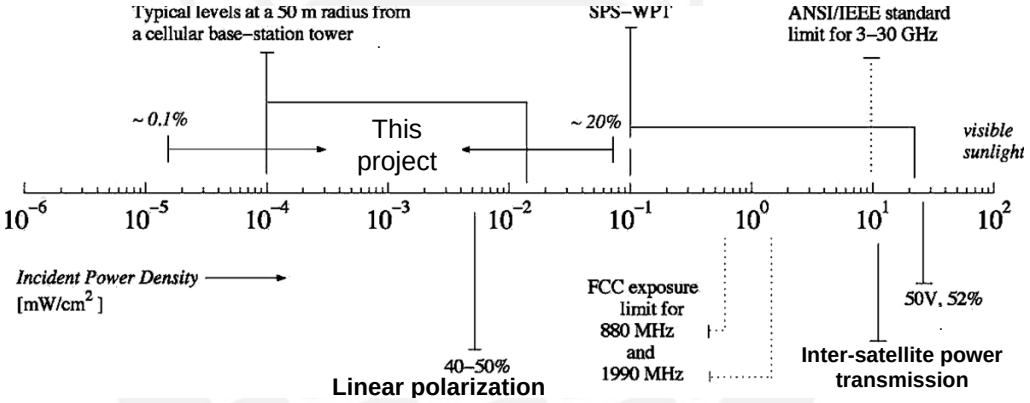

FIGURE 2.3: Diagram of various microwave power sources and their typical power density levels. The power density operating points of several rectenna designs found in the literature and their corresponding efficiencies are given. Also shown is the range of expected power densities used in the solar power satellite (SPS) and wireless power transmission (WPT) applications. The range of power densities for this work is indicated for comparison.

In the above referenced work (sections 2.1 and 2.2), rectification is performed for narrowband, essentially single-frequency, incident microwave radiation with relatively high power densities. Now a survey of the typical power densities associated with high power rectennas is given in figure 2.3, in which three examples are taken from [6],[7] and [9] along with the corresponding operating rectification efficiencies, also shown in the figure are expected power densities approx 50 meters away from a typical base-station tower operating at 880 and 1990 MHz [26], are usually asumed to be around $10^{-4} mW/cm^2$.

2.4 Electromagnetic Environment and Efficiency

There are several distinct scenarios for wireless powering, and the specific design is highly dependent on the incident waves that carry the energy:

- One or more high-directivity narrowband (single frequency) line-of-sight transmitters with well known and fixed polarization and well-known power levels. In this approach, used for power beaming, the efficiency of the rectenna can be very high. A reasonable application is transmitting power from one part of a satellite to another, eliminating heavy and bulky cables.
- One or more medium-power semi-directional transmitters that illuminate a range in space, with multipath present. In this case, the incident power density is known approximately, but there are multipath effects that change polarization and spatial distribution of power density. The transmitters can be single-frequency, multiple-frequency or broadband. An application of this scenario is for powering multiple sensors whose location is not precisely known, e.g. sensors that are placed behind walls or in a manufacturing environment. Another related application is for powering batteryless implanted devices.
- Unknown transmitters over a range of frequencies, power levels, generally unpolarized, with varying low-level spatial power densities. The application is energy harvesting or energy scavenging-recycling.

This work deals with the latter two cases, and some specific designs and applications are briefly described in the next sections. This chapter concludes with a comparative tables for rectennas and rectenna arrays.

The incident power density on the rectenna, $S(\theta, \phi, f, t)$, is a function of incident angles, and can vary over the spectrum and in time. The effective area of the antenna, $A_{eff}(\theta, \phi, f)$, will be different at different frequencies, for different incident polarizations and incidence angles. The average RF power over a range of frequencies at any instant in time is given by:

$$P_{RF}(t) = \frac{1}{f_{high} - f_{low}} \int_{f_{low}}^{f_{high}} \int_{0}^{4\Pi} S(\theta, \phi, f, t) A_{eff}(\theta, \phi, f) d\Omega df \tag{2.1}$$

The DC power for a single frequency (f_i) input RF power, is given by

$$P_{DC}(f_i) = P_{RF}(f_i, t)\eta[P_{RF}(f_i, t), \rho, Z_{DC}] \tag{2.2}$$

where η is the conversion efficiency:

$$\eta[P_{RF}(f_i,t),\rho,Z_{DC}] = \frac{P_{DC}(f_i)}{P_{RF}(f_i,t)} \tag{2.3}$$

which is a function of statistically varying incident RF power $P_{RF}(f_i,t)$ and depends on the impedance match $\rho(P_{RF},f)$ between the antenna and the rectifier circuit, as well as the DC load impedance. The reflection coefficient in turn is a nonlinear function of power and frequency. Therefore, in order to find the efficiency of the rectenna, we perform the following measurements:

1. Illuminate the rectenna from a known distance and incidence angle with a known frequency and power; thus $S(\theta,\phi,f,t)$ is known;
2. For each frequency of interest we will take the effective area from simulations. This is generally larger than the real effective area and therefore overestimates the received RF power.
3. Measure the DC power as a function of the DC load impedance (resistance);
4. Calculate the estimated conversion efficiency as P_{DC}/P_{RF} . Since the DC power is measured directly, and the RF power is over-estimated, the resulting efficiency will be an under-estimate.

This process should be done at each frequency in the range of interest. However, DC powers obtained in that way cannot be simply added in order to find a multifrequency efficiency, since the process is nonlinear. Thus, if simultaneous multifrequency or broadband operation is required, the above characterization needs to be performed with the actual incident power levels and spectral power density. Chapter 4 discusses in detail the efficiency ves incident power in our rectenna.

2.5 Example Rectenna Designs

Next, the study of the field strength in the center of tokio, also design and characteristics of several rectenna elements and arrays is overviewed, in the following order:

- Feasibility and potential application of power scavenging from environmental RF Signals in the center of Tokio [27].
- A linearly-polarized, single frequency (10 GHz.) conformal rectenna array for monitoring corrosion in aircraft wings [28].

- A dual-polarized rectenna element for small low-power sensor powering[28].
- Several broadband arrays for power recycling [28].

2.5.1 Feasibility and potential application of power scavenging from environmental RF signals

As a feasibility study a measurements of electrical field strength of the same place at the same time of day for 19 days and 16 places at the center of Tokyo made by the University of Tokyo is presented [27]. The place and route was selected based on the typical lifestyle of the people in Tokyo. Measurements were executed at major stations and trains including subways, small and large streets, and an office environment. The equipment used in the measurement allows to measure the individual contributions of multiple emitters and to generate a tabular or spectrum view of the total exposure over the 75 MHz to 3 GHz. frequency range.

As preliminary results, it turned out that one rectenna could supply stable DC electricity when the electrical field strength is more than about 0.5 - 1.0V/m. In each day, was calculated daily average (Ave), standard deviation (Dev), Duration (Dur: the percentage of the time when signal above 1.0 V/m is observed) of all the frequency from 75Mhz to 3 GHz. figure 2.4 show the summarized result of the measurement. In the bottom right, shows the geographical map of the place where measurement was taken place. Each bar chart (1-8) shows the average of all the measurement results of 19 days focused on three different frequency bands including FM Radio, TV and Mobile Phone(2 GHz.).

What is observed from the measurement result is that radiowave in mobile phone band is frequently observed at anywhere but very spiky and vary widely. This is because the strength of microwave radiated from mobile phones and a base station depends on the amount of the mobile phone traffic around the measurement place. Furthermore, as seen in No. 4 in figure 2.4, strength of FM radio and TV frequency band shows more stability (lower variance and higher duration). This is because a broadcasting tower (Tokyo Tower) located around the point No. 4.

After was introduced measurement results around Tokyo Tower as a follow-up experiment. figure 2.5 shows the average and standard deviation of FM radio, analog TV, and digital TV frequency band. Each measurement was executed for 15 minutes at different places where distance from the tower is from 100m to 1500m. The tower waas visible from all the measurement points except for (8). At point (6), only TV antenna is visible. Duration of the signal was 100% at all the points. Observed field strength was also more than 0.5V/m at many points where each distance from the tower is close enough.

Different from mobile phone signal, broadcasting signal is more suitable energy source in this point of view

Then field strength was strong enough (2V/m) at the place where it is not far from the tower. Using a directional antenna with 5 dBi gain, it will be able to harvest 1.73W near the Tokyo Tower. This estimation doesn't consider various losses resulted from antenna and rectifier. However, some of the real wireless sensor node only consumes 689 uW in average [29]. then it is feasible to operate this sensor node under this condition. Even if only insufficient amount of energy is scavenged from single rectenna, it is also possible to arrange multiple elements to receive more energy. Even if the strong signal appears intermittently, it is also possible to charge the energy to super capacitors and let the sensor node work intermittently. Such instabilities are also compensated by upper layer strategies such as network protocols [30] and application software.

2.5.2 Linearly-polarized medium-power rectenna array

The flight environment of an aircraft is very harsh due to large changes in humidity, temperature, pressure, speed, and loading conditions, which can result in corrosion and other failures. Using tomographic piezoelectric sensors, failures can be detected before they pose a significant risk to the aircraft. A wireless means of actuator excitation, communication, and sensor interrogation has many benefits such as fast inspection, less downtime, labor cost reduction, etc. Currently, wireless sensors contain an on-board miniaturized antenna, and a multi-channel circuit for data acquisition. Batteries, magnetic coupling or solar cells can be used to power the sensors, control, data collection and processing electronics. As an alternative to conventional powering methods, in this example a rectenna array was developed that provides DC power from incident microwave radiation. The specifications of the rectenna are derived from the requirements of the sensor system: $\pm 15V$ with $100mW$of continuous power for 5 minutes in order to complete corrosion inspection. The physical size requirements for the rectenna are an aperture of $15cm$ by $15cm$ using as thin of a substrate as possible to conform to the shape of the airframe. The transmitting antenna is linearly polarized and provides a power density of at most $10mW/cm^2$ incident on the rectenna array from a maximum distance of one meter with line of sight. The rectenna array for this example was designed starting from a single element. The number of elements and their DC connection is determined from the power obtained from the single element. For this application, the antenna element is a narrowband, linearly polarized patch antenna at 10 GHz. designed on a $0.25mm$ thick Rogers Duroid substrate with a relative permittivity of 2.2. The gain of the patch calculated from its physical area is 1.39 ($1.45dB$). The thin substrate is chosen because this allows the final rectenna array to be flexible enough to conform to

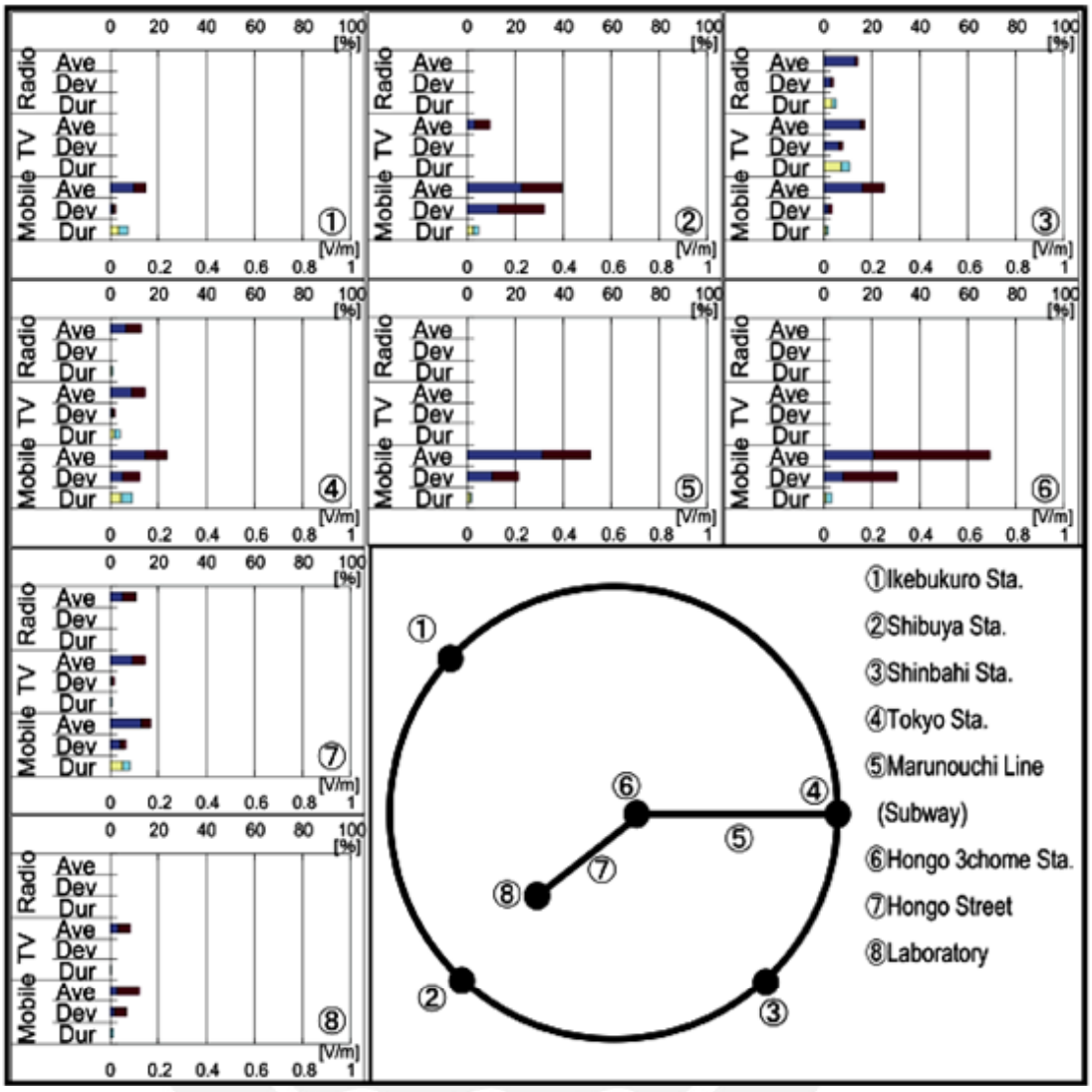

FIGURE 2.4: Measurement Result of Major Place in Tokyo.

the moderate curve of the airframe while desirable microwave properties are maintained. The rectifier diode was an Agilent HSMS-8101 Schottky mixer diode. The single element was simulated without considering connections to other rectenna elements. The maximum efficiency for the ideal circuit is 52% for an input power of 10 mW. Although the overall efficiency depends on how the rectenna elements are connected, all 25 elements in this rectenna are connected in series to maximize the output voltage as required by the electronics load.The trend for output voltage versus the resistive load is shown in figure 2.6. Series connection of 25 elements provides the required 15V output with approximately 100mW of DC power for a 2.4KΩ load. The estimated optimal efficiencies of 16, 19 and 25-element arrays are 44%, 44% and 39%, respectively. figure 2.7 shows the measured sensitivity of rectified DC power as a function of polarization mismatch between the transmitter and rectenna. The direct output voltage of the rectenna only

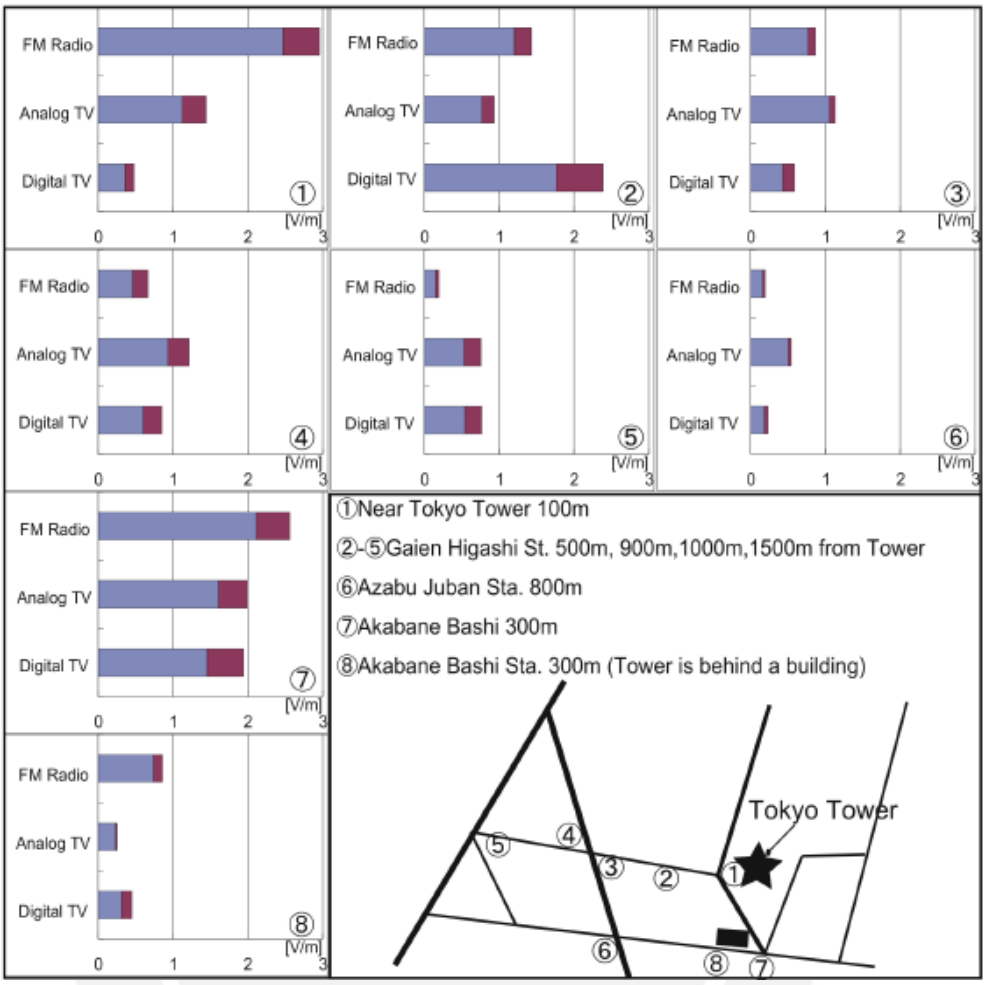

FIGURE 2.5: Measurement Results around Tokyo Tower.

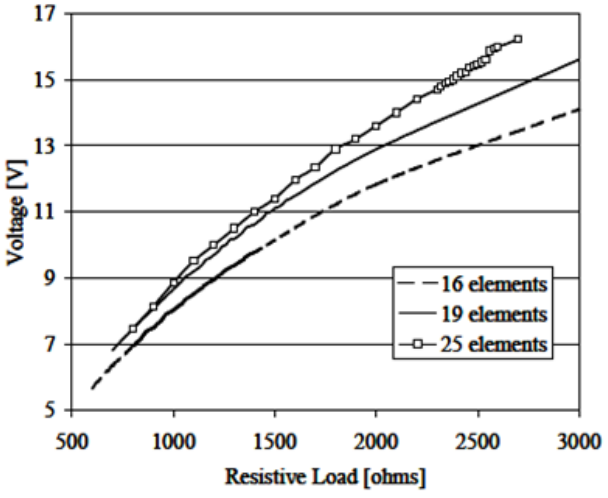

FIGURE 2.6: Measured DC voltage as a function of the DC resistive load for three array sizes.

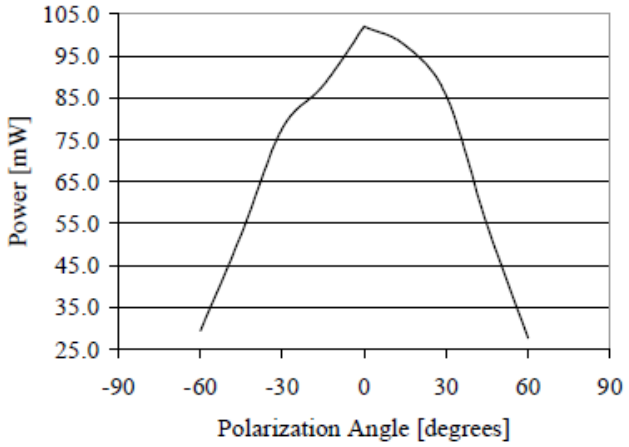

FIGURE 2.7: Measured DC power as a function of polarization mismatch between the transmitter and rectenna array. 0 degrees indicates linear polarization match.

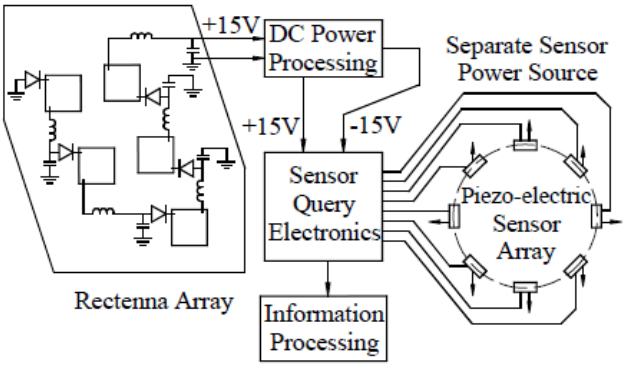

FIGURE 2.8: Block diagram of rectenna and sensor system. In the initial test, only the sensor control and processing electronics circuitry is powered by the rectenna.

provides positive or negative voltage and additional circuitry is required to provide both polarities. The Maxim ICL7662 inverter chip with 98% efficiency is used for this task (A more detailed discussion of dc-dc conversion is presented in chapter 5). The system block diagram is shown in figure 2.8.

2.5.3 Dual-polarized low-power rectenna element

The un-licensed ISM band around 2.4 GHz. is an appropriate frequency range for low-power wireless sensor powering. In this case, the application is a human health-function monitoring sensor for senior-citizen assistant living. The wireless sensor contains an accelerometer, temperature sensor and skin conductivity sensor. The sensor and power management circuit is controlled through a low-power microcontroller, and the collected

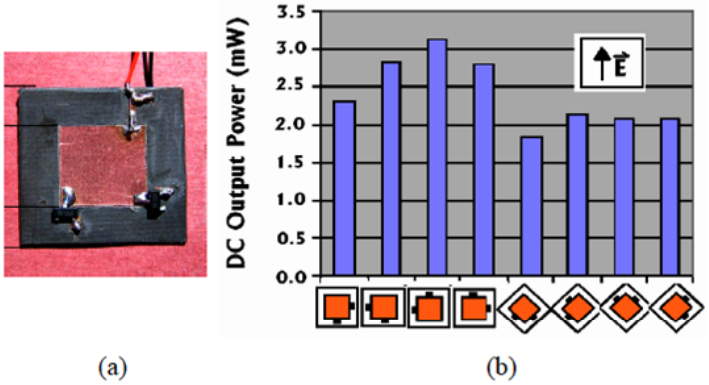

FIGURE 2.9: Photograph of dual-polarized 2.4 GHz. patch rectenna (a), and histogram of measured power levels for an incident power level of 170 uW/cm^2 for different incident polarization levels (b).

data is transmitted via a commercial low-power ISM band transmitter (from Chipcon). In this scenario, the sensor is mobile and therefore the polarization changes. Thus, the rectenna is designed to be dual-polarized with two rectifier diodes. Each diodes rectifies one of the two received polarizations, and the DC signals add. The rectenna is a $19mm$ x $19mm$ square patch, with a $6cm$ x $6cm$ square ground plane on a Rogers Duroid 6010 substrate ($\varepsilon_r = 10.2$, thickness=$50mil$) chosen to reduce the antenna size. An Agilent HSMS8101 diode is connected at each of the two centers of the two orthogonally-polarized patch radiating edges, figure2.9 (a). . A via terminates each diode to RF/DC ground, which is structurally isolated from the patch ground plane and interfaces with a PCB layer (behind patch ground plane) through a 2.7-nH inductor. Figure 2.9 (b) shows a histogram of measured power levels for an incident power level of $170uW/cm^2$ for different incident polarization combinations, which will all be present in the multipath environment envisioned in this application. It is interesting to compare these to the results in figure 2.7, which are measured for a similar patch antenna but with a single diode receiving one linear polarization. Not only is the DC power larger in this case, as both polarizations are received and rectified, but the variation of received power is reduced by approximately a factor of two.This rectenna operates with incident power levels as low as $10uW/cm^2$ and is capable of powering a low-power wireless sensor.

2.5.4 Broadband rectenna arrays for low-power arbitrarily polarized incident radiation with high power dynamic range

For low power applications, as is the case for collected ambient energy, there is generally not enough power to drive the diode in a high efficiency mode. Furthermore, rectification requires a different approach from standard matching techniques. In a rectenna

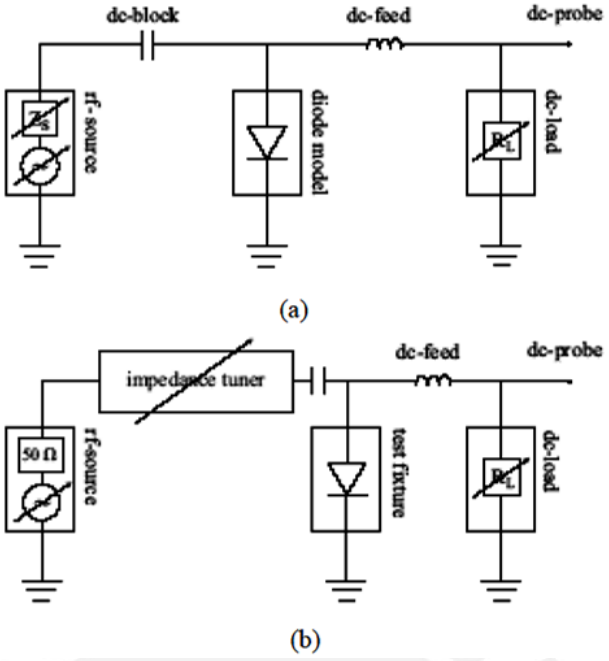

FIGURE 2.10: Circuit diagram of the Harmonic Balance simulation (a) and diagram of the equivalent source-pull measurement setup (b).

application, the antenna itself can be used as the matching mechanism instead of using a transmission-line or lumped-element matching circuit. The antenna's design is therefore heavily dependent on the diode characteristics.

Design of a broadband antenna integrated with a power and frequency dependent diode impedance is a challenge. A source-pull of the diode is a sweep of RF input source impedance values over a given area of the Smith chart. figure 2.11 shows the HB simulation approach using Agilent ADS as well as the measurement approach using impedance tuners. In both simulation and measurements, for a variety of input powers the resulting DC voltage is quantified for each source impedance and plotted on the Smith chart.

The region of optimal source impedance is later used for optimizing the antenna's design so that the antenna presents the proper equivalent source impedance to the diode. Usually, the optimal source impedance moves counter-clockwise along a constant admittance circle with increasing frequency due to the junction capacitance.

For maximal power transfer, the antenna impedance would match the optimal diode impedance for all frequencies. Since this is difficult to accomplish, a possible sub-optimal approach is to present a constant impedance to the diode by using a frequency independent antenna element. An equiangular spiral was chosen as the array element since it is uniplanar with convenient feed point for diode connection, and can be left or right-hand

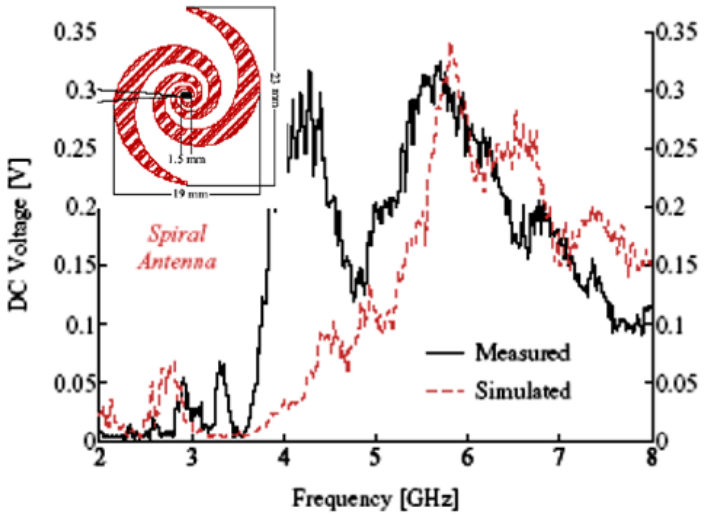

FIGURE 2.11: Nonlinear harmonic-balance simulation and measurements of theDC rectified voltage response across 60 ohms for the spiral antenna in the inset.

circularly polarized. A single element was simulated with full-wave CAD tools resulting in a one-port frequency dependent impedance that becomes the diode load in the rectenna. A diode is connected at the antenna feed and the resulting rectenna element performance is shown in figure 2.11. The disagreement around 4 GHz. is believed to be caused by the 1-cm long unbalanced coax feed. A 64-element array of left and right hand circularly polarized spiral elements is designed, so that each spiral element is directly connected to a rectifier diode. Therefore, the RF powers received independently by each element are summed upon rectification as DC currents and/or voltages. A sweep of the input power is performed and the resulting DC output and re-radiated power is quantified. The measurement,figure 2.12, is made with broadside linearly polarized radiation at 3 GHz. with incident power densities ranging from tens of nW/cm^2 to $0.1mW/cm^2$.

The DC voltage is measured across a 100-ohm load. The rectification efficiency reaches the 20% range for an incident power density of $0.1mW/cm^2$ and arbitrary polarization.

Also shown in figure 2.12 is the relative amount of reflected power along with the radiated power of the 2nd through 5th harmonics. The reflected power is found from S_{11} measurement using a vector network analyzer. The result, consistent with simulation results, indicates that the reflected power varies linearly with input power up to $0.1mW/cm^2$. Simulations suggest, however, that the reflections begin to drop as higher power levels are applied and a larger fraction of incident power is converted to DC and power at the harmonics. The array scaling in size is trivial, since there is not RF feed network, and only the DC output network is required. If space allows, this type of array

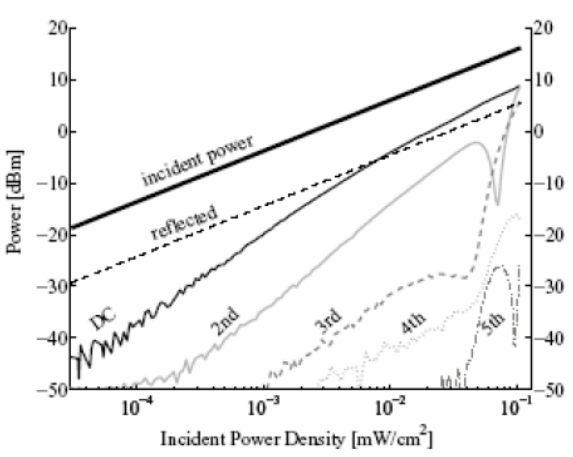

FIGURE 2.12: Measured reflected, rectified, and re-radiated harmonic power as a function of incident power density.

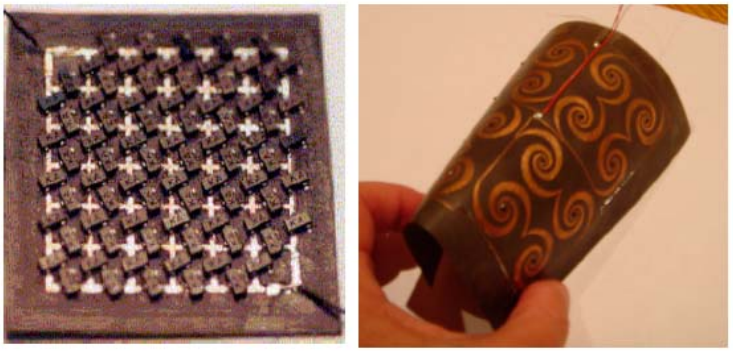

FIGURE 2.13: A dense dual-linearly polarized grid-rectenna array(left) and a dual-circularly polarized spiral antenna array fabricated on a flexible conformal substrate and operating between 2 and 18 GHz.(right)

can be made in the form of wall-paper for collecting as much power as possible. Further, the DC collecting lines can be made to be reconfigurable, so that either current or voltage are summed, depending on the DC load. The spiral array is dual-circularly polarized, but the same concept of separately rectifying two orthogonal polarizations applies to linear vertical and horizontal polarization. A grid-type dual-linear dense array is shown in figure 2.13 (left). Such arrays can be made on flexible substrates, as is shown in 2.13 (right) where a small spiral array is designed to decorate a coffee cup and provide DC power to a sensor with only $50uW/cm^2$ incident power density.

In resume:

-	Incident power required	Bandwith	Efficiency	Rectifier circuits	Application
Linear Polarization	mW/cm^2	Single freq.	low	1	wireless powering with dedicated source
Dual Polarization	uW/cm^2	Narrow band	medium	2	wireless powering with dedicated source(more distance)
Circular Polarization	uW/cm^2	Narrow band	medium	1-2	wireless powering with dedicated source(more distance)

TABLE 2.1: Comparison between polarizations of one element rectenna

- The rectenna's behavior is known, wireless power transmission is strongly developed technology.
- Is feasible to operate sensor nodes under the harvest electric energy from the RF signals that have been radiated by communication and broadcasting systems
- It shown consistent development of rectennas working with low incident powers.
- It recognizes the importance of polarization on the performance of the rectenna.
- In most cases linear polarization is useful for working in a single frequency, in this case, the rectenna depends on a exclusive transmitter and requires higher power incident.
- For energy recycling, to collect energy on any range, is always desirable to capture greatest amount of waves. The rectenas will be more efficient while is not limited by polarization and have the maximun frequency bandwidth.
- The arrays increase the amount of DC output and allow work in broadband applications, the drawback is the difficult to match all elements

Tables2.1 and 2.2 show important results about referenced work in this chapter.

-	Incident power required	Bandwith	Efficiency	Rectifier circuits	Application
Linear Polarization	mW/cm^2	Narrow band	medium	one for element	wireless powering with dedicated source(more distance)
Dual Polarization	nW/cm^2 uW/cm^2	Broad band	high	one for element	energy recycling and wireless powering
Circular Polarization	nW/cm^2 uW/cm^2	Broad band	high	one for element	energy recycling and wireless powering

TABLE 2.2: Comparison between polarizations in an array of rectennas

Chapter 3

Rectenna Design

This chapter describes the design and results of simulations of a single rectenna working at ISM band center in 2.45 GHz. First is presented a brief background about simulation methods used, microstrip antennas and rectifier circuits. As antena was chosen a microstrip square patch aperture coupled antenna, the design try to have lower dimensions and better polarization bandwidth that a traditional of this kind, this is achieved using a cross-slot in the patch [31] and two feed line each for one polarization,this last to increase the range of incident power; then a dual linear polarization antenna was achieved. As a rectifier was chosen Villard voltage doubler. The tool used to simulate the rectenna with Harmonic Balance (HB) method for the circuit and momentum electromagnetic full-wave analysis for the antenna is Agilent advanced design software (ADS) simulator. The results of the simulations will be compared with measurements in order to assess the usefulness of the simulation tool for our design(chapter 4).

3.1 A brief Background Information

3.1.1 Harmonic Balance Simulation

For analyzing nonlinear circuits, two major techniques are known: the time domain based large signal - small signal and the frequency domain based harmonic balance analysis. Since this work only applies single tone excitation to circuits, the decision was made to use the harmonic balance method. This also has the advantage of avoiding time constants, which are much greater than the inverse of the excitation frequency and require integration over many periods. These can differ from each other by several orders of magnitude, which would cause problems for numerical solvers of the nonlinear differential equations.

HB analysis is performed in the frequency domain Fourier space, thus avoiding differential equations. The entire circuit is split up into a linear and a nonlinear sub-circuit connected by N ports. Because the nonlinear devices create harmonics, the port-voltages must not only be known for the sinusoidal fundamental frequency of the excitation, but for all harmonics $k = 1 ::: K$, up to a given cut-off. For the entire circuit, assuming it is an M-port, the following systems can be written:

$$\begin{bmatrix} I_{1,k} \\ \vdots \\ I_{N,k} \\ I_{N+1,k} \\ \vdots \\ I_{M+N,k} \end{bmatrix} = Y_{lin} \cdot \begin{bmatrix} U_{1,k} \\ \vdots \\ U_{N,k} \\ U_{N+1,k} \\ \vdots \\ U_{M+N,k} \end{bmatrix} \tag{3.1}$$

$$\begin{bmatrix} \hat{I}_{1,k} \\ \vdots \\ \hat{I}_{N,k} \end{bmatrix} = \hat{Y}_{nlin} \cdot \begin{bmatrix} \hat{U}_{1,k} \\ \vdots \\ \hat{U}_{N,k} \end{bmatrix} \tag{3.2}$$

where $U_{m,k}$ and $I_{m,k}$ are k-th harmonics of port voltages, or respective currents, and Y_{lin} and $\hat{Y}_{nlin}$ are the admittance matrices of the sub-circuits. The hat notation relates to the nonlinear sub-circuit, whereas letters without hats belong to the linear sub-circuit. For the N connecting ports, $I_{n,k} = -\hat{I}_{n,k}$, i.e. Kirchhoff's current law, and $U_{n,k} = \hat{U}_{n,k}$, i.e. Kirchhoff's voltage law, must be satisfied for all $n = 1 ::: N$. To solve for the entire circuit, port-voltages $U_{n,k}$ have to be found, that solve both Eqs.3.1 and 3.2, so that $I_{n,k} = -\hat{I}_{n,k}$. As soon as those voltages are found, the circuit is analyzed. A more detailed discussion on the harmonic balance technique can be found in [32].

3.1.2 Square Patch Microstrip Antenna

A microstrip patch antenna consists of a very thin metallic patch (usually gold or copper) placed a small fraction of a wavelength above a conducting ground plane, separated by a dielectric substrate. Microstrip antennas have numerous advantages, they are light weight, they can be designed to operate over a large range of frequencies (1- 40 GHz.), they can easily be combined to form linear or planar arrays, and they can generate linear, dual, and circular polarizations. These antennas are inexpensive to fabricate using printed circuit board etching, which makes them very useful for integrated active antennas in which circuit functions are integrated with the antenna to produce compact transceivers. Microstrip antennas can be in various shapes and configurations but for the purpose of this work only a square patch microstrip antennas are of interest. The

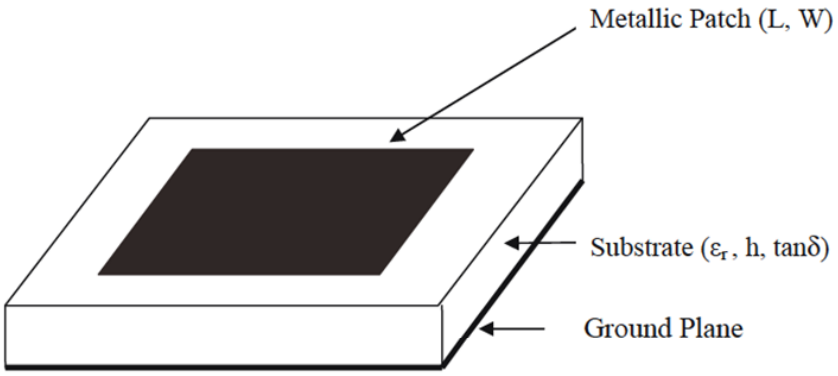

FIGURE 3.1: Rectangular microstrip antenna configuration.

basic antenna element is a thin conductor of dimensions L x W on a dielectric substrate of permittivity ε_r , loss tangent $\tan\delta$ and thickness h backed by a conducting ground plane. This configuration is shown in figure3.1. The material covered in this sections known as microstrip antenna theory is from ([33][34][35][36][37]). Next sections includes an overview of microstrip antennas modeling and feeding techniques.

3.1.3 Microstrip Antenna Analytical Models

There are various ways to model a microstrip patch. This modeling is used to predict characteristics of a microstrip patch such as resonant frequency, bandwidth, radiation pattern, etc.the usually used are transmission line model and the cavity model, these models are based on some assumptions, which simplify the calculations at the cost of less accuracy. There are other models that provide more accuracy such as the momemtum full-wave model but are also more complicated to analyze.

For a given antenna structure the conductors can be broken into "segments", and the currents on the segments can then be determined. The "moment" is numerically the size of vector of current describing the little segment (length and orientation). A set of "basis functions" may be assumed into which the current distributions are decomposed.

In the simplest case, the basis functions are rectangular approximations to the Dirac delta function. Because the widths of the rectangular sections are non-zero, only a finite (reasonably small) number of them are needed to cover the antenna structure. The exact Green's functions in spectral domain form are used to find the components from electric and magnetic currents by integrating each slab(there is a mesh of slabs), in general, the "n-th moment" is obtained by integrating the product of the Green's function with the

n-th basis function. This Green's function incorporates electrostatic coupling between the moments for the spatial change of the currents.

When the current distribution across the antenna structure has been determined, (by integration) is feasible predict characteristics of an antenna. The simulation of the antenna was done using Agilent Momentum method for electromagnetical analysis.

3.1.4 Microstrip Antenna Feeding Techniques

Impedance matching is the most important aspect in feeding an antenna no matter what technique is being used. This matching assures that most of the power is transferred from the feed to the radiating patch. But also associated with impedance matching are spurious radiation and surface wave losses, which are caused by discontinuities such as bends, junctions, stubs, and stepped impedance transformers. It is also important to consider the suitability of a feed for antenna arrays. The most common feeding techniques are coaxial probe feed, the coplanar microstrip line feed and the aperture-coupled feed. Aperture-coupled feeding is discussed in more detail since is the technique used in this design.

3.1.4.1 Aperture-coupled Feeding

In this technique the feed network is separated from the radiating patch by a common ground plane.The radiating microstrip patch element is etched on the top of the antenna substrate and the microstrip feed line is etched on the bottom of the feed substrate, energy is electromagnetically coupled through an aperture in the ground plane.The thickness and dielectric constants of these two substrates may thus be chosen independently to optimize the distinct electrical functions of radiation and circuitry. Although the original prototype antenna used a circular coupling aperture, it was quickly realized that the use of a rectangular slot would improve the coupling, for a given aperture area, due to its increased magnetic polarizability, Most aperture coupled microstrip antennas now use rectangular slots, or variations thereof. This aperture is usually centered with respect to the patch where the patch has its maximum magnetic field. For maximum coupling it has been suggested that a rectangular slot parallel to the two radiating edges should be used. Two very similar coupling mechanisms take place, one between the feed line and the slot and another between the slot and the patch, figure 3.2 shows the geometry of the basic aperture coupled patch antenna.

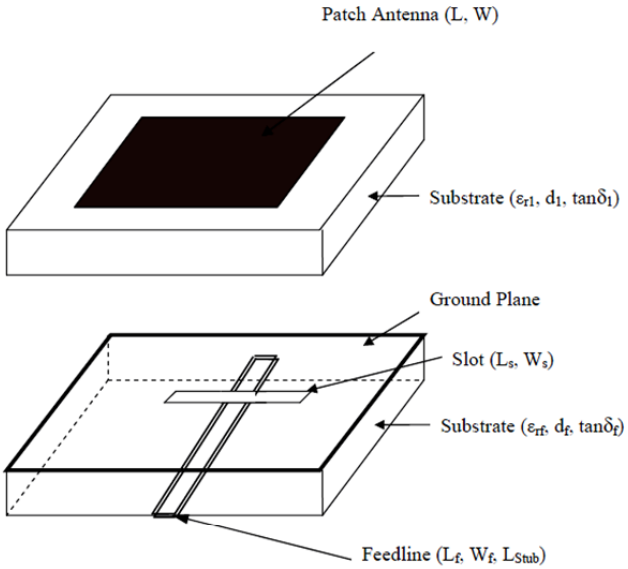

FIGURE 3.2: Geometry of the basic aperture coupled microstrip antenna.

3.1.5 Basic Operation of the Aperture Coupled Microstrip Antenna

The aperture coupled microstrip antenna involves over a dozen material and dimensional parameters, figure3.3 show a typical smith chart for this kind of antenna and the result of increasing the tuning stub length.The basic trends with variation of these parameters is presented bellow:

- **Antenna substrate dielectric constant**: This primarily affects the bandwidth and radiation efficiency of the antenna, with lower permittivity giving wider impedance bandwidth and reduced surface wave excitation.
- **Antenna substrate thickness**:Substrate thickness affects bandwidth and coupling level. A thicker substrate results in wider bandwidth, but less coupling for a given aperture size.
- **microstrip patch length**:The length of the patch radiator determines the resonant frequency of the antenna.
- **microstrip patch width**:The width of the patch affects the resonant resistance of the antenna, with a wider patch giving a lower resistance.
- **feed substrate dielectric constant**:This should be selected for good microstrip circuit qualities, typically in the range of 2 to 10.

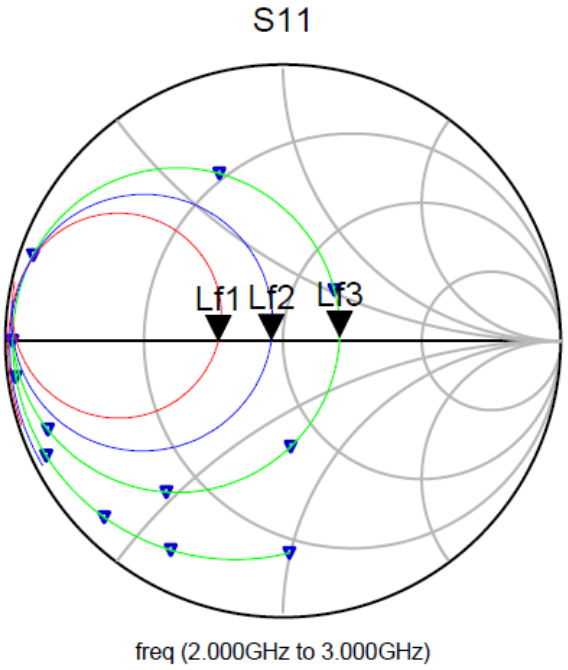

FIGURE 3.3: Calculated input impedance as a function of stub length (Lf), Lf1<Lf2<Lf3; by varing the stub and slot length is posible an exactly match. This figure is a result of trial and error simulations until get the desirable matching level.

- **feed substrate thickness**:Thinner microstrip substrates result in less spurious radiation from feed lines, but higher loss. A compromise of 0.01λ to 0.02λ is usually good.
- **slot length**:The coupling level is primarily determined by the length of the coupling slot, as well as the back radiation level. The slot should therefore be made no larger than is required for impedance matching.
- **slot width**:The width of the slot also affects the coupling level, but to a much less degree than the slot length. The ratio of slot length to width is typically 1/10.
- **feed line width**:Besides controlling the characteristic impedance of the feed line, the width of the feed line affects the coupling to the slot. To a certain degree, thinner feed lines couple more strongly to the slot.
- **feed line position relative to slot**: For maximum coupling, the feed line should be positioned at right angles to the center of the slot. Skewing the feed line from the slot will reduce the coupling, as will positioning the feed line towards the edge of the slot.

- **position of the patch relative to the slot**:For maximum coupling, the patch should be centered over the slot. Moving the patch relative to the slot in the Hplane direction has little effect, while moving the patch relative to the slot in the E-plane (resonant) direction will decrease the coupling level.

- **length of tuning stub**:The tuning stub is used to tune the excess reactance of the slot coupled antenna. The stub is typically slightly less than $\lambda_g/4$ in length; shortening the stub will move the impedance locus in the capacitive direction on the Smith chart.

3.1.6 Variations on the Aperture Coupled Microstrip Antenna

Since the first aperture coupled microstrip antenna was proposed, a large number of variations in geometry have been suggested by workers around the world. The fact that the aperture coupled antenna geometry lends itself so well to such modifications is due in part to the nature of printed antenna technology itself, but also to the multi-layer structure of the antenna. Below is categorized some of the modifed designs that have evolved from the basic aperture coupled antenna geometry:

- **radiating elements**: The original aperture coupled antenna used a single rectangular patch. Since then, workers have successfully demonstrated the use of circular patches, stacked patches, parasitically coupled patches, patches with loading slots, and radiating elements consisting of multiple thin printed dipoles. Most of these modifications are intended to yield improved bandwidth.

- **slot shape**:The shape of the coupling aperture has a significant impact on the strength of coupling between the feed line and patch. Thin rectangular coupling slots have been used in the majority of aperture coupled microstrip antennas, as these give better coupling than round apertures. Slots with enlarged ends, such as dogbone, bow-tie, or H-shaped apertures can further improve coupling.

- **type of feed line**:The microstrip feed line can be replaced with other planar lines, such as stripline, coplanar waveguide, dielectric waveguide, and similar. The coupling level may be reduced with such lines, however. It is also possible to invert the feed substrate, inserting an additional dielectric layer so that the feed line is between the ground plane and the patch element.

- **polarization**: Besides linear polarization, it has been demonstrated that dual polarization and circular polarization can be obtained with aperture coupled elements.

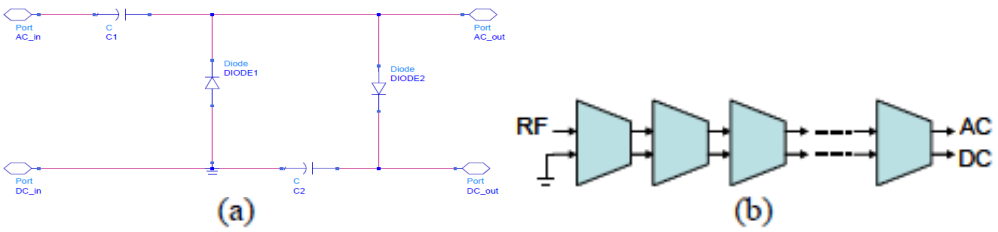

FIGURE 3.4: Single Villard voltage double (a) and cascaded Villard voltage doublers (b).

- **dielectric layers**:As with other types of microstrip antennas, it is easy to add a radome layer to an aperture coupled antenna, either directly over the radiating element, or spaced above the element. It is also possible to form the antenna and feed substrates from multiple layers, such as foam with thin dielectric skins for the etched conductors.

. In its basis geometry configuration, like figure 3.2; the aperture coupled microstrip antenna has a linear polarization and high quality factor; this traduce in impedance bandwidths ranging from 1 to 5% (narrowband).

3.1.7 RF to DC Rectifier

A basic schematic of a Villard voltage doubler, sometimes also called Cockcroft-Walton voltage multiplier [38], is shown in figure 3.4 (a). A DC voltage of twice the peak amplitude of the input AC signal can be generated at the DC output. And ideally, arbitrary output DC voltage can be reached by building cascaded stages of the doubler, figure 3.4 (b). In the real case, the amplitude of the AC signal will be divided by coupling capacitors and the junction capacitance of the diode. Also the reverse leakage current of the diode and the resistance of the diode will limit the feasible DC output. Therefore, to obtain the maximum voltage, large coupling and charge-storage capacitance is preferred. In addition, larger capacitance stores more energy and consequently provides more current when discharging. Low series resistance Schottky diodes are most suitable for implementing the circuit due to its high forward bias current for a given voltage. According to the analysis above, the junction capacitance should be minimized to achieve higher output voltage, then this is the main condition to properly choice of diode, this will be seen in section3.3.1 .

The equivalent input impedance of the rectifiers is decided by the diode junction capacitance, which is much smaller than the serially connected coupling and storage capacitance. By other hand, like in transformers, when voltage is stepped up, the output current decreases. This is also true of voltage multipliers. Although the measured output voltage of a voltage multiplier may be several times greater than the input voltage, once a load is connected the value of the output voltage decreases. Also any small fluctuation of load impedance causes a large fluctuation in the output voltage of the multiplier. For this reason, voltage multipliers are used only in special applications where the load is constant and has a high impedance or where input voltage stability is not critical.

3.2 Antena Design

This section addresses the design procedure of an aperture-coupled square patch microstrip antenna in ISM frequencies 2.4-2.5 GHz. whit an input line of 50Ω. Three similar antenna structures were designed using different geometric parameters (patch sizes,lengths of aperture coupling, and stub coupling, and insert a second feed line) with the same substrates material. There are two reasons for designing three antennas (1) to reduce the dimensions without affecting the bandwidth achieved almost at the same cost material; the second and third antenna will be more thick because has a double intermediate substrates but with less patch size; and (2) to increase the polarization bandwidth. the Two optimum antennas was fabricated and measured for show the improvements and the better was used to integrate the rectifier. These antennas were designed beginning from its basic geometry configuration (figure 3.2) and then by changing some of this parameters in shape, position and length we success increase the bandwidth; as it is important to receive the greatest possible amount of RF radiation.

In its basic configuration a single linearly polarized antennas are expected, with two feed lines properly positioned a dual linear poralization is achieved; this will be discussed in section 3.4 and showed in figures 3.16, 3.17 and 3.17. There is no exactly step-by-step design procedure for this kind of structure due to the number of interacting design parameters. The following design is a combination of tuning and modeling to arrive at a functional design that meets the above requirements. There is just one point to start with the modeling and tuning: is necessary define a basic dimensions, this and design process are discussed in the following sections.

-	Arlon 25N(A25N)	Rohacell51
Er	3.38	1.05
TanD	0.0025	0.0008
H	0.508 mm	3 mm
Cond (cupper)	$5.813 \cdot 10^7$	-

TABLE 3.1: Substrates parameters used

3.2.1 Simulation Setup and Design Process

To start with the modeling, first we need to define the layers setup for our antena, figure3.5 shows this configuration in Agilent ADS, then is necessary define the basic dimensions of our antenna, also by using Line Calculator tool from Agiltent ADS; in which is inserted the important parameters of specific substrate as: dielectric constant "Er", substrate thickness "H", tangencial losses " tan D", metal thickness "T", and conductivity "Cond"; the work frequency "Freq", electric length E_{Eff} and input impedance "Z0" and this calculates the dimensions of the line when is resonant at our frequency whit the above characteristics. Substrates were made from a thick layer of Rohacell51 foam and a thin layer of Arlon 25N for patch metallization, the feed substrate is also Arlon 25N. Rohacell51 is a Polymethacrylimide (PMI) hard foam, which is used as a core material for sandwich constructions. This material has permittivity close to air ($\sim$1). It also shows outstanding mechanical and thermal properties,is inexpensive, light weight, and it has a high heat resistance. Arlon 25N is woven fiberglass reinforced, ceramic-filled composite materials with a nominal dielectric constant of 3.38 and a loss tangent of 0.0025 at 10 GHz., engineered for use in microwave and RF multilayer printed circuit boards.These are the substrates availables in the laboratory and have a good performance for our design. Inserting values of table 3.2 in the "Line Calc" tool, figure3.6 and leaving other values by default, we can get the first dimensions of the patch and the width of the feed line for 50Ω input impedance, now we can start tuning the lengths to get the optimum design (patch and other lengths in order to match at 2.45 GHz.).

After several and tiresome trials, the square patch's size was fixed to 47mm, this value is different that the line calc, since now; the patch interacts with the foam and aperture, the length of the tuning stub on the feedline was set to 14mm, and its width 1.14mm. The aperture length was 24mm with 1.14mm width. The -10dB impedance bandwidth was 3.77% (figure 3.10) and the expected linear polarization was achieved (for a basic square

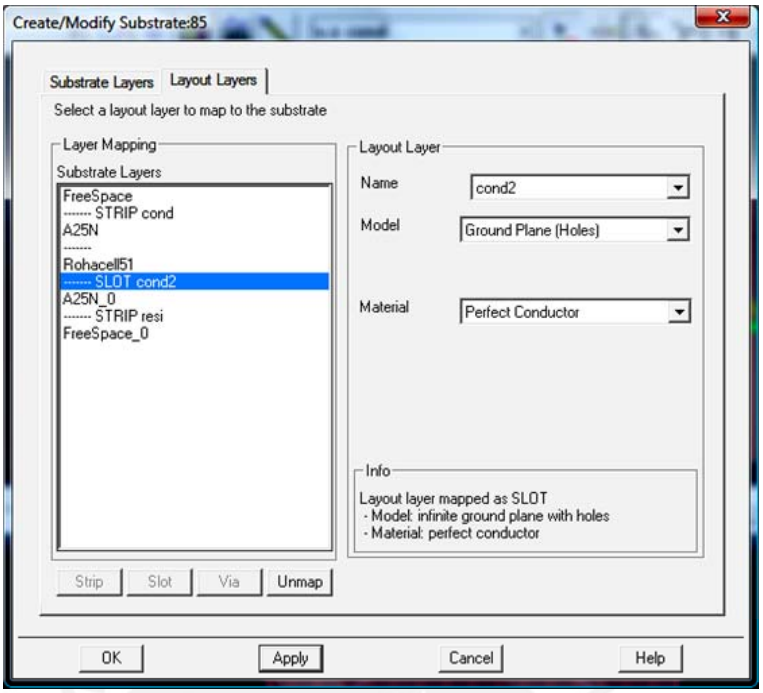

FIGURE 3.5: The figure show the multilayer setup for our antenna, first A25N substrate with a strip for square patch in the top and empty in the bottom, below a Rohacell51 foam and below the second A25N with a slot as a coupling aperture in the top and strip for the feed line in the bottom. there is a "free space" in both sides of the antena.

patch aperture coupled microstrip antenna geometry configuration), these dimensions are summarized in the table 3.2. the graphics results are below displayed with the second antenna results.

Then, with the main objective of reduce the patch size traduced in reduce the antenna size and without detriment to bandwidth, was designed the second antenna. This is achieved by inserting a cross slot centered in the square patch with equal lengths in both directions to reduce the operation frequency without changes in polarization [31], this corresponds the reduction of $\sim$ 28% of antenna's size; this method proposes an inclined slot coupled where the inclination angle respect to the feed line is $\arctan(W/L)$ or in our case is 45 degrees, since is a square patch; because the cross slots on the patch don't work with apertures collinear underneath. This method slightly increase the difficulty to match. To maintain bandwidth became two things: (1) A second Rohacell51 foam was introduced, this can be explained by the fact that the aperture acts as a second resonator in combination with patch element, this creates an effect simular to stacked patch antenna, which uses two patches of slightly different resonant frequency to achieve more bandwidth. (2) Tuning the widths of each slot in the cross slot but both with the same length (see figure 3.7), this is due to each slot's width modifies

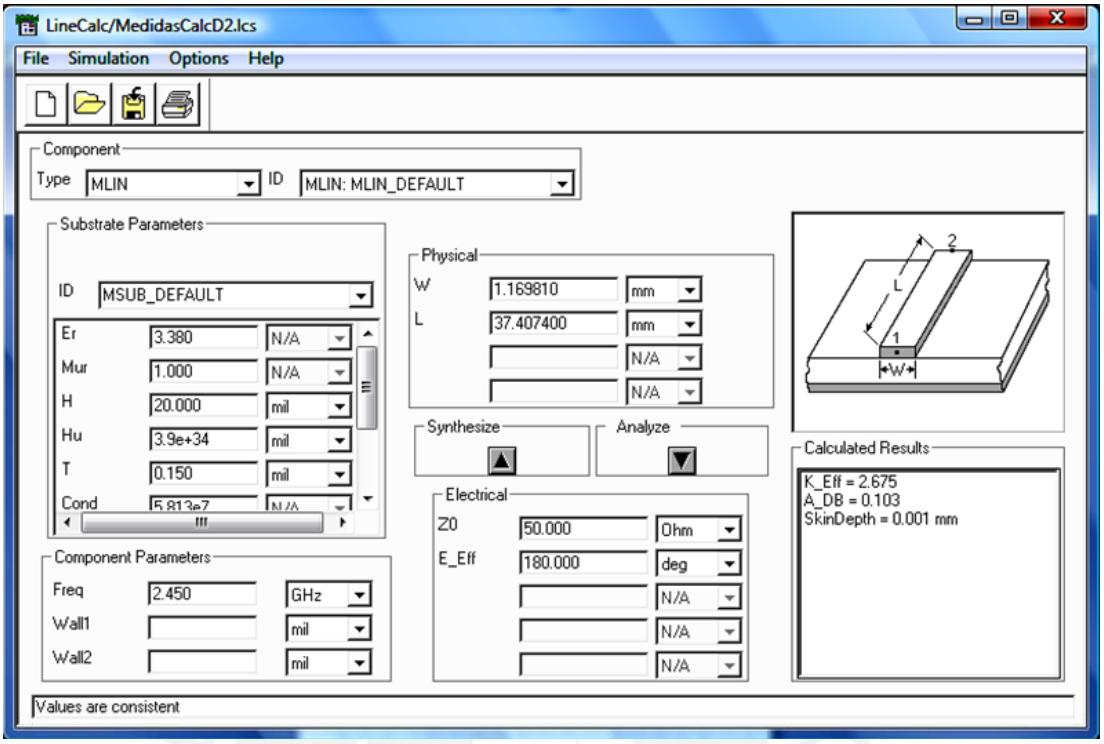

FIGURE 3.6: Figure shows how to calculate the dimensions of a "microstrip transmission line" by inserting the substrate parameters in "LineCalc" tool of Agilent ADS. This was used to know the first dimension of our resonant patch at 2.45 GHz. and the feed line's width for 50Ω input impedance.

Layer	Material	Dimension
Top Patch	Copper	47mm x 47mm
Top Substrate	A25N/Rohacell51	0.508mm/3mm (thickness)
GroundPlane/ Aperture	Copper/ Air	100mm x 100mm/ 24mm x 1.14mm
Feed Substrate	A25N	0.508mm (thickness)
Feedline/ Tuning Stub	Copper	Feed/ 14mm

TABLE 3.2: First antenna dimensions

Layer	Material	Dimension
Top Patch	Copper	33.95 x 33.95mm
Top Substrate	A25N/2xRohacell51	0.508mm/ 2x3mm (thickness)
GroundPlane/ Aperture	Copper/Air	73mm x 73mm/ 27 x 1.14mm
Feed Substrate	A25N	0.508mm (thickness)
Feedline/ Tuning Stub	Cooper	Feed/7,24mm

TABLE 3.3: Second antenna dimensions

the coupling mechanism between slots and aperture. This method was discovered by trial and error.

The second antenna and with the same trial and error simulation process has the following geometric parameters: square patch's size 33.95mm, length of the tuning stub on the feed line 7.24mm, and its width 1.14mm., aperture length 27mm with 1.14mm width. The -10dB impedance bandwidth was 3.7% and now the expected linear polarization was achieved but rotated 45 degrees anticlockwise respect to before design, this can be explained by the fact that aperture was rotated 45 degrees in the same direction and the symetric geometry of our design causes the coupling of the waves in this orientation; this design has almost the same behavior of the first design only with the advantage of less patch size, these dimensions are summarized in the table3.3. Now we need to improve the bandwidth.

Now, with an optimize patch size; a third antenna with the same process was designed, now is introduced a second feed line perpendicular to the first one with intention to get also a second perpendicular polarization and increasing the bandwidth per polarization. The apertures for coupling now are different, because the cross slots on the patch don't work with apertures collinear underneath, these are shifted close to the patch's edges and bending in U-shaped, this method is also made in a trial and error process; now the feed lines start at antenna's center and the stubs are at the other end(see figure 3.9); the two feed lines and apertures are identical in geometry but only positioned different, in this design the rectifier circuit will be positioned in the center of the back side of the antenna (see figure 4.4).

Layer	Material	Dimension
Top Patch	Copper	33.95 x 33.95mm
Top Substrate	A25N/2xRohacell51	0.508mm/ 2x3mm (thickness)
GroundPlane/ 2 x U-shaped	Copper/	73mm x 73mm/ long arm 19.20mm
Aperture	Air	short arm 8.28mm width 1.14mm
Feed Substrate	A25N	0.508mm (thickness)
Feedline/ 2 x Tuning Stub	Cooper	Feed/6,73mm

TABLE 3.4: Optimized antenna dimensions

This antenna has the following geometric parameters: square patch's size 47mm, length of the tuning stub on the feed line 14mm, and its width 1.14mm., U-shaped aperture with long arm length of 19.20mm, short arm length 8.28mm and both with 1.14mm width. The -10dB impedance bandwidth was 3.77% and now the expected dual linear polarization was achieved, this can be explained by the fact that there are two perpendiculars feed lines each acting almost independently causing waves coupling in the each aperture orientation to each feed line; this is great advantage to our purpose of receive the greatest possible amount of RF radiation and recycle producing DC voltage. Dimensions of this last design are summarized in the table. A more detailed discussion of each antenna parameter and its plots are following discussed, final notes of each design are summarized in the table3.5.

Figures 3.7 (a) and (b) show the 2D view of the first and second antenna designed respectively, figures 3.8 (a) and (b) show the 3D view also for the first and second antenna designed in Agilent ADS. Figures 3.9(a) and (b) show 2D and 3D view respectively of the third designed antenna.

Figure 3.10 shows the simulated return loss of first two designed antennas. It can be seen that the impedance matchs at frequencies close to ISM band center at 2.45 GHz. In the first design(blue line), the -10dB impedance bandwidth is of 90MHz (3.77%), second design(red line) also has an -10dB impedance bandwidth of 90 MHz (3.77%). The low bandwidth of the microstrip antennas is the main disadvantage. Figures 3.11 and 3.12 show the simulated return loss S11 and S22 respectively of third optimized

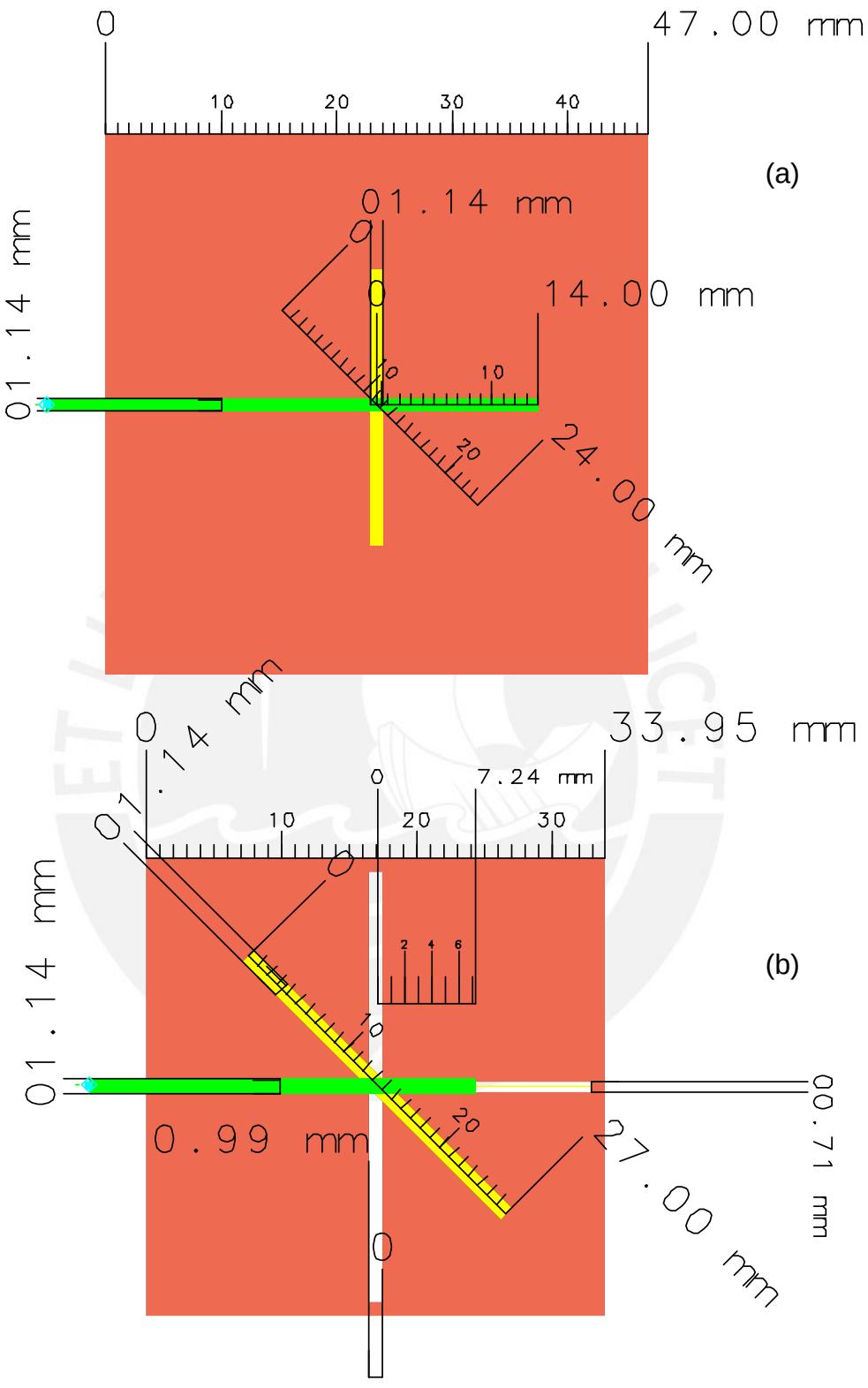

FIGURE 3.7: 2D views of the designed apeture-coupled square patch microstrip antennas with different dimensions, (Agilent ADS). Figure (a) shows the first design and (b) optimized design with a size reduction of 28%.

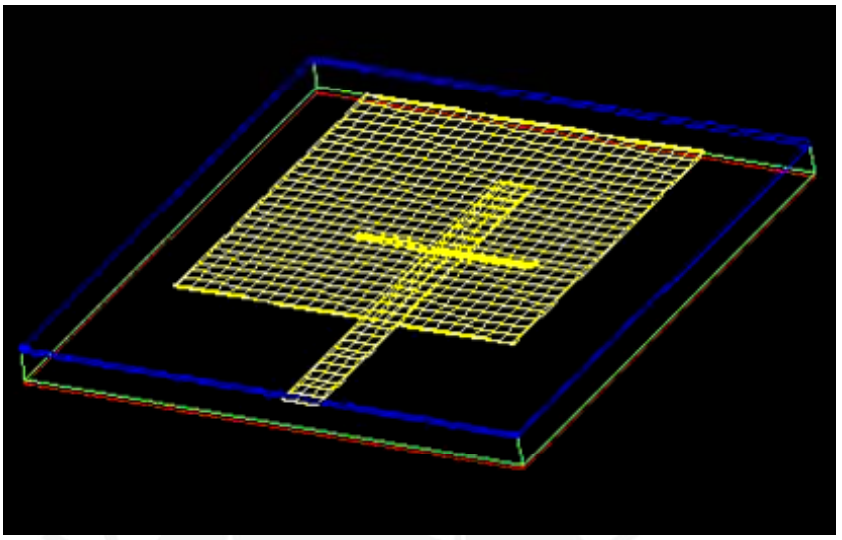

(a)

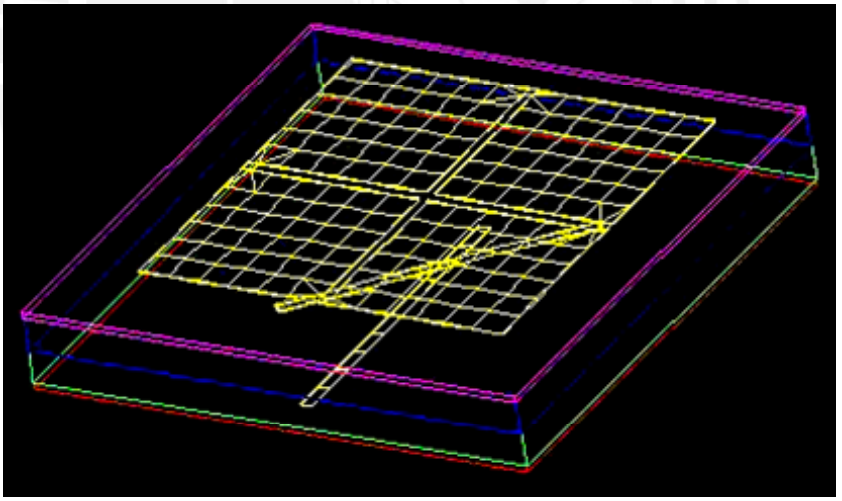

(b)

FIGURE 3.8: 3D views of the designed aperture-coupled square patch microstrip antennas with different dimensions, (Agilent ADS). Figure (a) shows the first design and (b) 28% optimized size antenna; in (b) it can be seen the effect of introduce a second foam, now the estructure is thicker

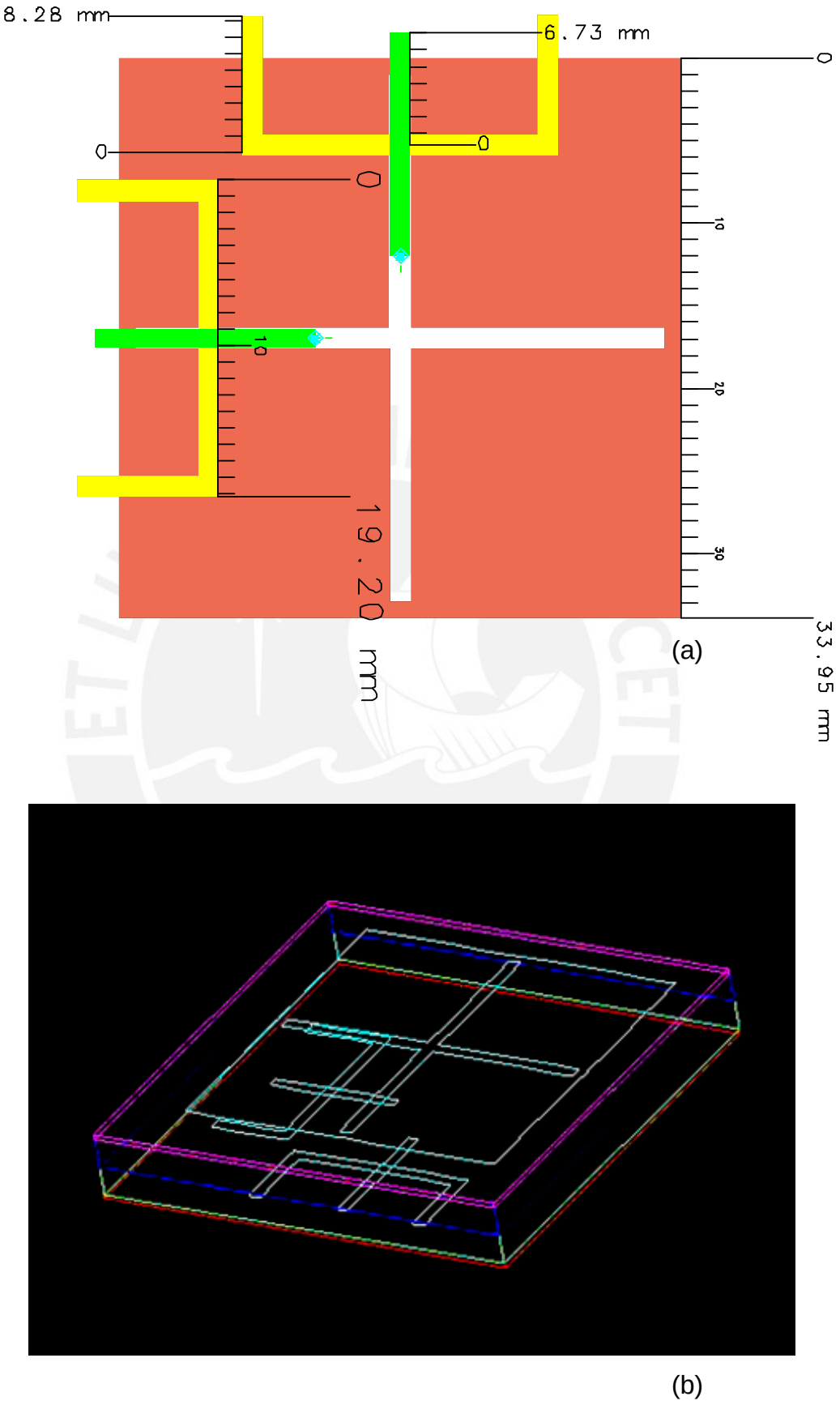

FIGURE 3.9: 2D and 3D views of the optimized design, dual feed aperture-coupled square patch microstrip antenna, (Agilent ADS). Figure (a) shows the dimensions and (b) 3D view.

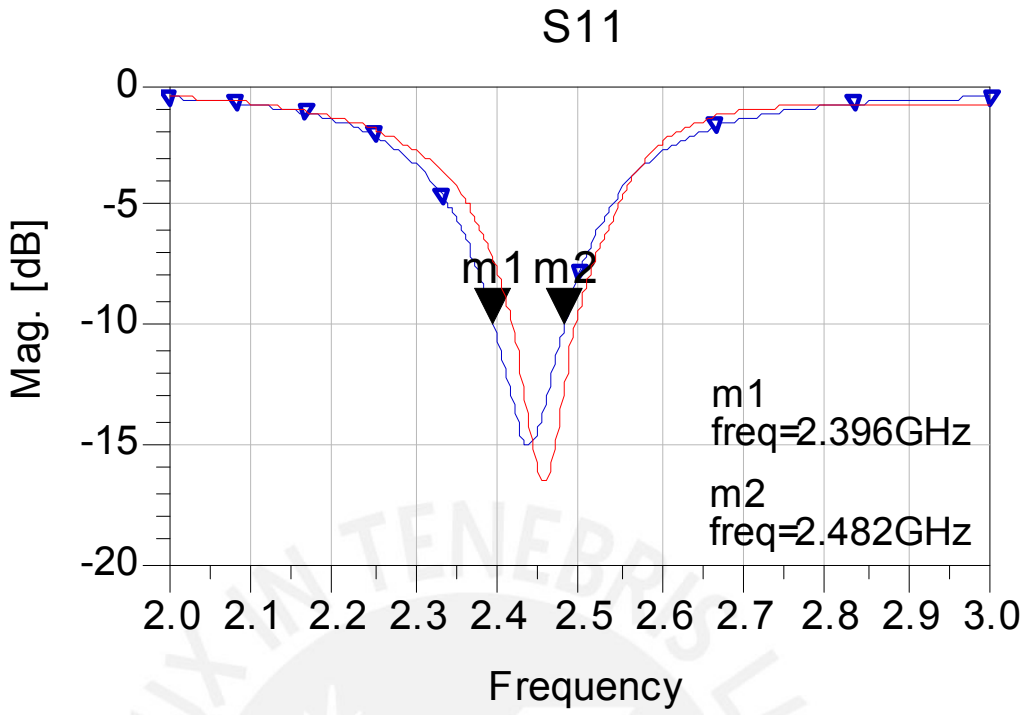

FIGURE 3.10: Simulated return loss of the first two designed antennas measured at the input port (Agilent ADS). First design in blue and second one in.

design antenna per each feed line. also It can be seen matching close to ISM band center at 2.45 GHz. for each one .The -10dB impedance bandwidth for both are 75MHz (3.07%). There is a few decreasing in bandwidth respect to second design per feed line, this is because the new design inserts new coupling elements damaging slightly the matching, but it is negligible as now antenna can receive a double RF radiation, now we duplicated the polarization bandwidth.

Figure 3.13 shows the impedance locus of the antennas, these are as typical described in section 3.1.5, where the higher frequency loop is due to the coupling of the patch and the slot. Markers 1 and 2, show the impedances which define the -10dB impedance bandwidth in figure 3.10, now also the blue line is for the first design and red line for the second. It can be seen that the frequency loop is larger and further from the center of the Smith chart, which is to be expected due to smaller bandwidth achieved; for achieve a larger bandwidth, must have a loop more concentrated at the center of the Smith chart. Figures 3.14 and 3.15 show also the impedance locus per each input port or feed line of the optimized dual feed line antenna these are presented in the same order of the return loss plots; these have the same loop's shape because the identical geometry of each feed line and aperture coupling.

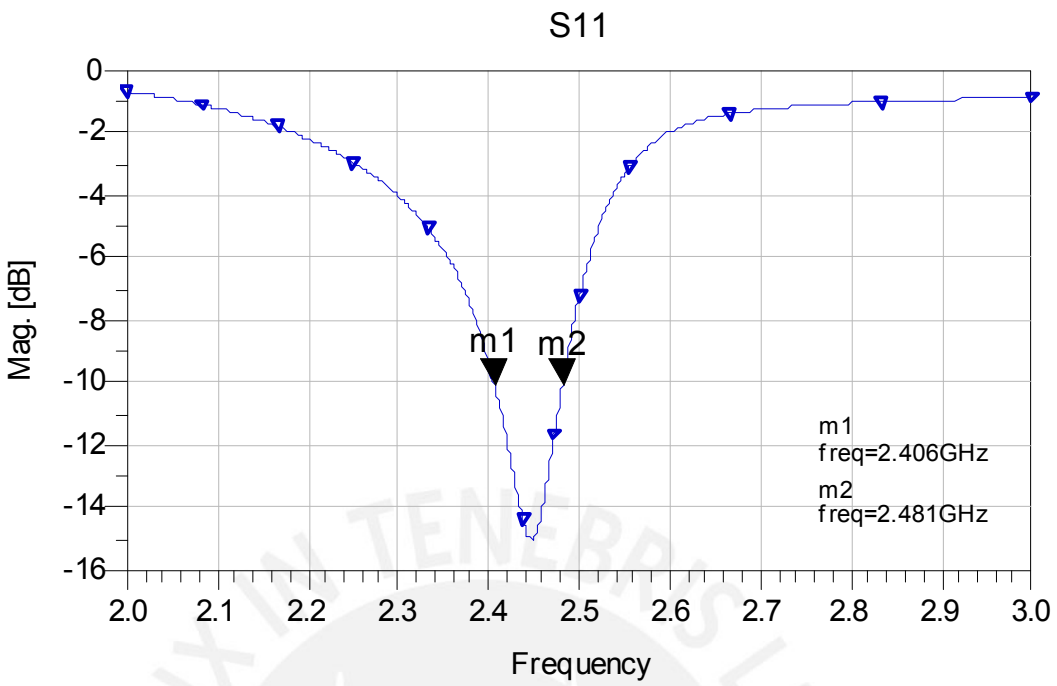

FIGURE 3.11: Simulated return loss of port 1 or first feed line in the dual feed line optimized size and polarization bandwidth antenna's design (Agilent ADS).

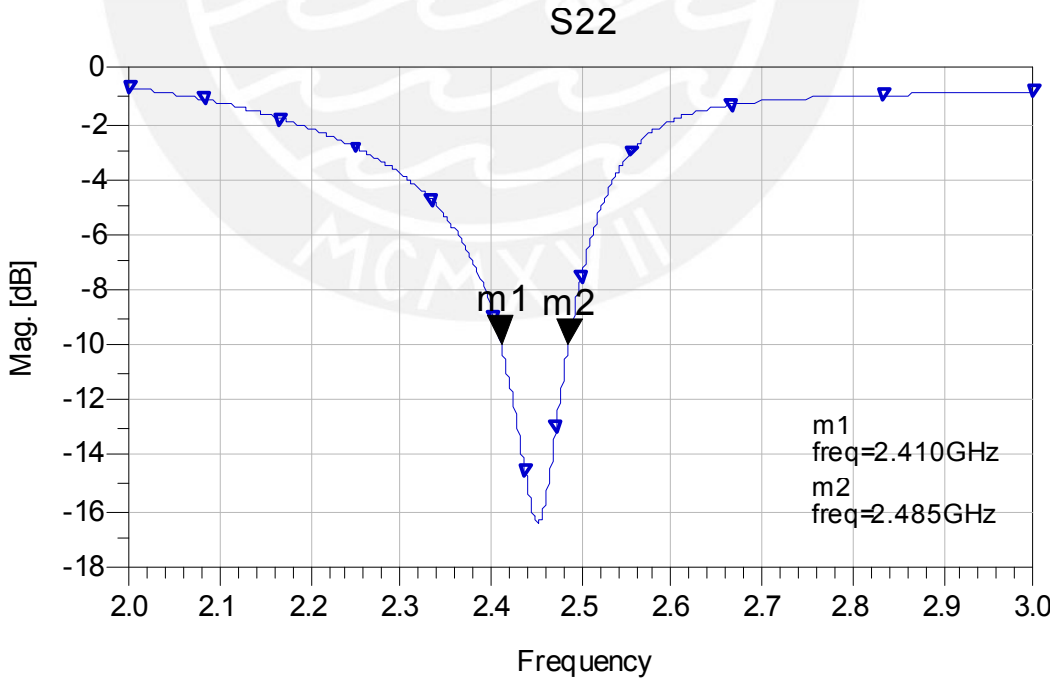

FIGURE 3.12: Simulated return loss of port 2 in the dual feed line optimized size and polarization bandwidth antenna's design (Agilent ADS).

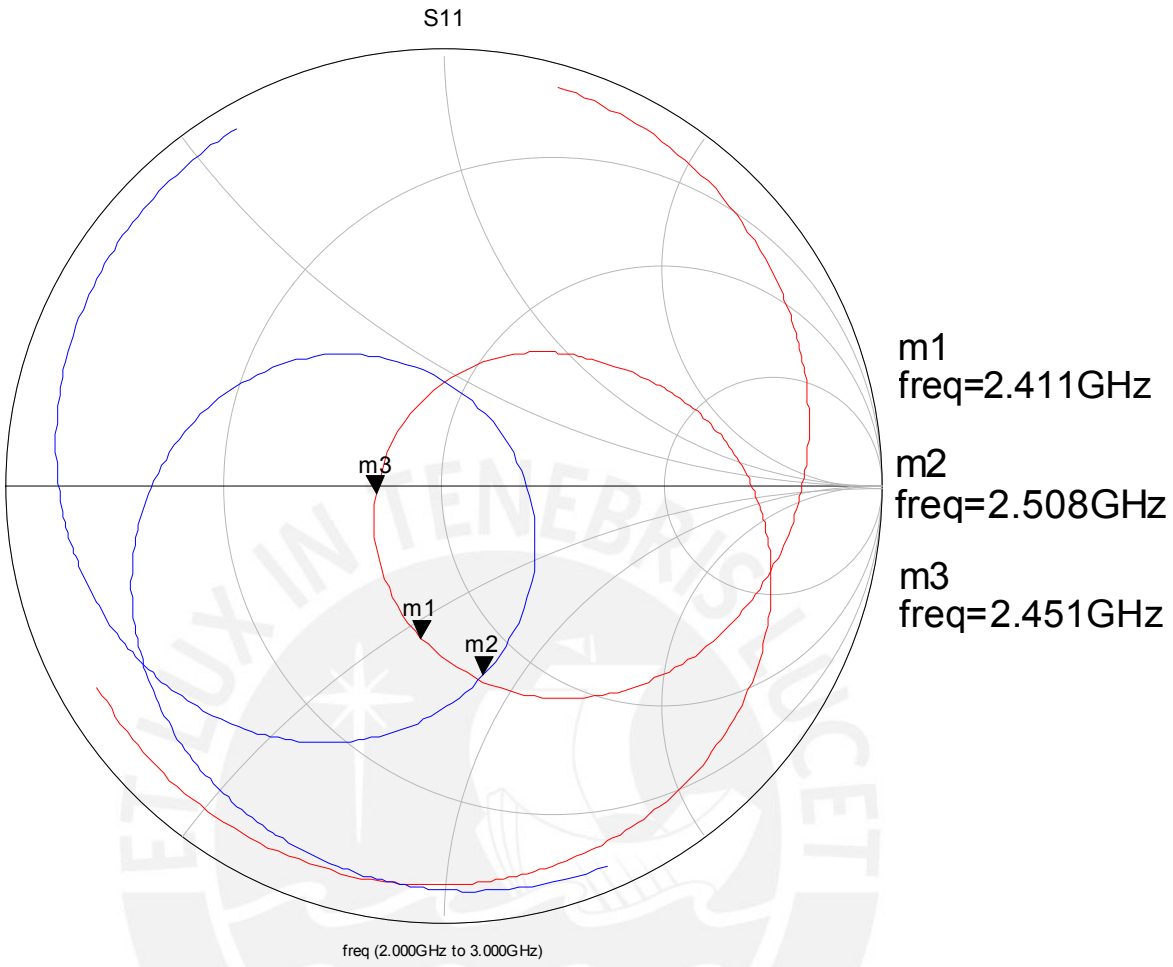

FIGURE 3.13: Simulated impedance locus of two antenna designed; blue line for the first design and red line for the second one (Agilent ADS).

Figures 3.16 (a) and (b) show the E ($\phi = 0°$) and H($\phi = 90°$) fields respectively, and its components theta and phi for the first antenna designed, it can be seen that the electric field vector has only E_{theta} component in the broadside direction, this means that a linear polarization is expected. Figure 3.17 (a) (b) also shows the E ($\phi = 0°$) and H($\phi = 90°$) fields respectively for the second antenna, now the electric field vector has equals its two components theta and phi, this means that there could be a rotated linear, circular or eliptical polarization depending of the phase between components, this will be determined with the polarization plots(figure 3.25).

Figure 3.18 shows the E ($\phi = 0°$) and H($\phi = 90°$) planes respectively and its components theta and phi for the last optimum antena's design for each port 1 and 2 separately in the top and bottom respectively. Figures 3.18 (a) and (b) at top, show the simulated

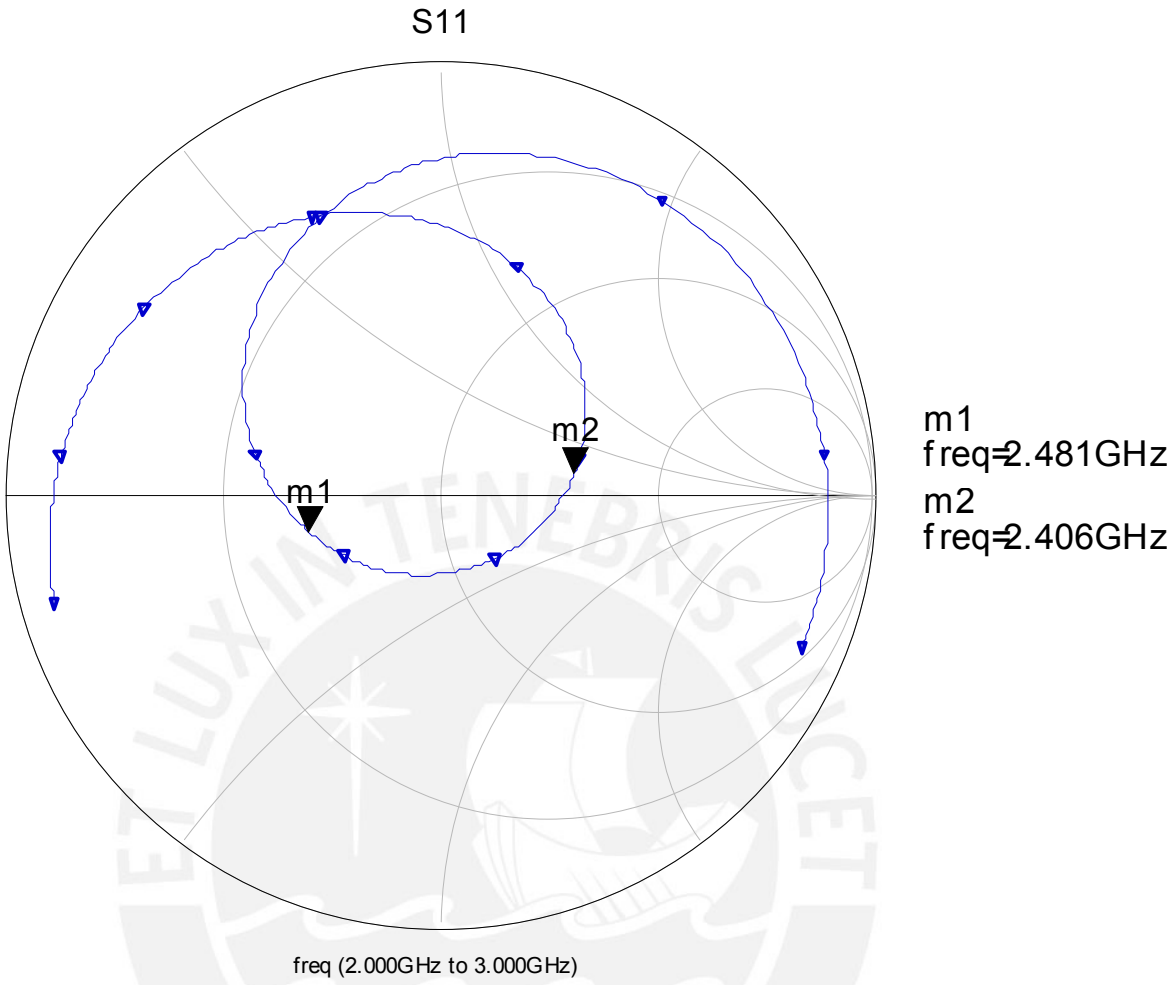

FIGURE 3.14: Simulated impedance locus of first port in the dual feed optimized size and polarization bandwidth antenna's design (Agilent ADS).

fields for the first port, feeding only this while the second is connected to a 50Ω load, in these top figures can be seen that there is only a predominant E_{theta} component in the broadside direction, as we expected; a linear polarization; figures 3.18 (c) and (d) at bottom, with the same idea show the fields for the second port also with a 50Ω load in the first one, these top figures show also that there is only a predominant component E_{phi} in its broadside direction, as we expected; this is also a linear polarization. As we can see each port has a different predominant component from the E field, this can be explained by the fact that the ports 1 and 2 are mutually perpendicular, each component will produce also a mutually perpendicular linear polarization, this will be shown in its polarization plots (figure 3.26).

Figure 3.19 (a) and (b) show the 2D radiation patterns for the first and second antenna

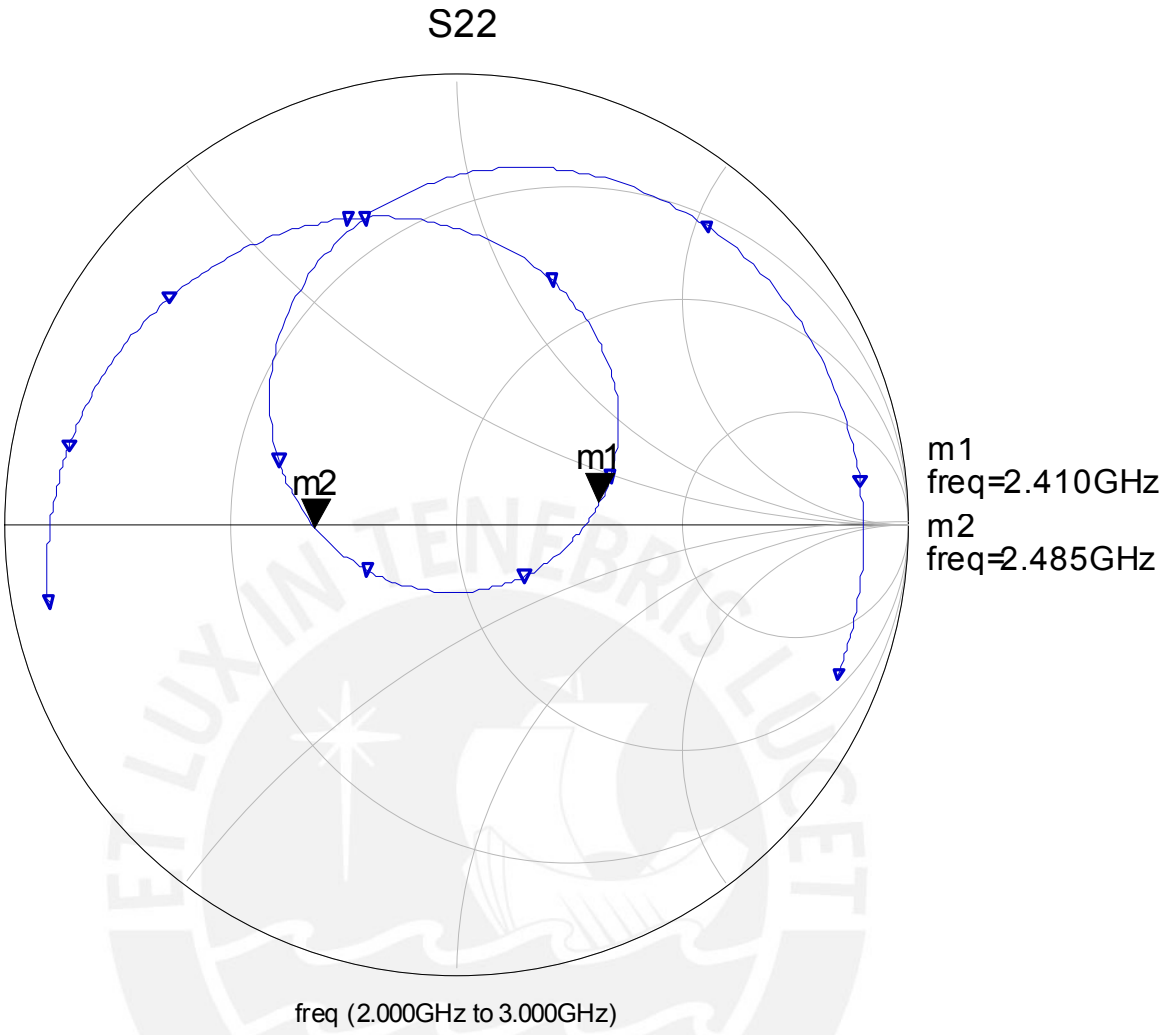

FIGURE 3.15: Simulated impedance locus of the second port in the dual feed optimized size and polarization bandwidth antenna's design (Agilent ADS).

respectively, remember that first antenna is slightly larger. In top figure 3.19 (a) can be seen that in broadside direction, 4.63 dB of gain and 4.84 dB of directivity is achieved. Other characteristics of this pattern are: half-power beam width at -3dB (HPBW) of about 90°, beam width between first nulls (FNBW) of 180° and Front to Back Ratio (FBR) of 9.6dB. Also In bottom figure 3.19 (b) can be seen that in broadside direction, 7.10 dB of gain and 7.91 dB of directivity is achieved for the second antenna; also the half-power beam width at -3dB (HPBW) of around 76°, beam width between first nulls (FNBW) of 180° and Front to Back Ratio (FBR) of 17dB. The increase in gain is due to the increase of aperture's length related with the patch's size.

Figure 3.20 (a) and (b) show the contribution for the 2D radiation pattern from ports 1 in (a) and 2 in (b) separately for the optimized antenna's design.In top figure 3.20

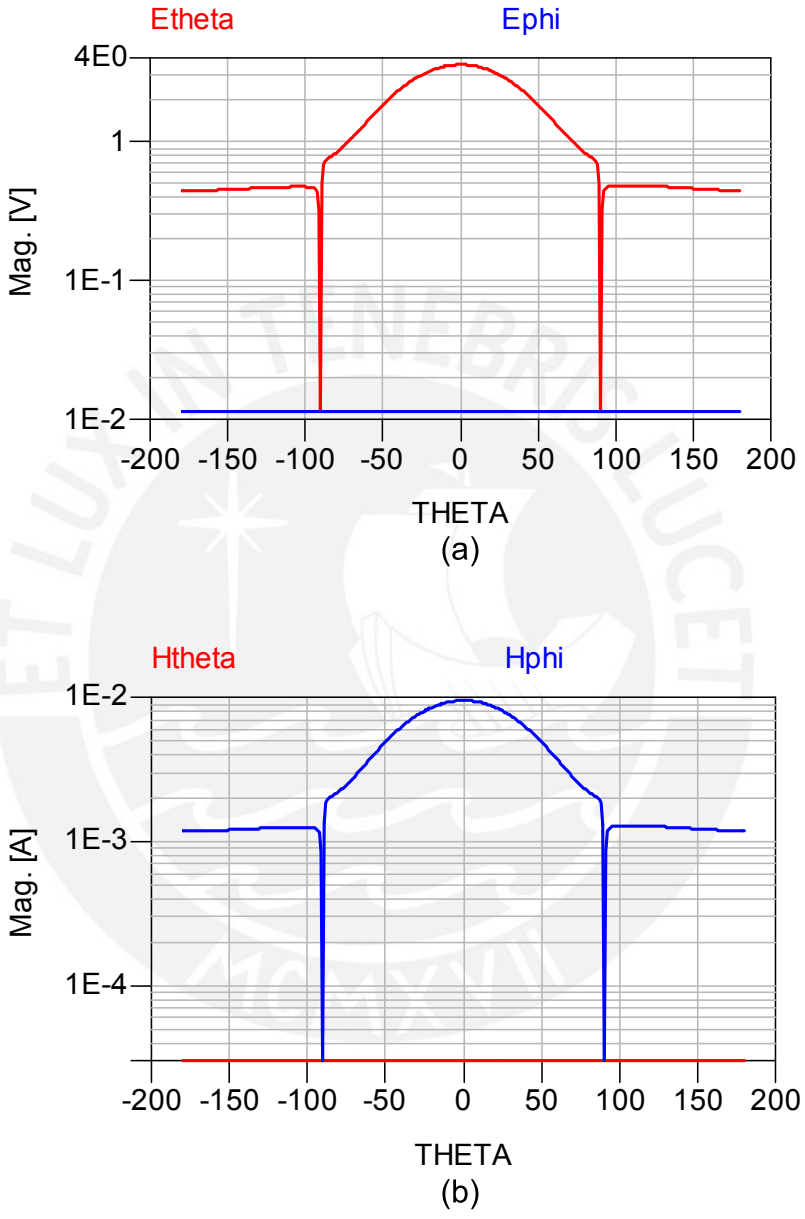

FIGURE 3.16: Absolute fields E at top (a) and H at bottoma (b) for the first antenna designed. E field with only one component; a linear polarization is expected (Agilent ADS).

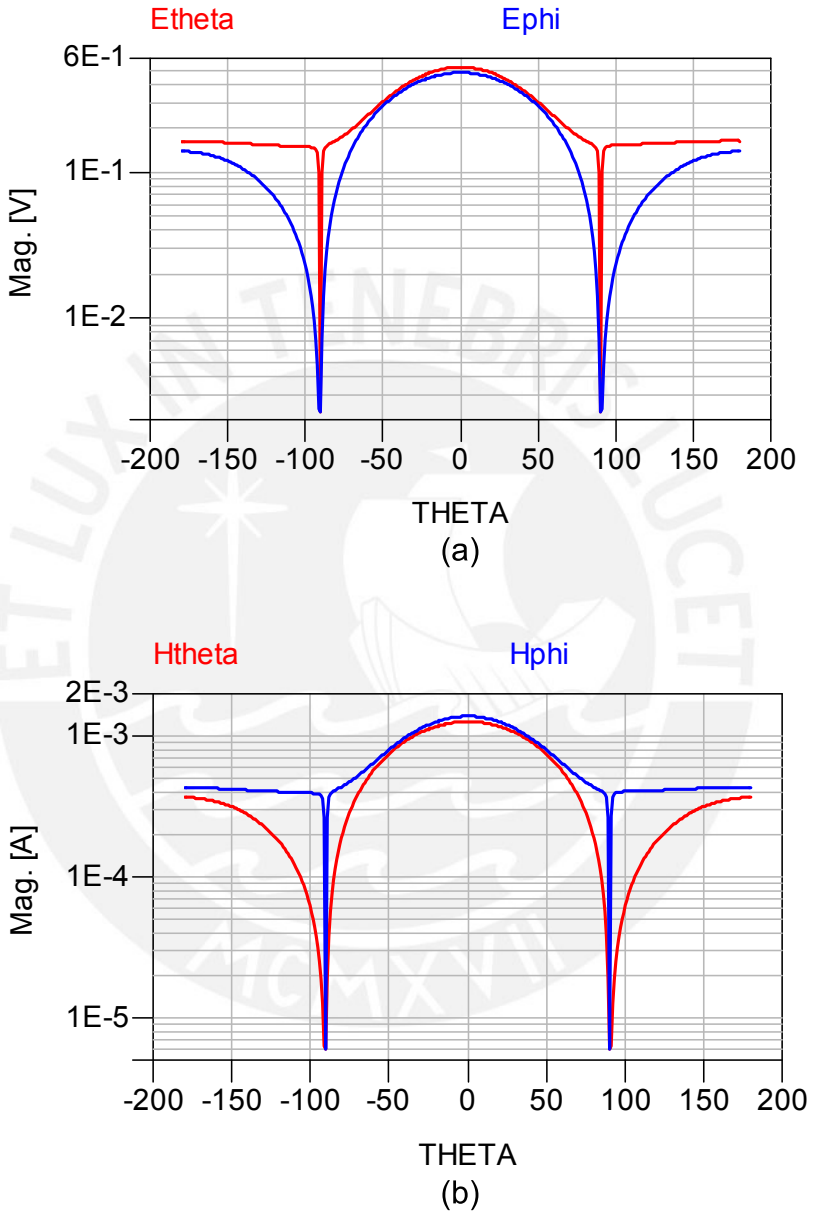

FIGURE 3.17: Absolute fields E at top (a) and H at bottom (b) for the second antenna designed. E field with its two components (Agilent ADS).

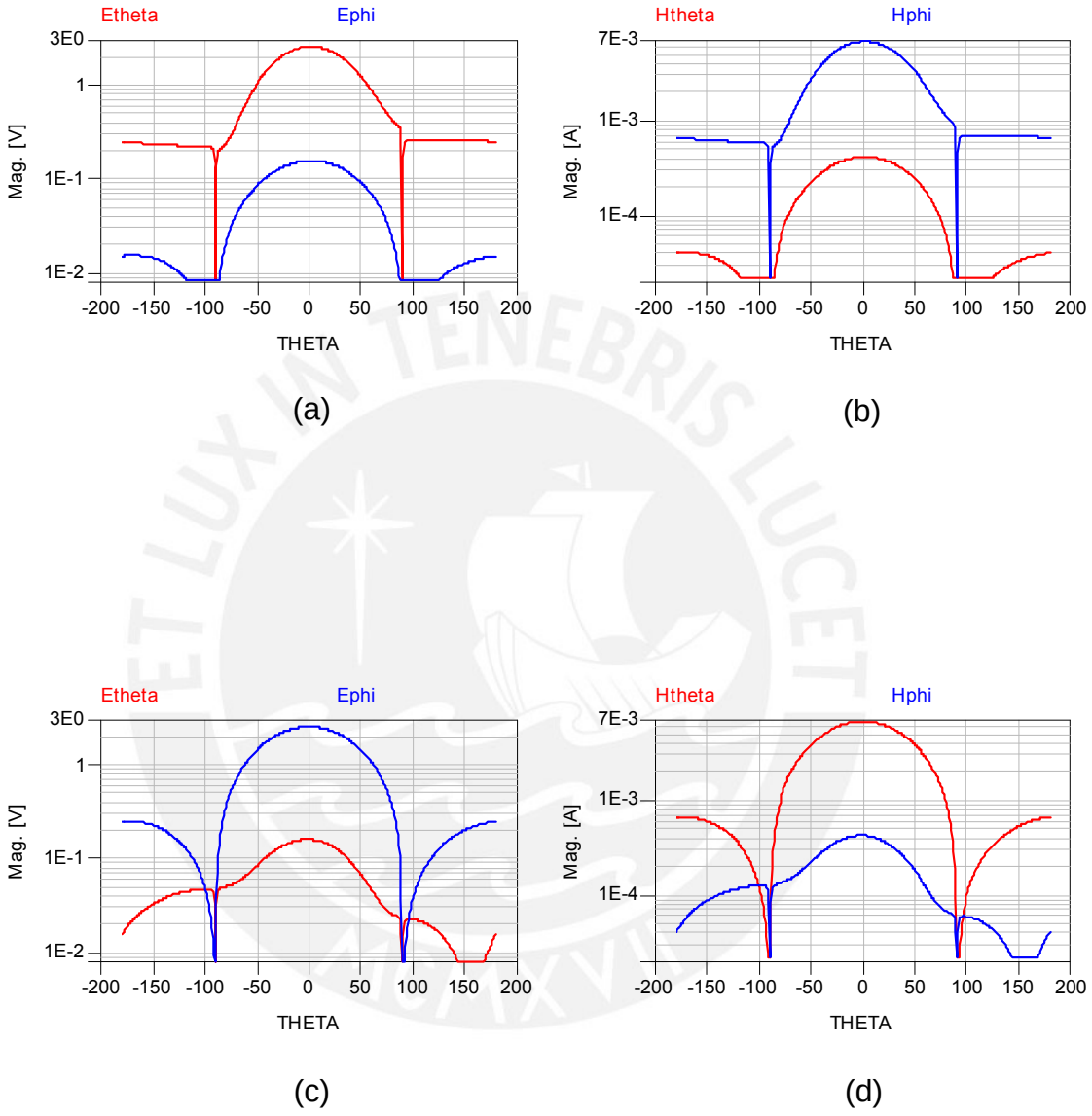

FIGURE 3.18: Absolute fields E and H per each port in the dual feed optimized size and polarization bandwidth antenna's design (Agilent ADS); top figures (a) and (b) from the first port while the second connected to 50Ω load, bottom figures (c) and (d) from the second port while first one is also connected to 50Ω. Plots show only one predominant E component per port.

(a) can be seen that at broadside a gain of 8.75dB and 8.91db of directivity is achieved. Other characteristics are: half-power beam width at -3dB (HPBW) of around 70°, beam width between first nulls (FNBW) of 180° and Front to Back Ratio (FBR) of 17.75dB. Also In bottom figure 3.20 (b) can be seen that at broadside a gain of 8.75dB is achieved for the second port; also the half-power beam width at -3dB (HPBW) of around 70°, beam width between first nulls (FNBW) of 180° and Front to Back Ratio (FBR) of 17.75dB. Now is achieved a gain properly as the apertures coupled are perpendicular to theirs feed lines like the first antenna designed. Figures 3.21,3.22 and 3.23show views by Agilent ADS of the 3D radiation pattern for the first, second and third antenna designed respectively.

Figure 3.24 shows the behavior of the electric field at co-polar in red line (same polarization as the excitation) and cross polar in blue line (turn it 90° referred to excitation polarization) in magnitud(a) and phase (b) of the first antenna designed. In figure 3.24 (a) can be seen that there is a matching only in co-polar orientation,the cross polar is to attenuated, then; there is a linar polarization, as we expected; when the aperture coupled slot orientation coincides with the excitation polarization, figure 3.24 (b) no much information give us because there is only one component. Figure 3.25 shows also the behavior of the electric field at co-polar in red line and cross polar in blue line, in magnitud(a) and phase (b) of the second antenna designed. It can be seen that there is matching in co and cross-polar orientation and with the same magnitude; figure 3.25 (b) shows that both components co and cross-polar are in phase,then; there is a linar polarization as we expected; but now the two equal matching polarization levels in co and cross-polar can only mean that it is a rotated linear polarization with a symmetrical rotated angle, then this angle should be 45° and is exactly the same rotated angle of the aperture coupled slot. Finally we can say that the orientation of the polarization is defined by the aperture orientation.

Figure 3.26 shows the behavior of the electric field at co-polar in red and cross polar in blue, in magnitud (left) and phase (right) of the optimized size and polarization bandwidth antenna designed per port: port 1 at top and port 2 at bottom. In figures 3.26 (a) and (b) can be seen that there is a matching only in co-polar orientation,then; there is a linar polarization, as we expected; when the large arm of U-shaped aperture coupled slot orientation coincides with the excitation polarization, in phase no much information give us because there is only one component. Figure 3.26 (c) and (d) shows that there is matching only in cross-polar orientation, this also means that there is a linar polarization as we expected from the other port, in conclusion now is achieved a two ortogonal linear polarizations where each orientation depends from the large arm of the U-shaped aperture coupled slot from each port.

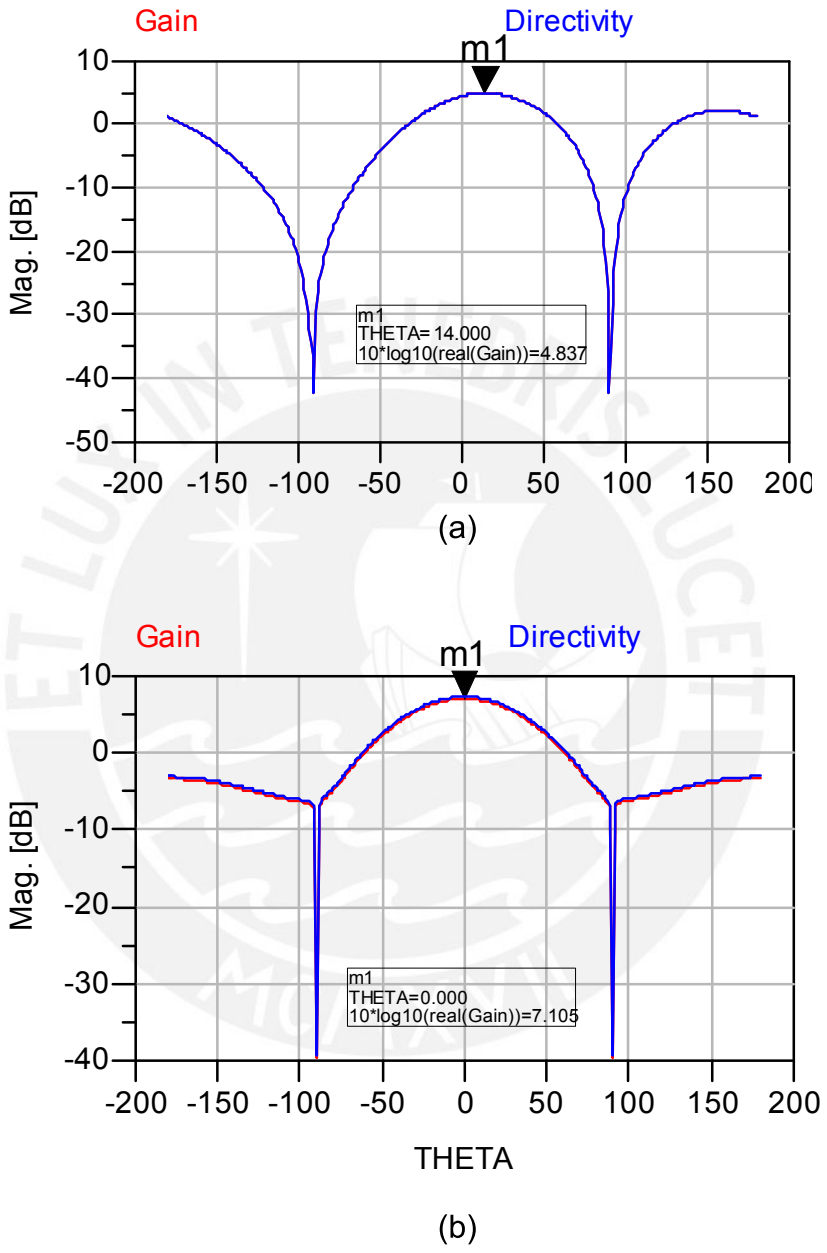

FIGURE 3.19: Simulated 2D radiation pattern, gain and directivity for both antennas designed, for largest antenna at top (a) and optimized size antenna at bottom (b) (Agilent ADS).

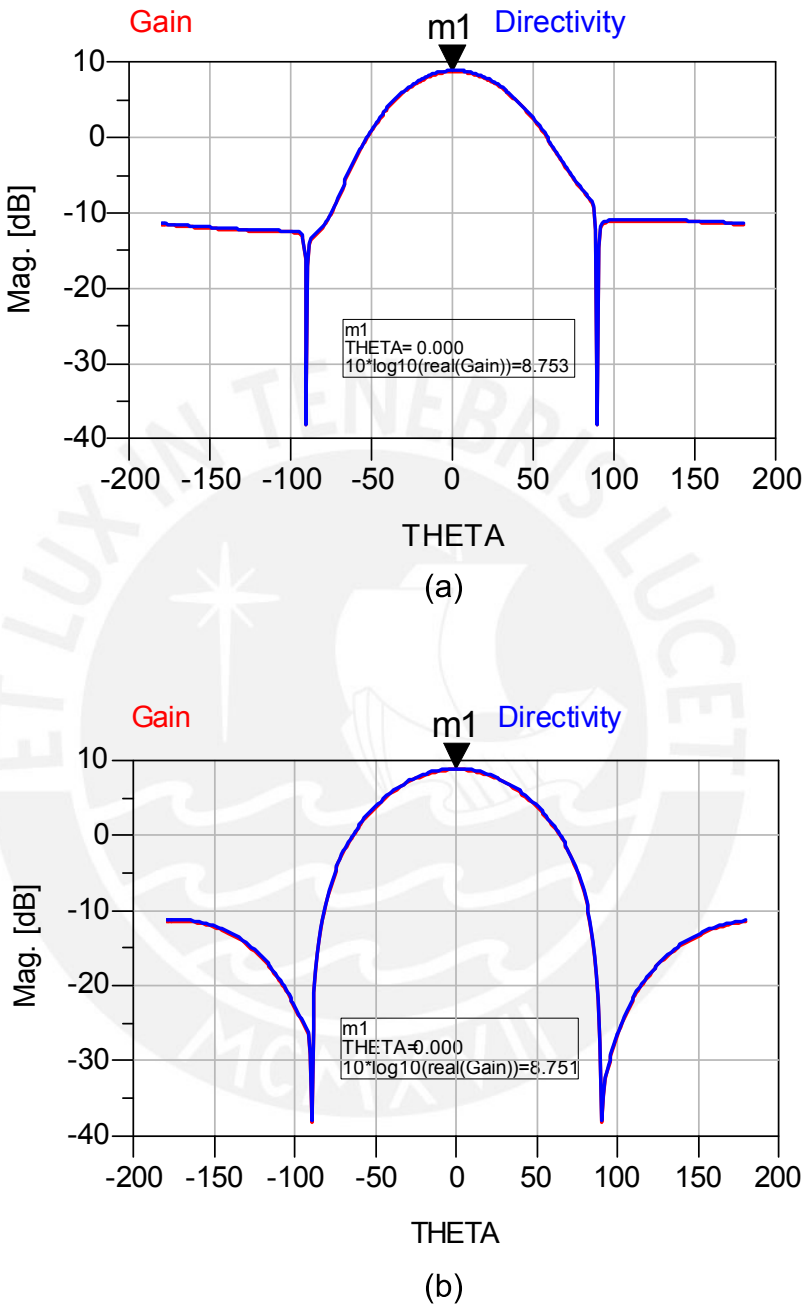

FIGURE 3.20: Simulated 2D radiation pattern gain and directivity for optimized size and polarization bandwidth antenna designed. Contributions per port, port 1 (a) at top and port 2 (b) at bottom (Agilent ADS).

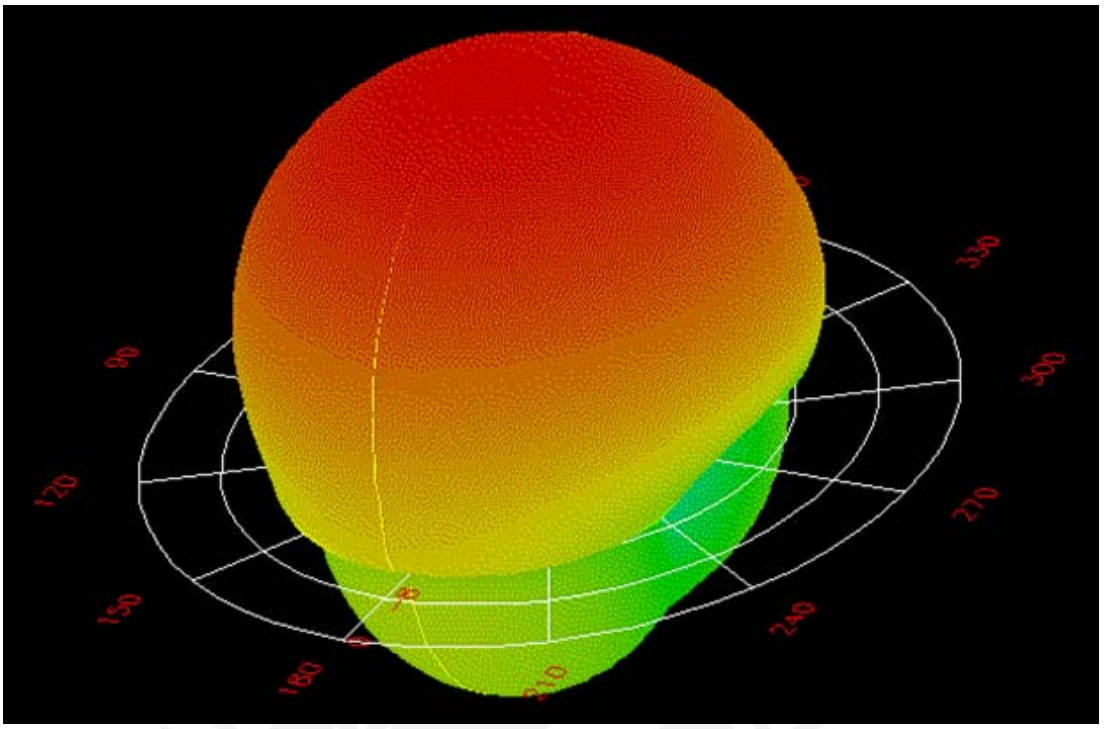

(a)

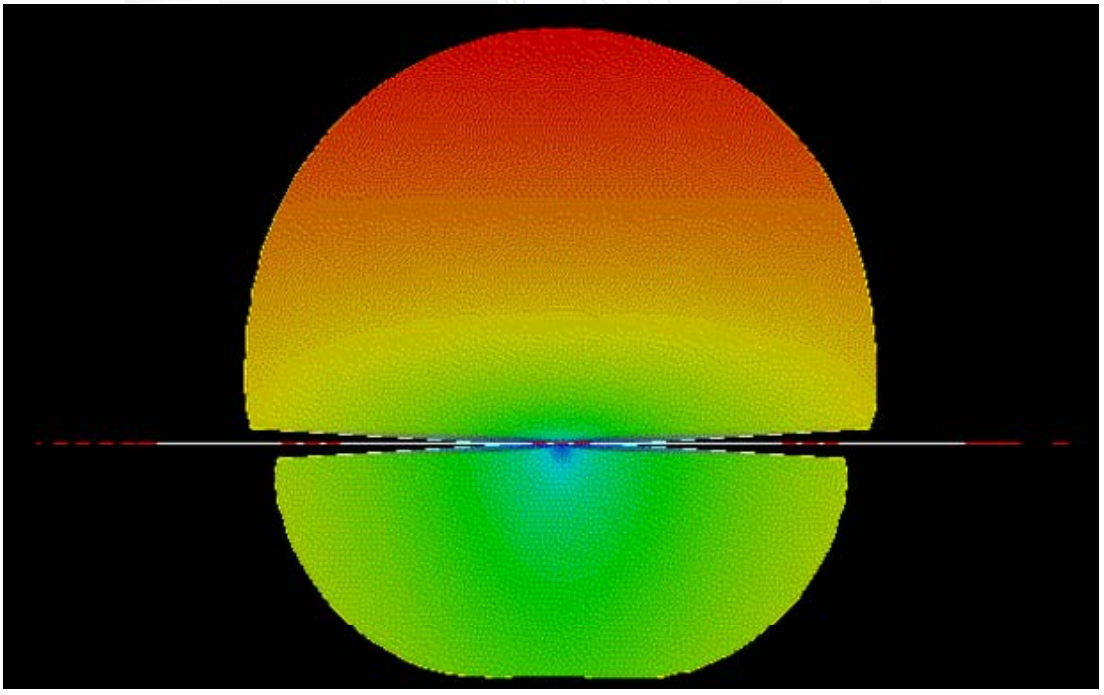

(b)

FIGURE 3.21: Simulated 3D radiation pattern of largest antenna (Agilent ADS). Front angle view (a) and side view (b).

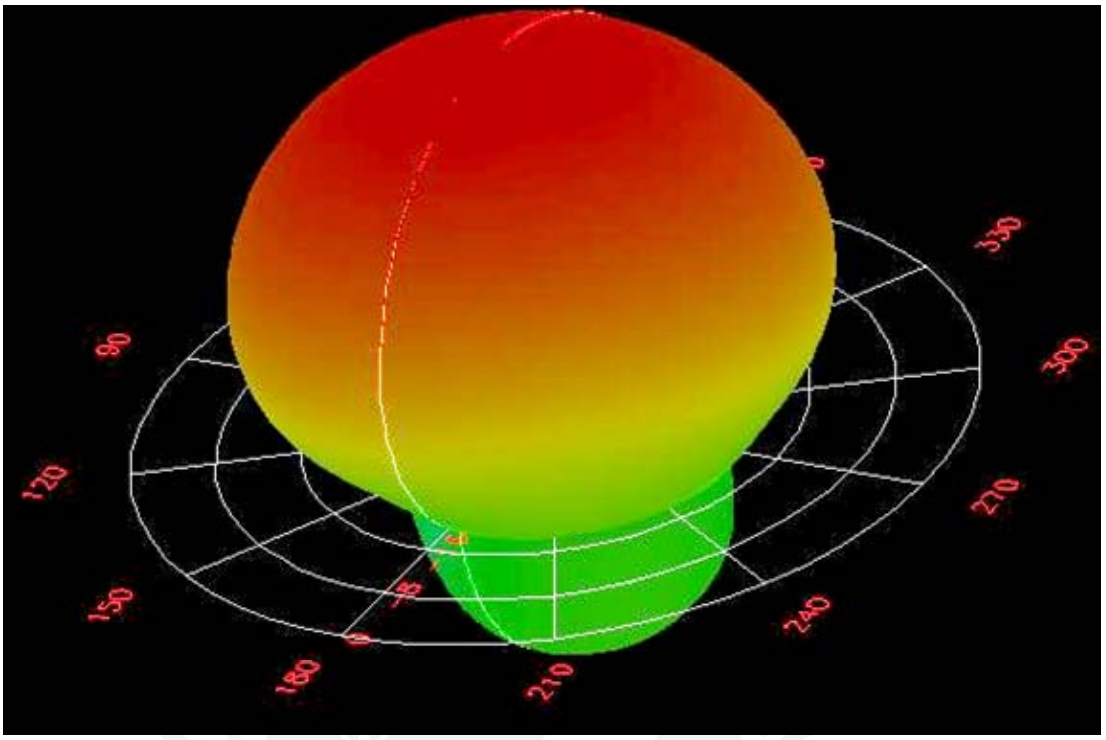

(a)

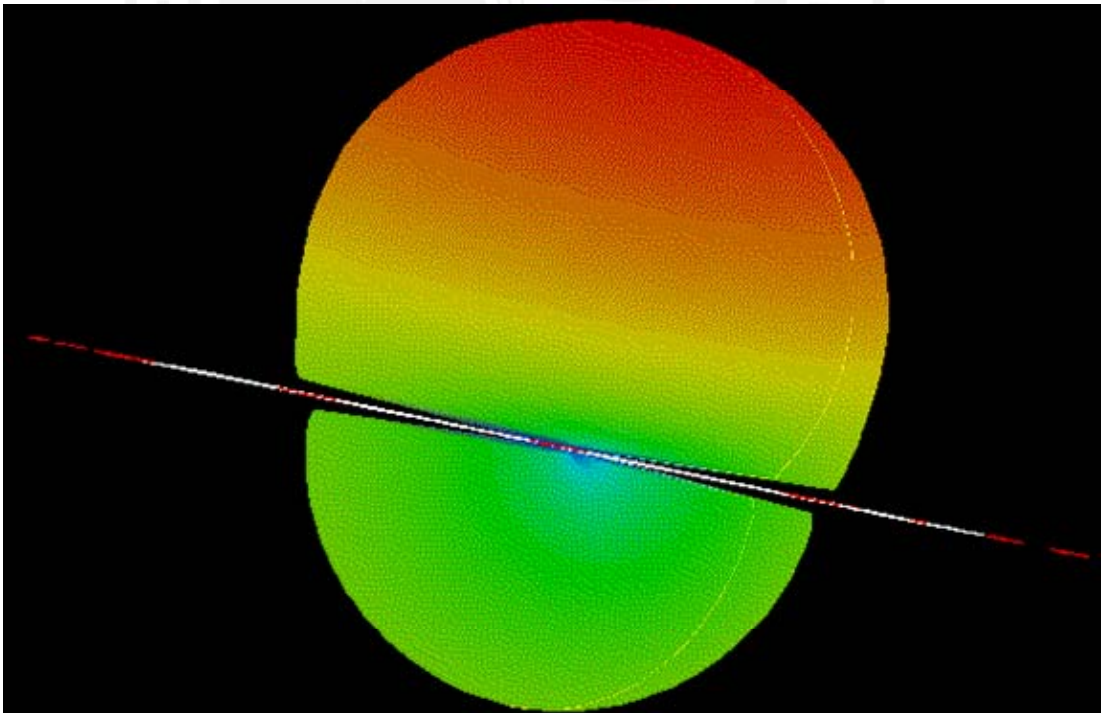

(b)

FIGURE 3.22: Simulated 3D radiation pattern of optimized size antenna's design (Agilent ADS). Front angle view (a) and side view (b).

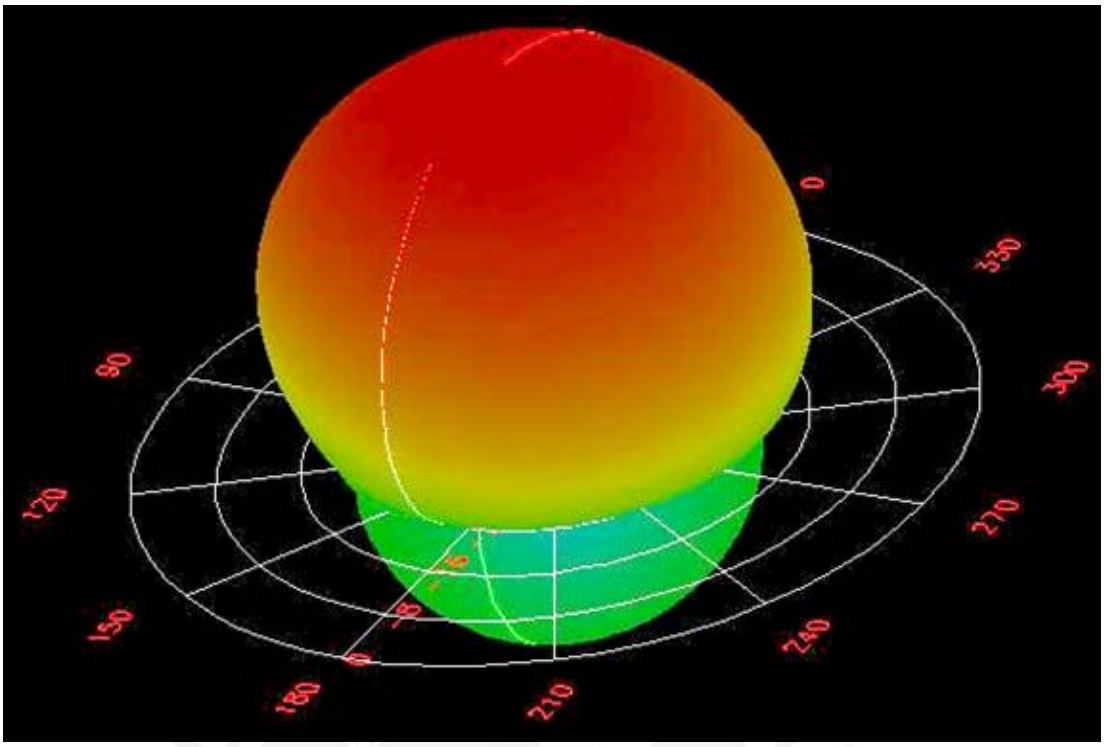

(a)

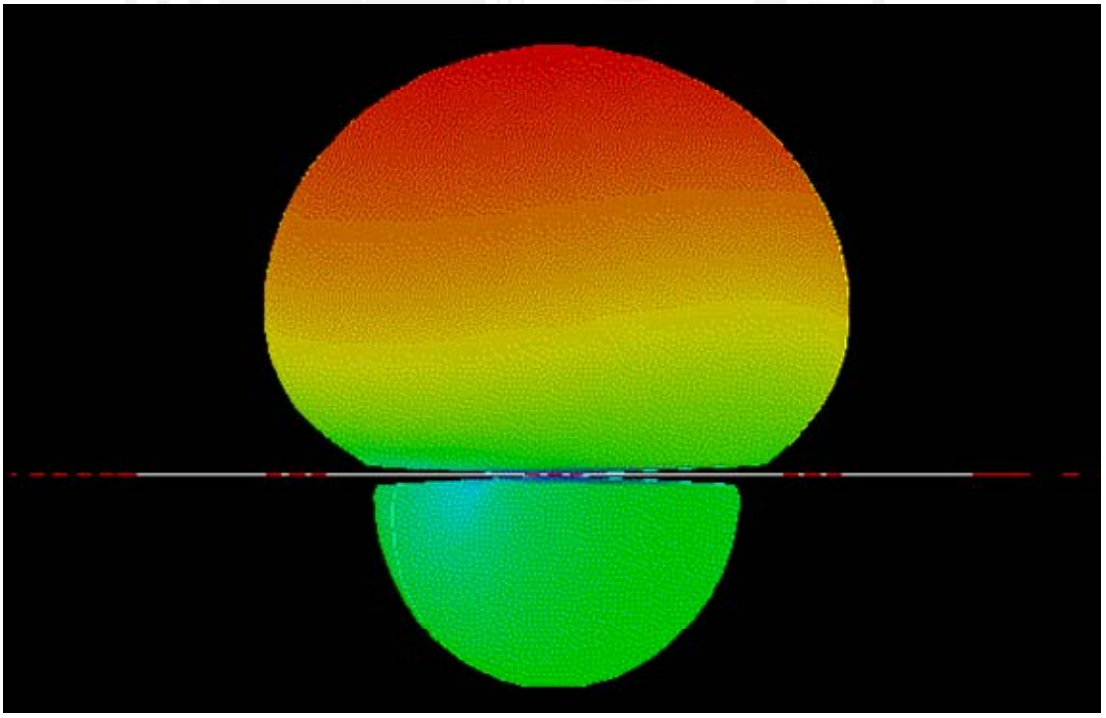

(b)

FIGURE 3.23: Simulated 3D radiation pattern of optimized size and polarization bandwidth antenna's design (Agilent ADS). Front angle view (a) and side view (b).

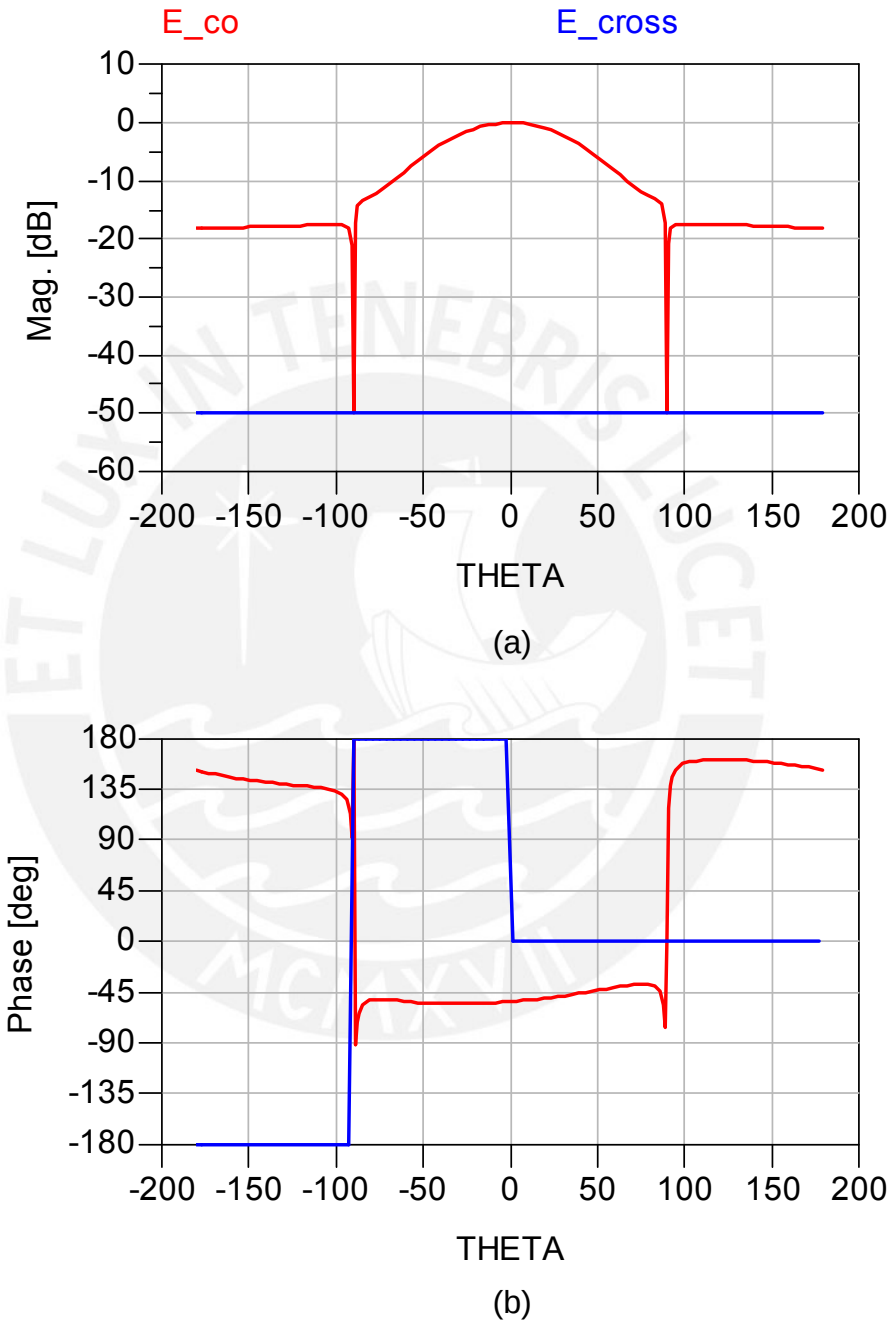

FIGURE 3.24: Simulated polarization in magnitude (a) top and phase (b) bottom, for the largest antenna (Agilent ADS).

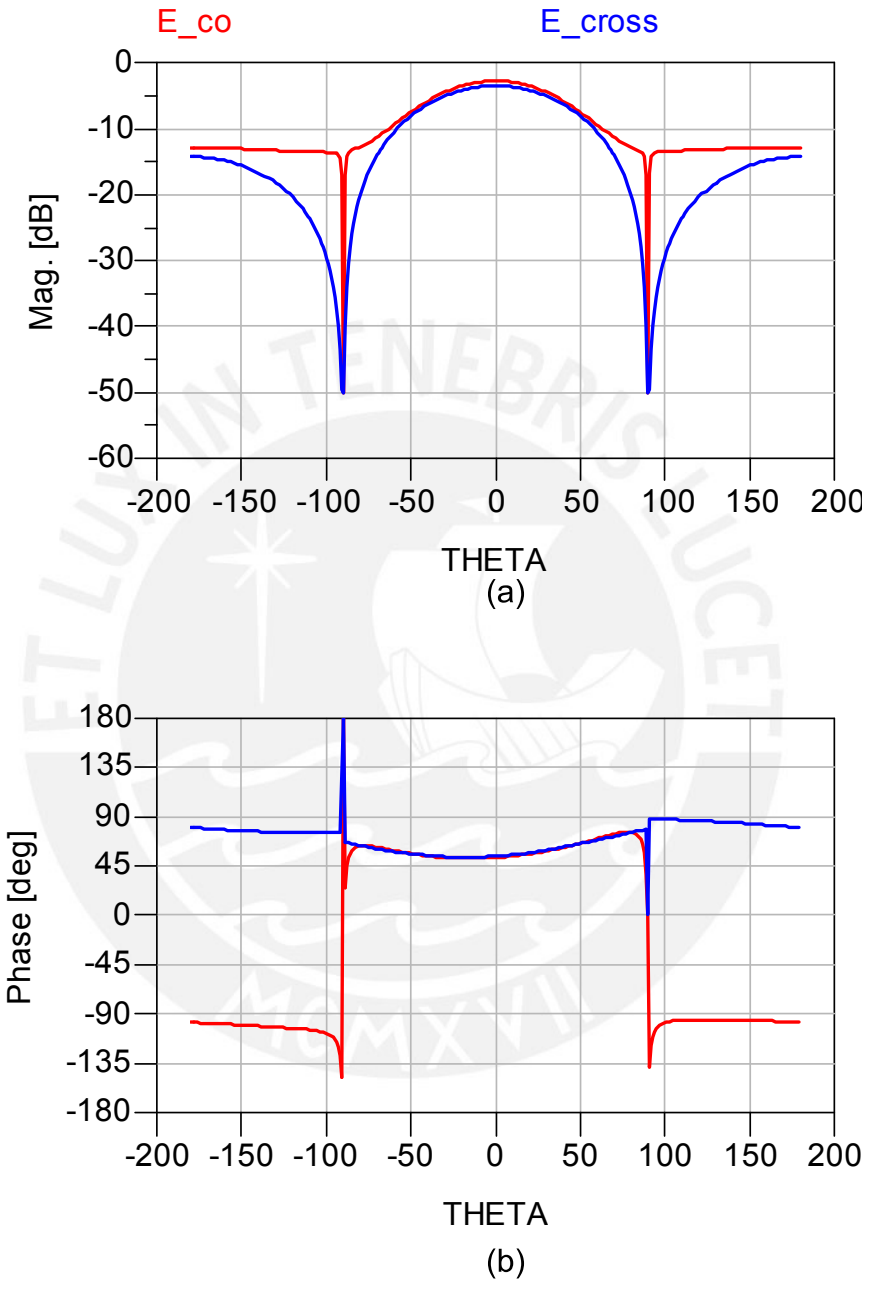

FIGURE 3.25: Simulated polarization in magnitude in the top(a) and phase in the bottom (b), for the optimized size antenna (Agilent ADS).

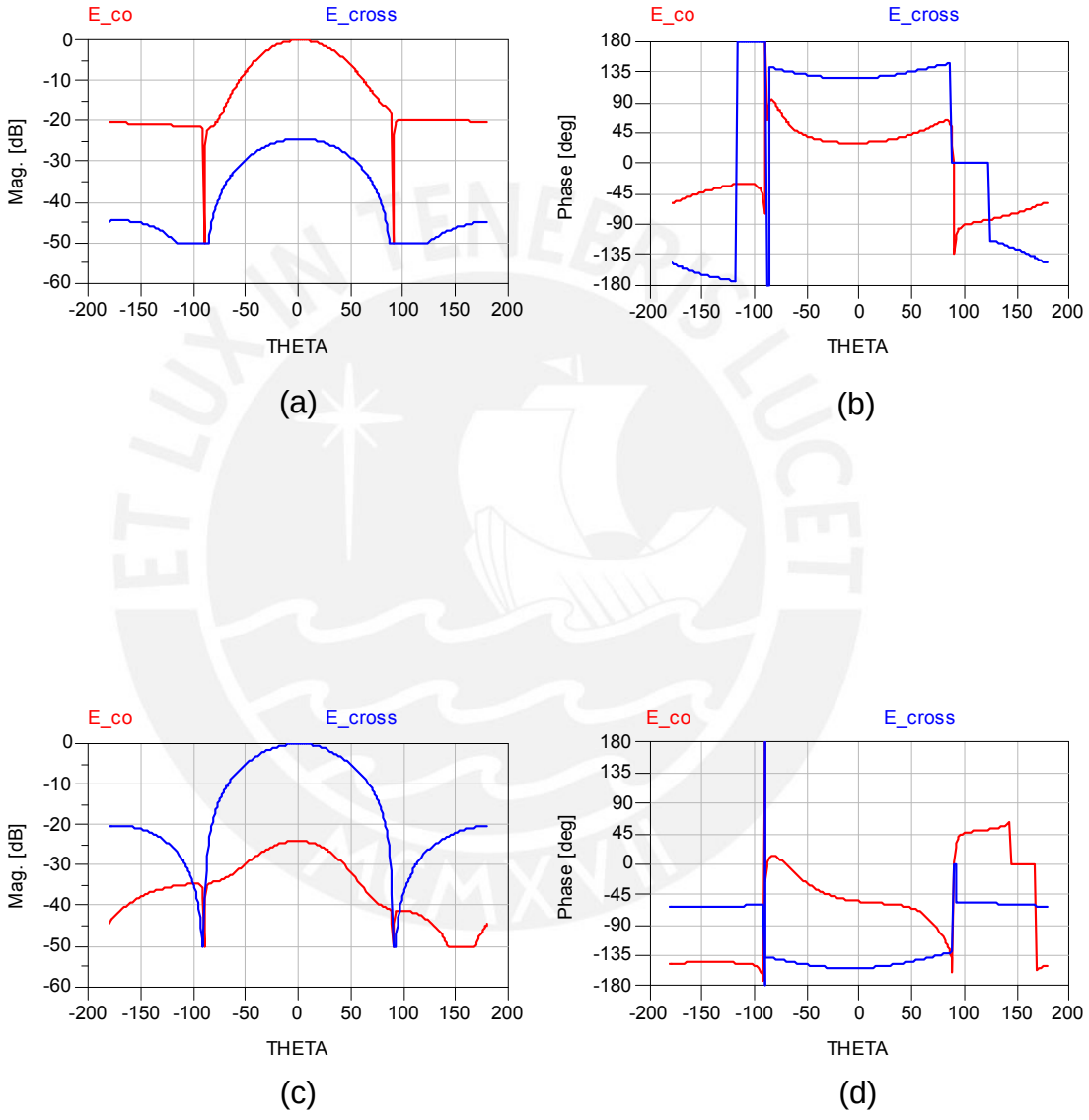

FIGURE 3.26: Simulated polarization in magnitude on the left and phase on the right per port; port 1 at top and port 2 at bottom (Agilent ADS). A dual linear polarization antenna is achieved.

Antenna Parameter	Design 1	Design 2	Design 3
Square patch size	47 x 47mm	33.95 x 33.95mm	33.95 x 33.95mm
Ports	Single feed line	Single feed line	Dual feed line
Aperture shape	Linear	Linear rotated	2 x U-shaped
Aperture inclination	Straight	45° rotated	2 x Straight
Polarization	Linear straight	Linear Rotated	2 x Linear straight
Bandwidth	3.77%	3.77%	3.07%
Gain	4.63dB	7.10dB	8.75dB
Directivity	4.84dB	7.91dB	8.91dB
Effective area	$0.004m^2$	$0.009m^2$	$0.009m^2$
HPBW	90°	76°	70°
FBR	9.6dB	17dB	17.75dB
Description	Basic Design	Optimized size design	Optimized Size and Bandwidth

TABLE 3.5: Parameters resume of three designed antennas

3.3 Rectifier Design

A basic rectifier circuit and behavior was introduced in section 3.1.7, it is called Villard voltage doubler and its schema is shows in figure 3.4.As antenna was chosen the last design that has the optimum size and polarization bandwidth with dual feed lines (2 ports), is necessary have two rectifier circuits, one per port and in the end these will joint its DC outputs in one load. A decrease in performance will be expected due to the coupling effects. To achieve this first we start designed one basic rectifier and then the process will be iterative. As we said above, the behavior of the rectifier depends of the diode's characteristics. Now we going to do an analysis of these, so we can choose

an useful diode for our purpose; as first condition we now that the most suitable to implementing the circuit is Schottky diode due to its high forward bias current for a given voltage (see section 3.1.7).

Limiting Factors for the Diode Conversion Efficiency

The input power has a strong effect on RF to DC conversion efficiency, which drops sharply once the RF voltage stays below the turn-on voltage of the diode. This is due to the exponential nature of the vi-characteristic of the diode. Another limiting factor is the maximum frequency the diode can work at. This is set by the transit time of the charge carriers, given by the dimensions of the pn-junction and the charge carrier mobility. Even though the transit time for the diodes used is about one order of magnitude lower than $\frac{1}{f}$ in the frequency range investigated, losses in the diode grow significantly with frequency.

3.3.1 The Choice of the Diode

When looking for a rectifying diode in the context of RF recycling, a diode with a high conversion efficiency, even for very small incident power levels is required. So is desired a good trade off between the junction potential V_j, the zero bias junction capacitance C_{j0}, the series resistance R_s, the saturation current I_S, and the sensitivity of the efficiency to mismatch. figure 3.27 taken from [39] shows efficiency versus various parameters,the figure gives the efficiency for $R_s = 11\Omega$, $V_j = 0.4V$, $C_{j0} = 0.1pF$, $R_L = 1k\Omega$, and $V_0 = 0.3V$ at a frequency of 4 GHz. where V_0 is the DC part of the voltage applied to the diode. One of the parameters R_s,V_j, and C_{j0} was varied, whereas all the others were kept constant.

Three different types of silicon Schottky diodes with parameters shown in table 3.6 were compared. They were chosen from a variety of available diodes based on past simulation results of referenced work. The SMS7630 has the highest conversion efficiency over the frequency range from 2 to 8 GHz. Figure 3.28 taken from [40] shows the simulated results, these suggested the choice of the Alpha Industries Skyworks SMS7630 over the SMS7621 and the M/ACom MA4E2054.

Packaging is another concern when choosing the right diode. Basically, the smallest package is the best choice because of diminished parasitic effects. But there was a limitation for the size: solder onto the antenna's back side may by more difficult.

Diodes measured had SC-79 (max 1.7mm x 0.9 mm), SOD-323 (max 2.7mm x 1.35mm) and SOT-23 (max 2.8mm x 2.6mm) packages. Because SOT-23 has a third unused metal connector, which can cause more unwanted effects than the rest of the package, this was

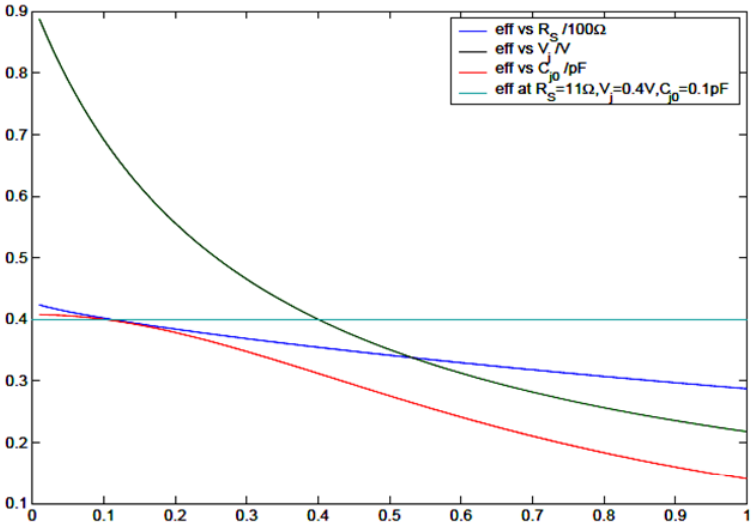

FIGURE 3.27: Efficiency of a diode vs. various parameters, one parameter is varied as all others are kept constant.

Parameter	SMS7630	SMS7621	MA4E2054
I_sA	$5 \cdot 10^{-6}$	$4 \cdot 10^{-8}$	$3 \cdot 10^{-8}$
$R_s\Omega$	20	12	11
N	1.05	1.05	1.05
TT seg	$1 \cdot 10^{-11}$	$1 \cdot 10^{-11}$	0
C_{j0} pF	0.14	0.10	0.10
V_j V	0.34	0.51	0.40
M	0.40	0.35	0.50
E_g eV	0.69	0.69	0.69
XTI	2	2	-
F_c	0.5	0.5	-
B_v V	2	3	5
I_{BV} A	$1 \cdot 10^{-4}$	$1 \cdot 10^{-5}$	$1 \cdot 10^{-5}$

TABLE 3.6: Diode parameters, as given in manufacturer's specifications

not used. results (figure 3.28) showed no significant differences between the SOD-323 and the SC-79 package. The reason for this might be the frequency range investigated.

3.4 Integrated Rectenna Design

Then, chosen SC-79 SMS7630 we can begin to make the topology of the rectifier circuit chosen, this is shows in figure 3.29; now we need the S-parameters of our antenna, for this, we import these from Agilent circuit simulator and insert in a data block.At the beginning only one antenna's port is used and the other connected to a 50Ω load; this

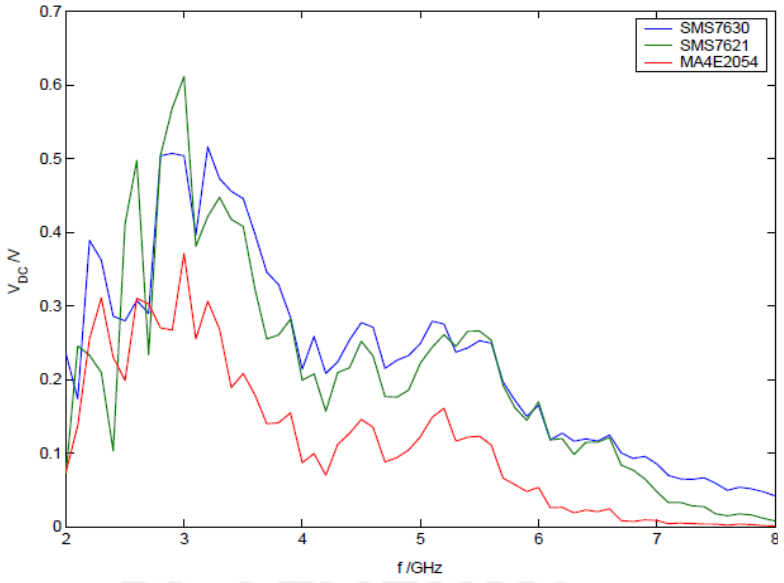

FIGURE 3.28: Comparison of the Schottky Diodes.

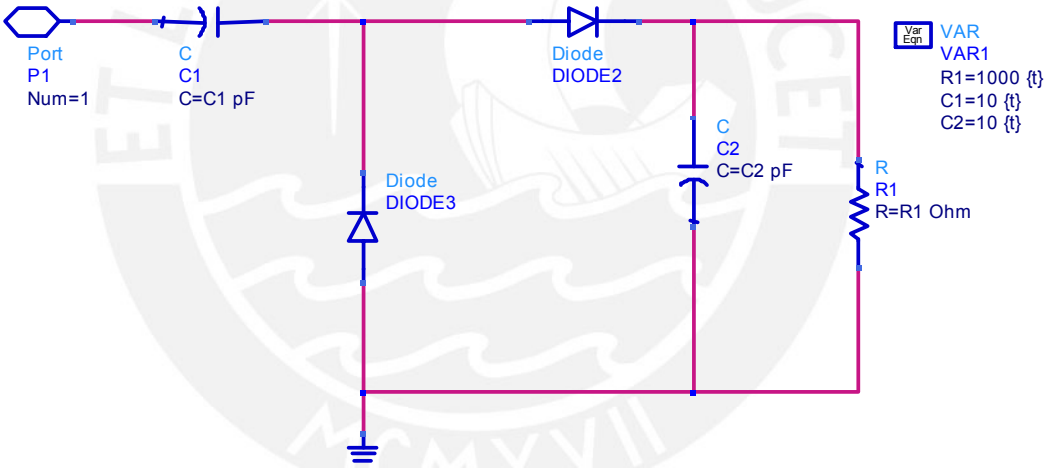

FIGURE 3.29: Basic topology of one branch rectifier circuit.

is to find the values from the basic rectifier circuit, then this will be duplicated at the other port. The antenna is simulated by a single tone voltage source plus antena's S-parameters,we apply the harmonic balance method for analyze this circuit in the frequency domain (see section 3.1.1), in this case with five Harmonics, then the S-parameters need to be between 0 and 5 x 2.45 GHz. These parameters were calculated from 0 to 13 GHz. in Agilent Momentum simulator. The single tone voltage source was configured for sweep in frequency to make a components matching analysis from 2 to 3 GHz.

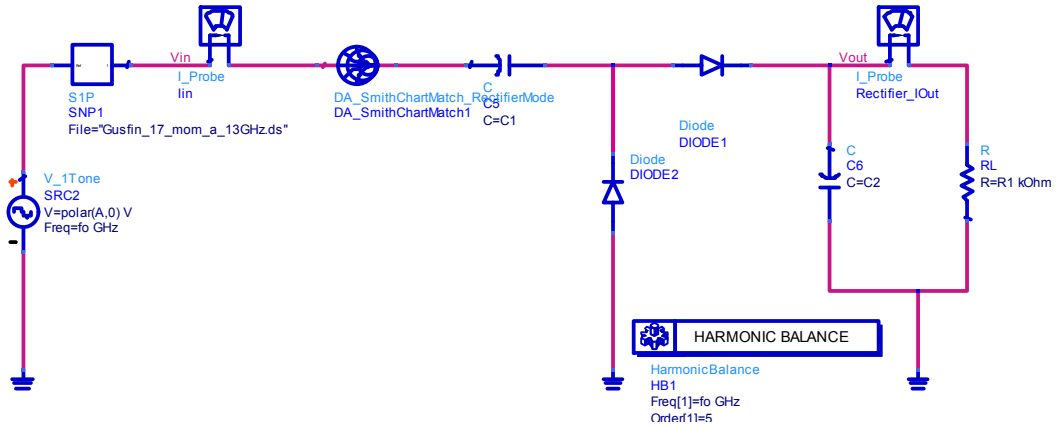

FIGURE 3.30: Entering the matching network with Smith Chart Matching tool (Agilent ADS).

To ensure maximum power transfer from the antenna to the load, the idea is find the best values for the matching network (will be calculated with Smith tool) and rectifier circtuit components(C1, C2 and R1) to matching the circuit at 2.45 GHz. with an impedance near antenna's impedance 50Ω and trying to not adversely affect the bandwidth always for low input power levels (see figures 3.38 3.40) to achieve our goal: ambient microwave energy recycling.

For get this purpose we will use the Tuning tool of Agilent ADS circuit simulator, from start values $C1 = C2 = 10pF$ and $R1 = 1000\Omega$ for the basic rectifier circuit, including a matching network with a Smith Chart Matching tool from Agilent ADS between the antenna's S-parameters block and rectifier circuit as figure(3.30), and make the first approximation of values of this network; Smith Chart Matching tool designed the topology of the matching network, choosing an inductance L1 in shunt and other in series L2 as we can see in figure (3.31), then with this topology and with the first approximated values, we need looking for better values for all components (L1,L2,C1,C2 and R1) and looking for good matching and a high efficiency as is posible; this is achieved using a Tuning tool as we can see in figure (3.32).

C1 and C2 functions: C1 is the first rectifier's capacitor to store energy from the antenna to reach the same voltage level that the signal coming from. C2 have two functions; is the second rectifier's capacitor to store energy from the antenna plus C1's energy , then reach twice voltage of the signal coming from the antenna (antennas's voltage plus C1 stored voltage); and the second function is cancel the harmonics of the output signal trying to obtain a DC without ripple; figure 3.33 shows the result of this second function, where the DC output signal is plotted versus time showing the harmonics effect (a little ripple). Inductors L1 and L2 are used only as part of the

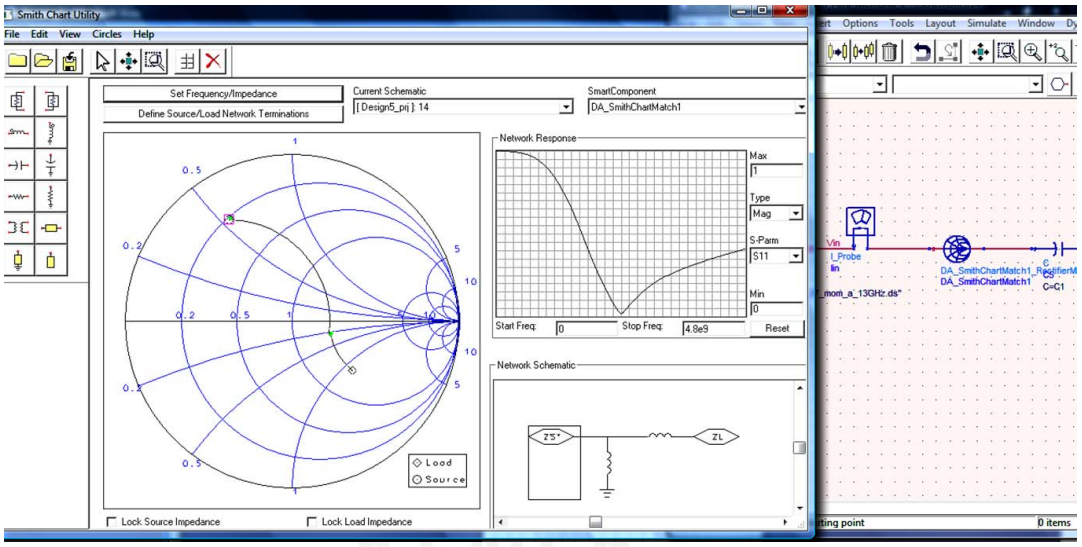

FIGURE 3.31: Working with Smith Chart Matching tool (Agilent ADS).

matching network to ensure the maximum power transmission from the antenna. The efficiency in figure 3.37 and 3.38, was calculated as a equation 3.4 where $P_{RF_{in}}$ in dbm, P_{DC} is calculated directly from the voltage in R1 according to equation3.3 due to is the power in a DC component and tends to be constant. This is an approximate and overestimate efficiency because now is assumed that all RF power is transferred to the rectenna with complete matching and this is not completely true. The incident RF power on the rectenna is a function of incident angles and effective area of the antenna, and can vary over the spectrum and in time, this concept was explained in more detail in section 2.4. A more accurately efficiency will be calculated in the measurements section 4.3.

$$P_{DC} = \frac{V^2}{R} \tag{3.3}$$

$$\eta = \frac{P_{DC}}{P_{RF_{in}}} = \frac{V^2 \cdot P_{in}}{R} \tag{3.4}$$

Equation 3.4 calculates an underestimate efficiency with $P_{RF_{in}}$ overestimate.

After this first tune, the components have values more accurately but are no the finals yet, because we need insert the effect of the microstrip pads and ground vias where we will solder all components. Now we can duplicate the rectifier circuit at other port of our antenna, the topology of the circuit is showed in figure 3.34. The circuit will be soldered in the back side of the antenna(A25N substrate) onto its thin cooper layer, this pads and ground vias also were designed with Momemtum method and its S-parameters are imported from circuit simulator into data blocks as we did with the antenna,the

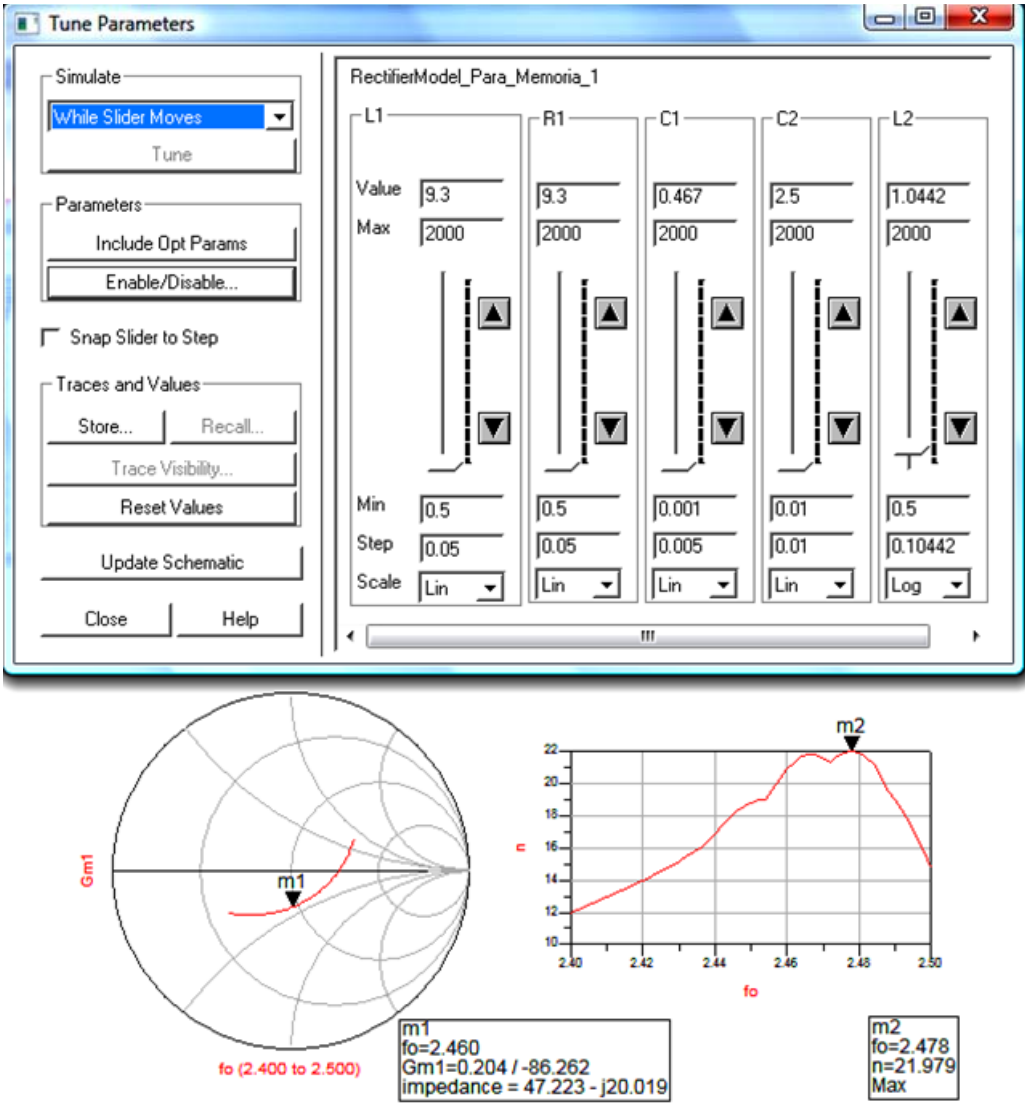

FIGURE 3.32: Tuning values for rectifier(C1,C2,R1) and matching network (L1, L2) components until get the optimum performance.

components size chosen to solder components was 0603(1.6mm 0.8mm), because is similar to diode package size SC-79 (max 1.7mm x 0.9mm) allowing soldered; the pads and ground vias was designed according to these size components. The final pads and grounds vias design in 2D is showed in figure 3.35. Figure3.36 show the 3D view of one ground pad, it can be seen its holes to be connect with the ground plane at other side of the substrate, this process is explained in the fabrication section 4.1.

Now, we need tune one more time to adjust the components values(now including the real effect of pads and grounds), this is done by trial and error until get the best behavior in matching and efficiency as in figure 3.32.Now and as last step, a last tuning including the manufacturer library components with a comercial available values close or the same

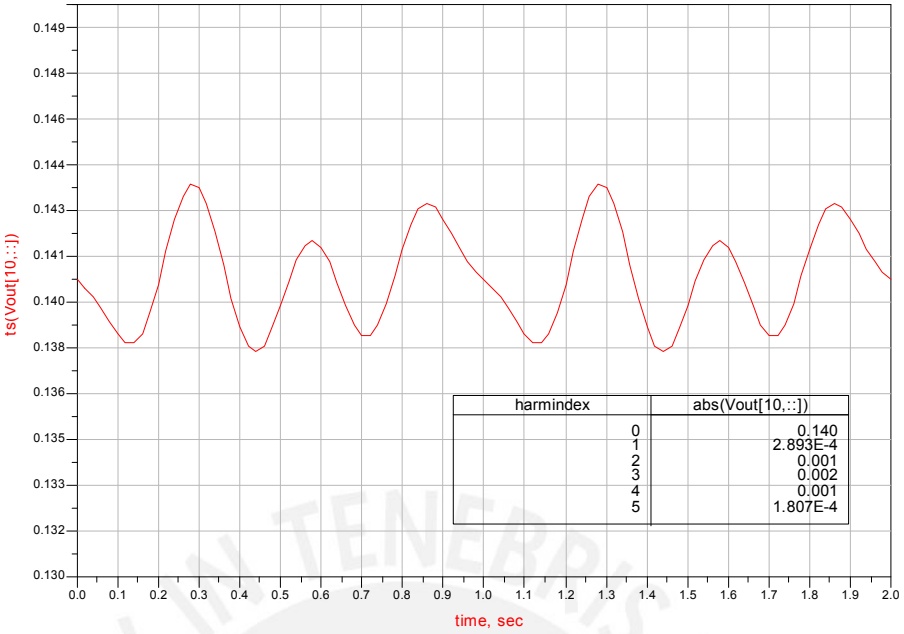

FIGURE 3.33: Simulated output DC voltage as a function of time, achieved at the one branch rectenna output (Agilent ADS).

to the calculated by tuning for capacitors (Murata) and Inductors (Coilcraft).There are three tuning steps for get accurately values, improving the accuracy between each try according to the real effects.

After the final tuning process, optimum values obtained for the circuit components at low input power levels are showed in table 3.7. Figure3.37 shows the obtained efficiency versus frequency calculated with a input power of -20 dbm, it shows a good results for our frequency band from 2.4 to 2.5 ($\eta_{max}(2.42GHz.) = 12.6\%$) GHz., the curve shows two peaks, one for each branch rectifier. Figure 3.38 shows the behavior for low input power levels from -20 to -0 dbm (calculated at 2.42 GHz.), obtaining ($\eta_(- 20.3dbm) = 12.05\%$) and ($\eta_(- 0.13dbm) = 38.42\%$). Rectenna's input impedance matched around 2.45 GHz. and around -20 dbm of input power are displayed in figures 3.39 and 3.40 respectively; each color shows the behavior from each branch rectifier, figures 3.41 and 3.42 show the DC output voltage as a function of frequency and input power respectively; around 66.8mV is obtained for -20,33 dbm and 1.2V for 0 dbm. These results are consequences with the intent to recycle energy and represent good results according with the referenced work (see section 2.3, figure 2.3).

Observation. In the case of sweep in Pin, it can seen that the Pin axis is moved 7 dBm below (see "Pin-7" on markers 1 and 2 from figures 3.38 and 3.42) this is due to the +10 dB of coupling factor of the directional coupler (from ouput to input), used

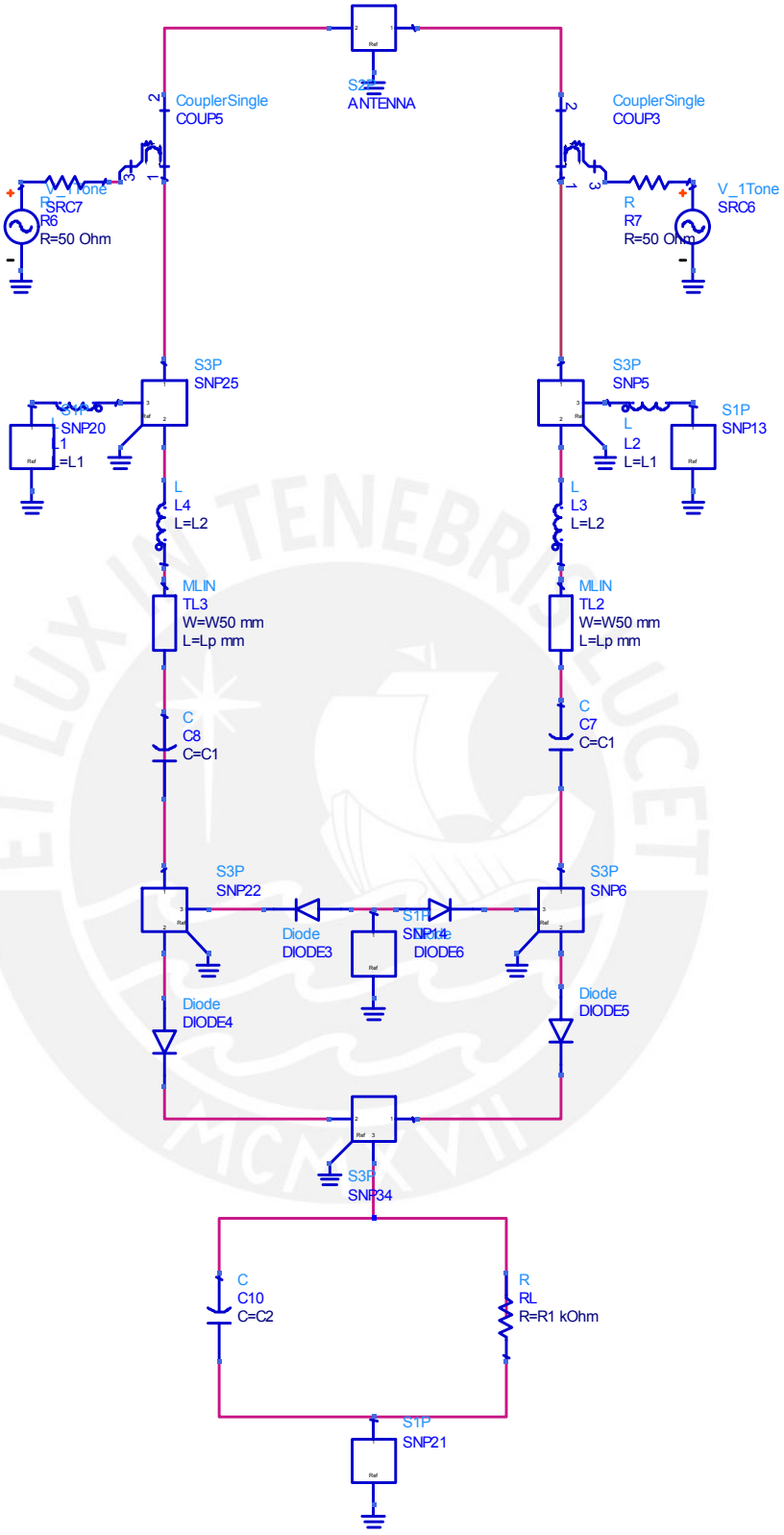

FIGURE 3.34: Final topology of the rectifier with two rectifier branches (Agilent ADS). A 10 dB directional coupler is used to join the inputs(antenna's S-parameters and V1 tone source) only as simulation purpose

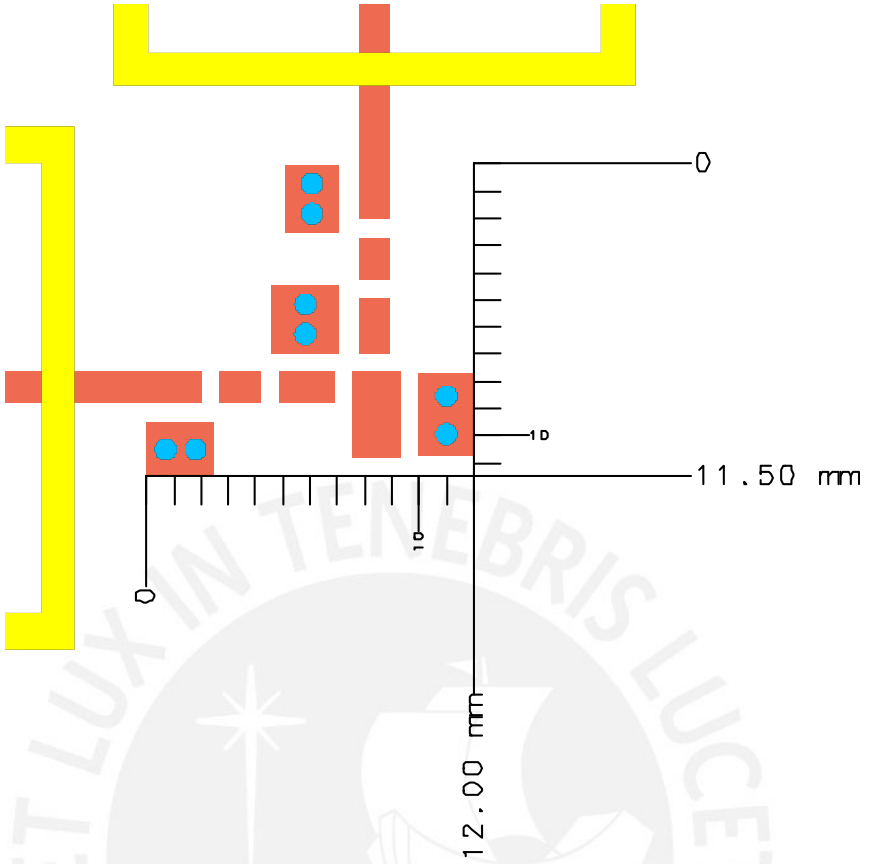

FIGURE 3.35: Ground vias and pads dimensions (Momemtum Agilent ADS). Designed under back side of the antenna to interconnect rectifier circuit components.

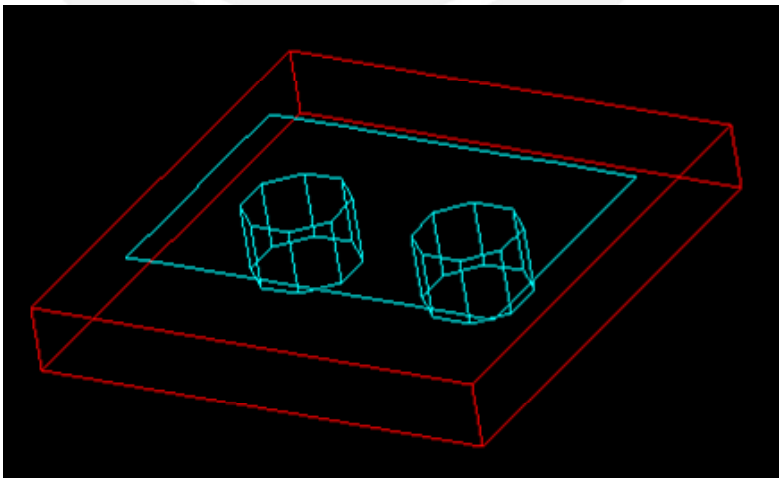

FIGURE 3.36: 3D view of the ground pad designe (Momemtum Agilent ADS). Used to interconnect rectifier circuit ground with the ground plane.

Component	Value	Dimension
Inductor L1 Coilcraft	1.8nH	0603 (1.6mm x 0.8mm)
Inductor L2 Coilcraft	5.6nH	0603 (1.6mm x 0.8mm)
Capacitor C1 Murata	1.5pF	0603 (1.6mm x 0.8mm)
Capacitor C2 Murata	5.6pF	0603 (1.6mm x 0.8mm)
Resistance R1	4kOhm	0603 (1.6mm x 0.8mm)
Diodes Skyworks SMS7630	see table 3.6	SC-079 1.7mm x 0.9mm

TABLE 3.7: Final values for rectenna components

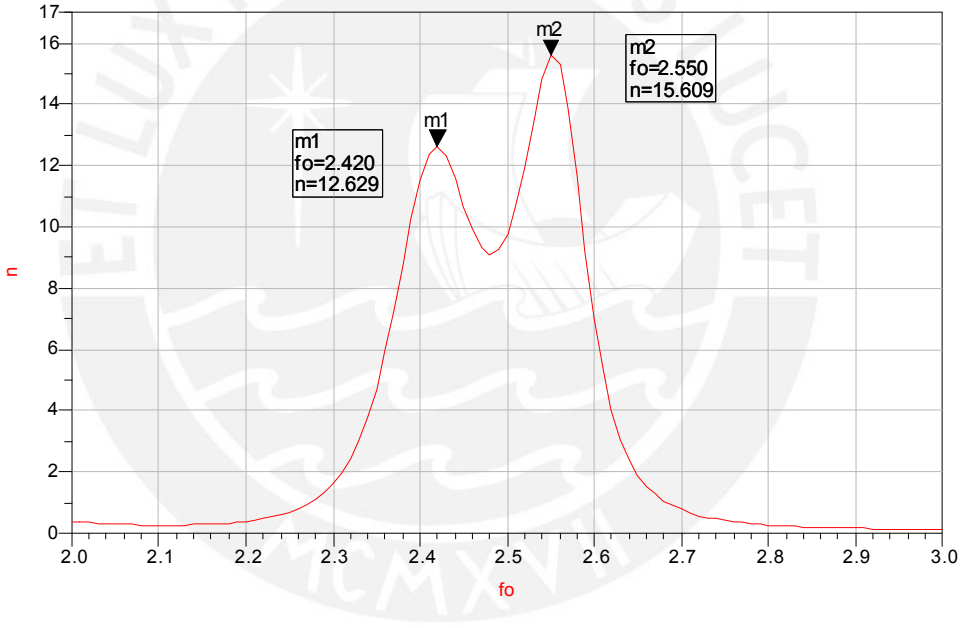

FIGURE 3.37: Rectenna efficiency versus frequency showing the behavior at 2.45 GHz. (Agilent ADS).

in the simulation (see figure 3.34) and −3 dB due to input power is divided in two branches rectifier, then; the Pin is overestimate in +7 dB; e.g. if we need -20 dBm as input power, is necessary to set it at -13 dBm (least 7 dBm), this setup is only for simulation purposes, the directional coupler is used to join two inputs: V1 tone source and antenna's S-parameters block, both to simulate a signal from antenna.

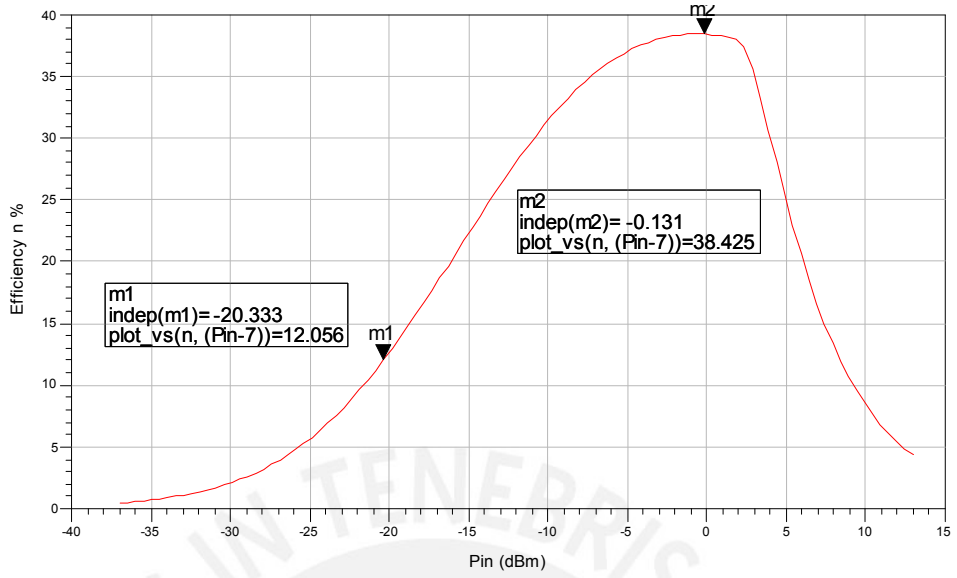

FIGURE 3.38: Rectenna efficiency versus input power showing its behavior for low input power(Agilent ADS).

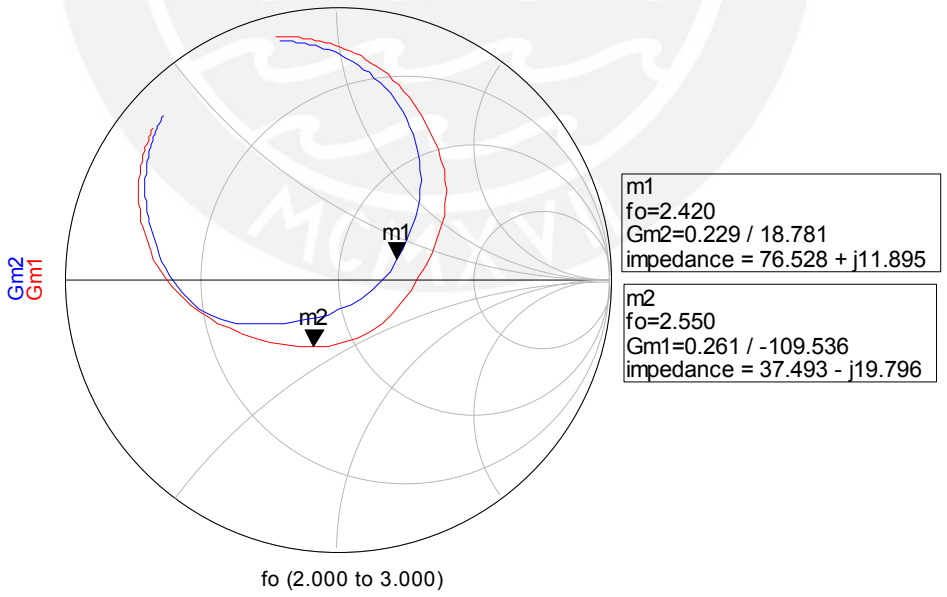

FIGURE 3.39: Rectenna's input impedance matched around 2.45 GHz. (Agilent ADS). Each color represent the impedance for each branch rectifier.

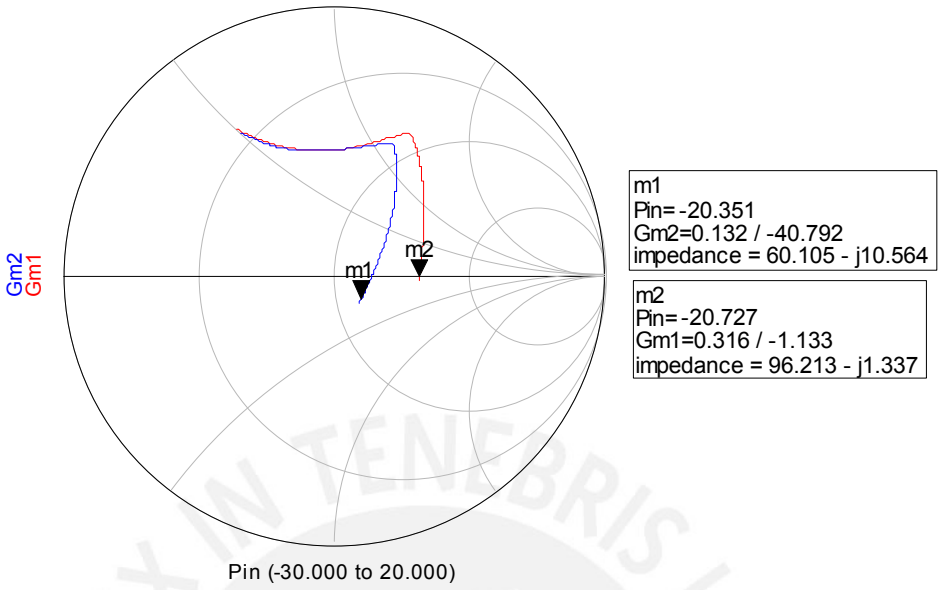

FIGURE 3.40: Rectenna's input impedance versus input power, matched around -20dbm (Agilent ADS).Each color represent the impedance for each branch rectifier.

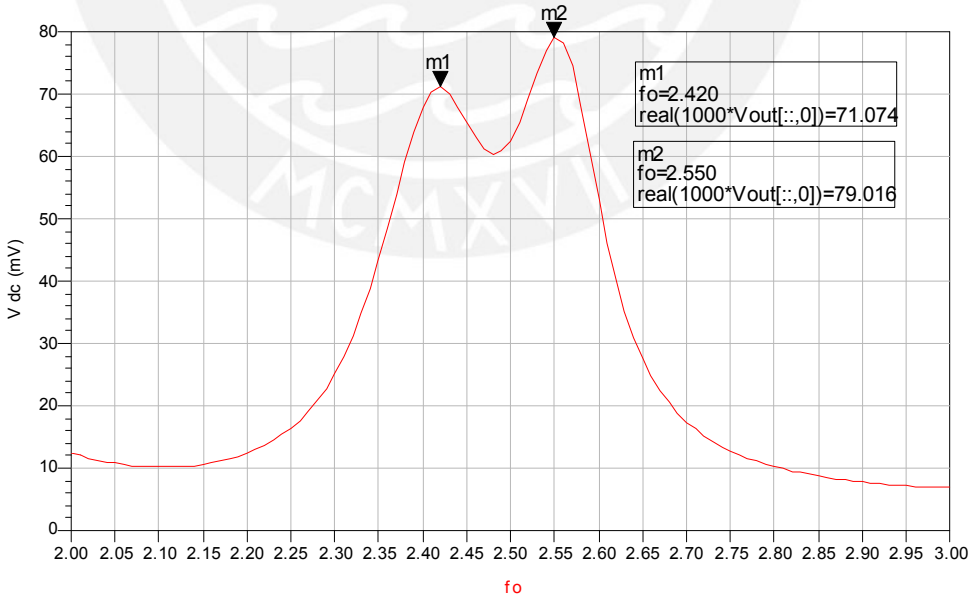

FIGURE 3.41: Rectenna's DC output voltage versus frequency (Agilent ADS).

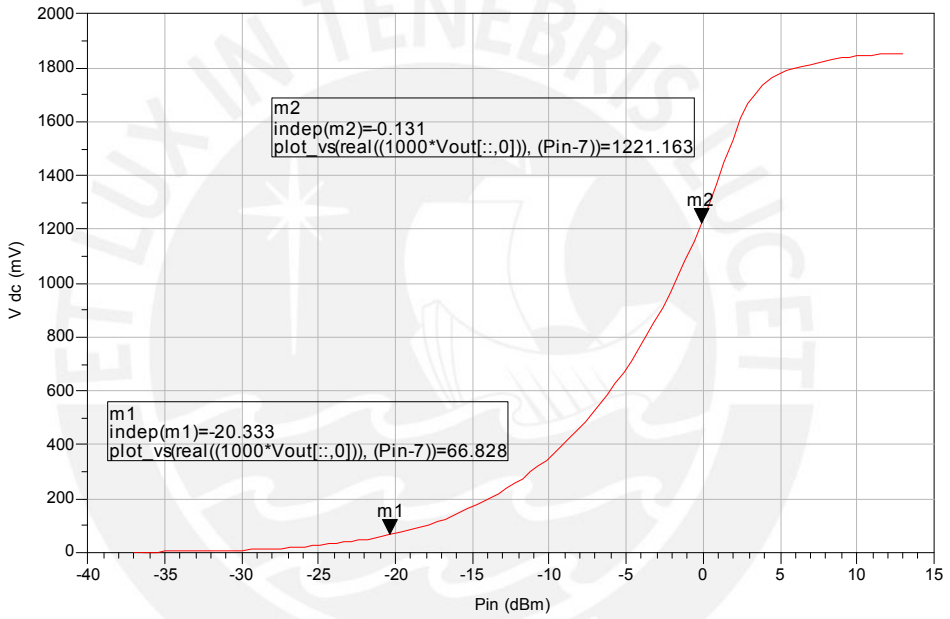

FIGURE 3.42: Rectenna's DC output voltage versus input power (Agilent ADS).

Chapter 4

Fabrication and Measurements

4.1 Fabrication

The last two designed antennas: (1) optimized size and (2) optimized size and bandwidth, circuit pads, one branch rectifier, complete rectifier with to branches and integrated rectenna were fabricated in the "CTTC design laboratory". Here's a summary of the process:

1. At first, all data from Agilent ADS momentum simulation is exported to LPKF milling machine software.
2. The A25N substrate (for front and back side of our antenna) is fixed into the work surface of LPKF milling machine in which the shadows of the patch and pads over the copper are marked, ground vias holes made and substrate cut at the ground plane size.Unfortunately at the first try the mill over the patch was to depth and was necessary a second try.(figure 4.1)
3. The unwanted copper is removed by hand using a cutter and following the marks made by the machine (figure 4.2)
4. The two Rohacell51 foams were easily cut by hand with a cutter (figure 4.3)
5. The back side A25N substrate is cover with a paste and inserted into a chamber in which is heated to metallize the ground via holes and connect these with the ground plane.
6. After each layer is properly milled and cut (figure 4.3); the inductors, capacitor and resistor are soldered in the back side of the antenna under the ground plane side, over the pads and ground vias designed (figure 4.4). In the separately antenna

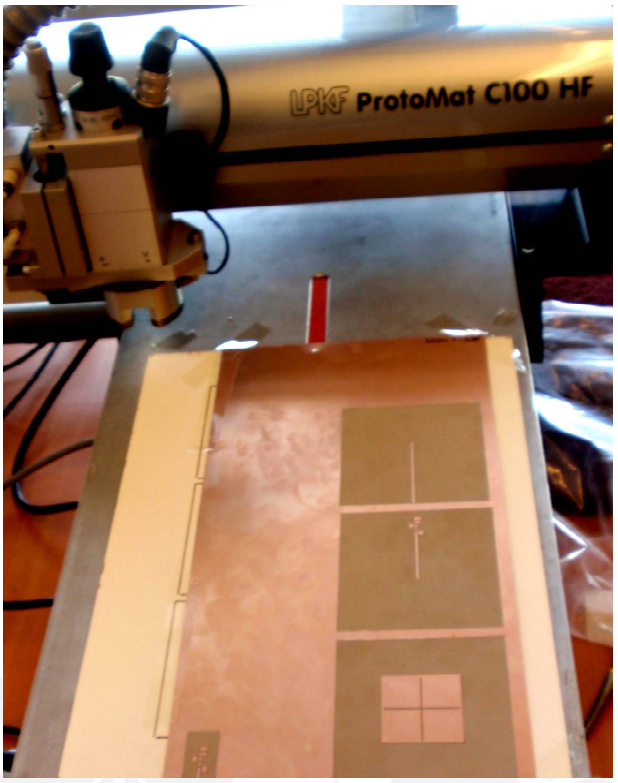

FIGURE 4.1: The A25N substrate (for front and back side of our antenna) fixed into the work surface of LPKF milling machine in which the shadows of the patch and pads over the copper are marked, this figure corresponds to the optimized size antenna.

and branches rectifier cases a SMA connectors are soldered to each port (figure 4.5 and 4.6).

7. The layers are bonded.The two Rohacell51 foams and A25N were bonded with an uniformly layer of glue spray over each surface (figure 4.7).

The above describes the followed fabrication process for an integrated rectenna where the antenna is over the top layer and rectifier under the bottom layer due to the structure of the microstrip aperture coupled antennas allowed. With the same fabrication process, also a separately antennas (without behind circuit), one branch rectifier and complete rectifier circuit were fabricated to take measures of each one and assess their performance separately.

.

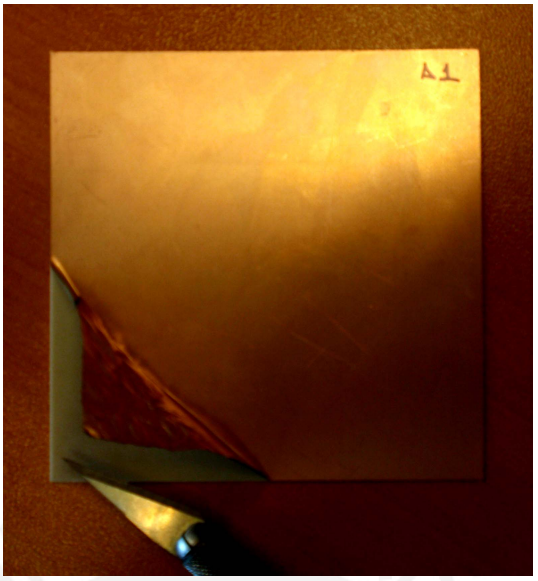

FIGURE 4.2: Removing the unwanted copper using a cutter and following the marks made by the milling machine,now is removed all the cooper from the back side of the patch.

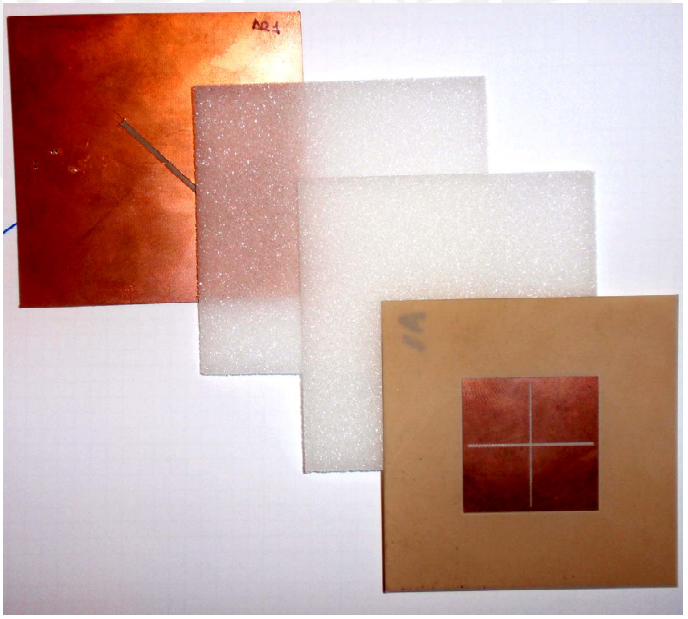

FIGURE 4.3: A25N and Rohacell51 layers ready to be stacked, the two Rohacell51 layers were easily cut by hand with a cutter; this figure corresponds to the optimized size antenna.

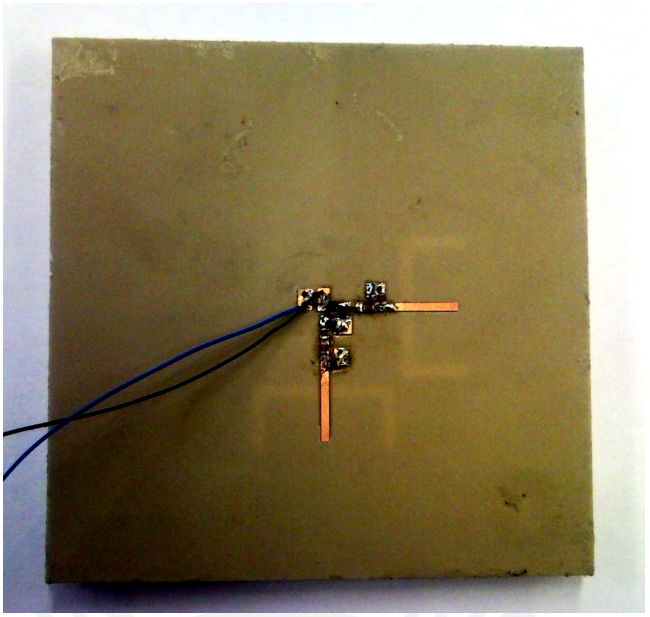

FIGURE 4.4: The inductors, capacitor and resistor are soldered in the back side of the antenna under the ground plane side, over the pads and ground vias designed; this figure corresponds to the integrated rectenna.

4.2 Measurements

Four sets of measurements will be made on: (1) the optimized size antenna, (2) the optimized size and polarization antenna, (3)one branch rectifier circuit and (4)the integrated rectenna. Antennas were tested for S11 parameters and radiation patterns; one branch rectifier circuit also was tested for their S11 parameters and RF-DC conversion efficiency as a function of frequency and input power, and the integrated rectenna for its RF-DC conversion efficiency as a function of frequency, incident power and polarization mismatch. The following results were obtained on the labs and anechoic chamber of the "Centre Tecnologic de telecomunicacions de Catalunya CTTC".

4.3 Measurement Setup and Limitations

Antennas measurements

Antennas were tested for its return losses and radiation patterns; the return losses was measured in a Rohde & Schwarz ZVA24 vector network analyzer with the properly calibration for S11 measure. In the patterns radiation cases, measurements were taken in a walk-in anechoic chamber. The transmission antenna was an open boundary quadridge horn model 3164-05 specified for use from 2 to 18 GHz. The receiving antenna was the

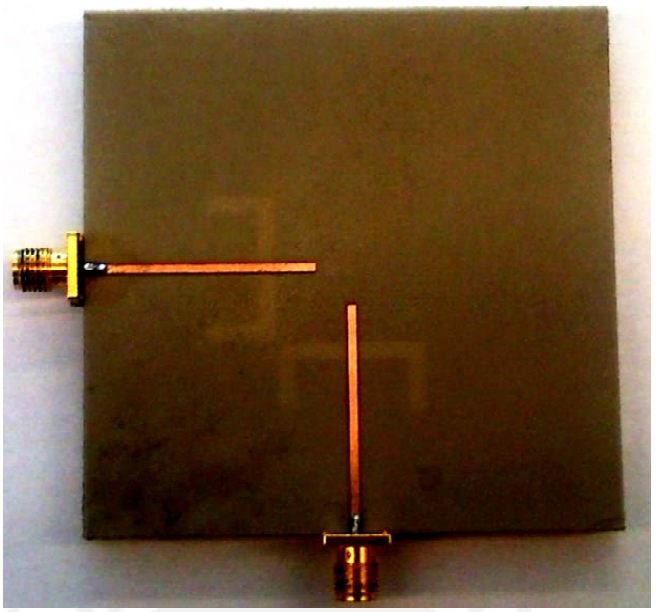

(a)

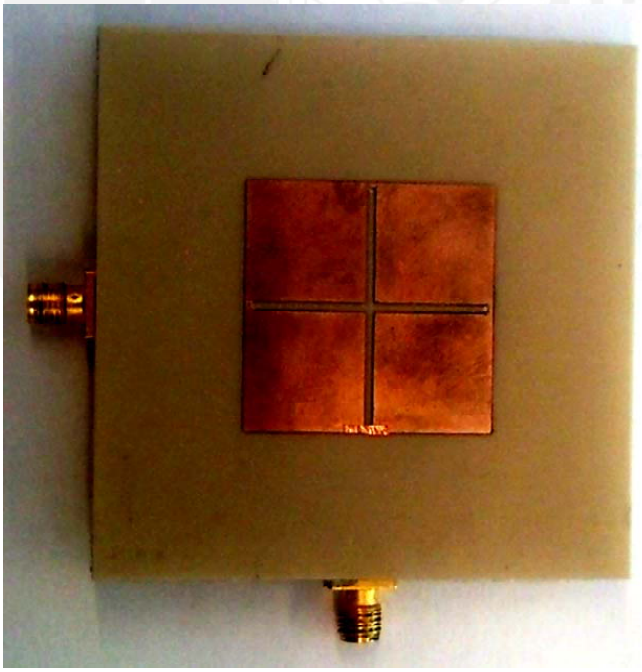

(b)

FIGURE 4.5: In the separately antenna cases a SMA connectors are soldered to each port; back (a) and front (b) views of the optimized size and polarization bandwidth antenna.

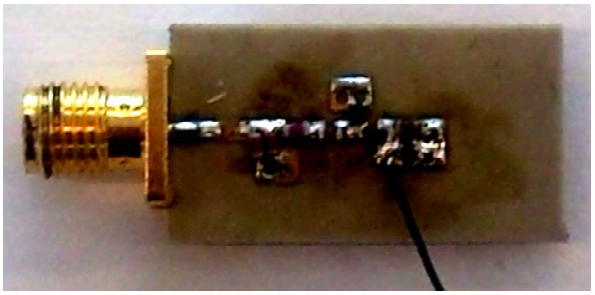

(a)

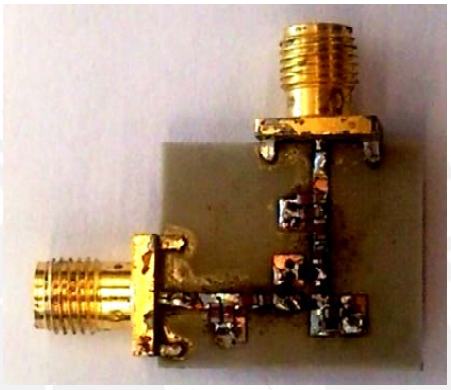

(b)

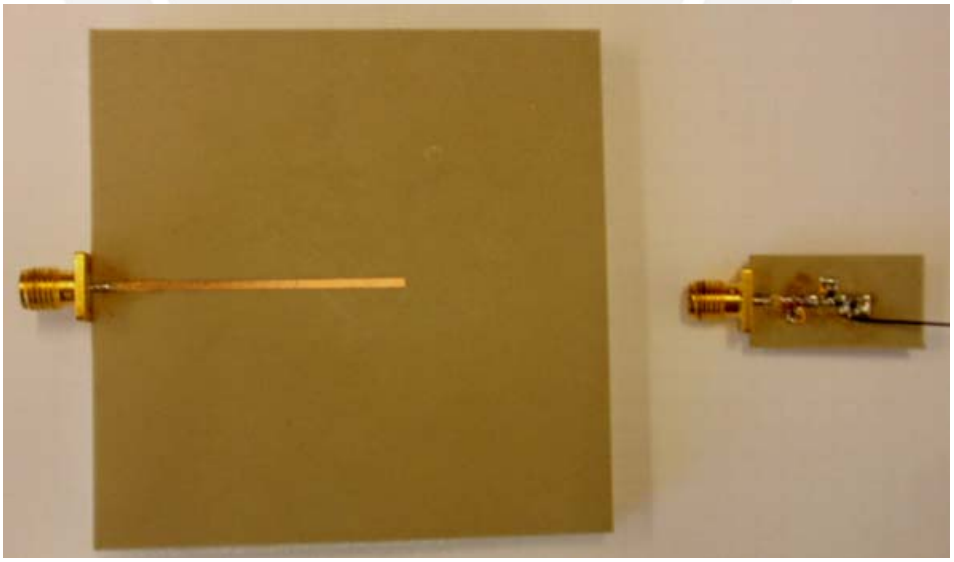

(c)

FIGURE 4.6: In the separately branches rectifier cases a SMA connectors are soldered to each port; figure (a) corresponds to a one branch rectifier, (b) is the complete rectifier with two branches rectifiers and (c) shows a comparative in sizes between the antenna and circuit.

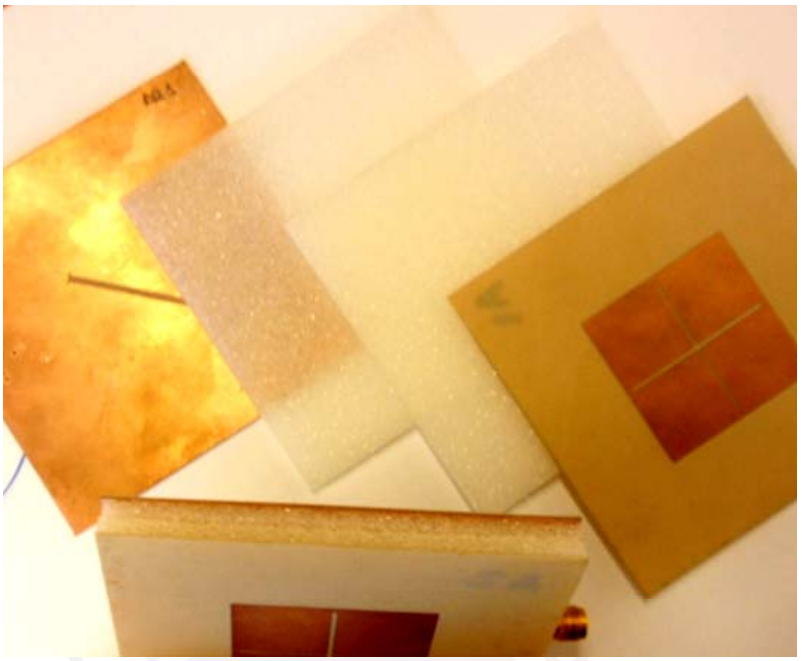

FIGURE 4.7: The layers are bonded.The two Rohacell51 foams and A25N were bonded with an uniformly layer of glue spray over each surface.

antenna under test AUT, i.e. were three ATUs, (1) the optimized size antenna, (2) the optimized size and polarization bandwidth antenna and (3) the integrated rectenna, the same antenna that case (2) but now with the rectifier circuit builded behind.

One branch rectifier measurements

The one branch rectifier efficiency was measured generating two kinds of input signal with a Agilent E4438C vector signal generator: (1) a single frequency signal (without modulation) and (2) with a 802.11b signal,(11Mbps, QPSK modulation, each channel of 22MHz with 11MHz of -3dB bandwidth) in the three European non overlopping channels (see figure 4.8) like RF input; and in the DC output was connected an Agilent 34401A Digital Multimeter.

Rectenna efficiency measurement

In the case of the integrated rectenna measurements each data-point consists of at least a DC voltage, i.e. the DC output of the rectenna, and was taken versus at least one of the following variables: transmitted power Pt, frequency f,elevation angle ϑ or azimuth angle φ. Figure 4.9 shows the measurement setup. For 1D measurements, the motors remain stationery, For 2D-radiation patterns measurements, only the ϑ-motor is turned and for 2D-polarization mismatch measurements the φ-motor is turned and ϑ-motor remain stationery

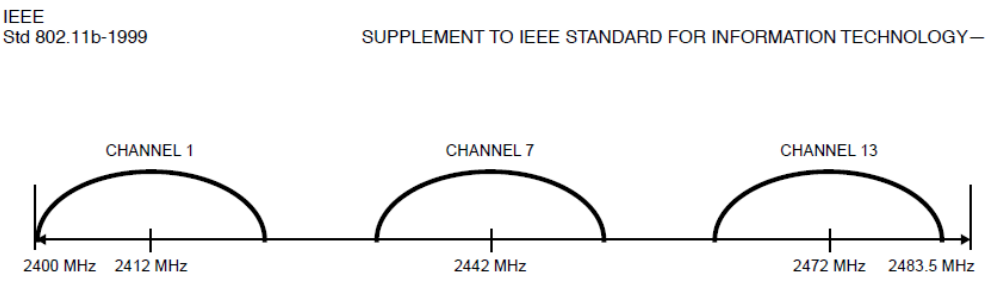

FIGURE 4.8: 802.11b European channel selection - non overlapping.

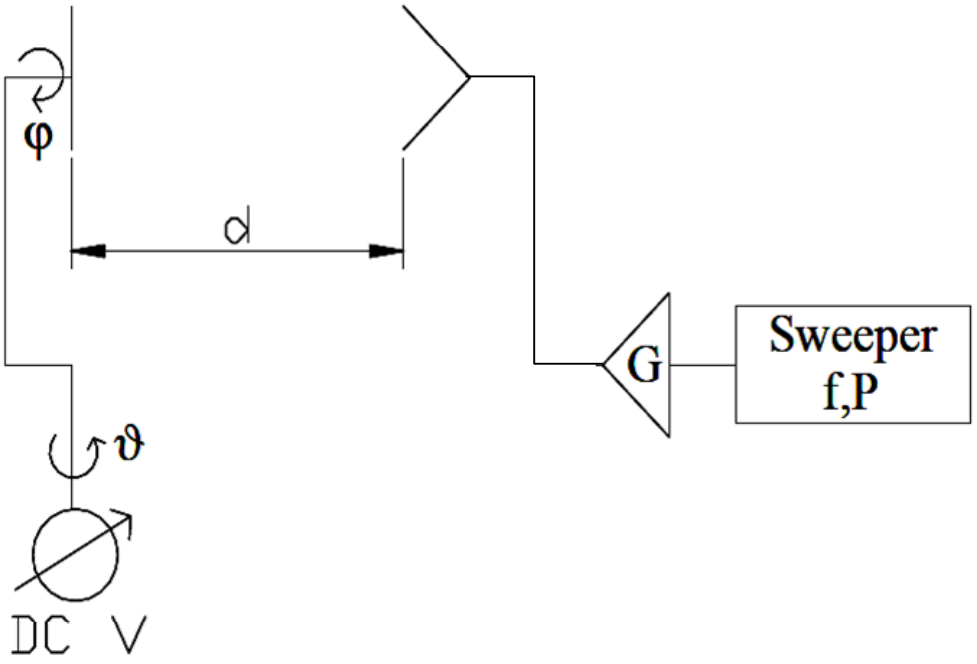

FIGURE 4.9: Measurement setup in the anechoic chamber.

In order to obtain the rectenna's efficiency, linearly polarized energy is transmited from the horn antenna to the rectenna located a distance d from the transmitting horn. The rectenna's efficiency η as was exposed in section 2.4 is the ratio of the converted dc power P_{DC} to the receive RF power $P_r = P_{RF}$ as:

$$\eta = \frac{P_{DC}}{P_r} \tag{4.1}$$

the DC power P_{DC} is:

$$P_{DC} = \frac{V_{DC}^2}{R_L} \tag{4.2}$$

and the received power was calculated with the Friis transmission (Eq. 4.3 and 5.4).

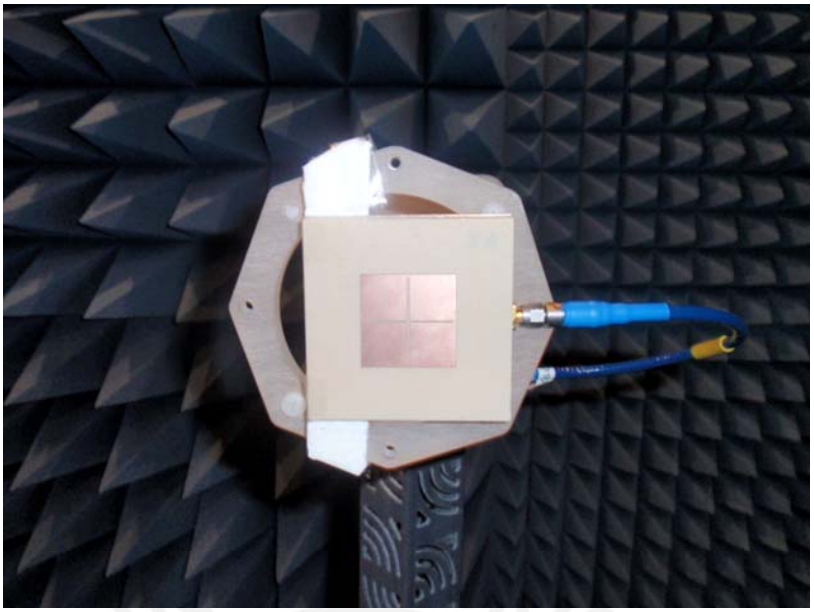

FIGURE 4.10: Fixing setup of the antenna under test on the anechoic chamber's rotor axis, it can seen the arm structure that holds the antenna.

The gain of the transmitter antenna, taken from its data sheet is 6dB for 2.5 GHz. [41]; the transmitted power was sweeping from 0 to 20 dbm and the distance d between the antennas was 3.63m. Whenever needed for the Friis equation, the effective area A_{eff} for the AUT was extracted from Agilent ADS simulations. It was only used for 1D, i.e. broadside measurements.

$$\frac{P_r}{P_t} = \left(\frac{\lambda}{4\pi \cdot d}\right)^2 \cdot G_{0t} \cdot G_{0r} \tag{4.3}$$

with G_{0t} the gain of the horn used for measurements, G_{0r} the gain of the AUT, and d the distance between transmitter and rectenna during measurements. Then, by expressing P_r as a density power and in terms of the AUT's effective area A_{eff}

$$P_r = \left(\frac{P_t G_{0t}}{4\pi d^2}\right) L_{pol} A_{eff} \tag{4.4}$$

L_{pol} represents the polarization mismatch between the transmitter and receiver antennas and in this case is 1 because our antenna has linear polarization and the incoming wave also is linearly polarized. Measurements on the rectenna were limited by the amplifier available (max 17.5 dBm) and the distance necessary between the transmit antenna and the AUT to guarantee far-field measurements.

1D Setup

For 1D measurements, transmitter and receiver had a fixed position with their broadsides facing and the parameters frequency and power varied. To calculate the received power

of the antenna, the Friis equation (4.3) was used. The broadside gain of the horn is known, as mentioned earlier, and the directivity of the antenna was taken from the simulations

2D Radiation pattern Setup

For 2D radiation pattern measurements, the elevation angle was swept over the range $0 \leq \vartheta \leq 2\pi$, with $\vartheta = 0$ specifying the z-axis. This process measure one plane (e.g. E o H) for the other plane measures is necessary to rotate the azimut angle $\pi/2$. **2D Polarization Setup** For 2D polarization measurements, the azimuth angle φ was swept over the range $0 \leq \varphi \leq 2\pi$, with $\varphi = 0$ specifying the x-axis.

4.4 Measurements of the Optimized Size Antenna

4.4.1 S11 Parameters

Figure 4.11 shows the S11 parameters measured for the optimized size antenna in blue in comparison with its S11 simulation in red. Return losses figure 4.11 (a) shows that there is a good matching at 2.45GHz., now the -10dB impedance bandwidth is 4.48%, can be seen that in the fabricated antenna is achieved more bandwidth than in its simulation (3.77%), also the loop in the smith chart for the measured antenna is a little more concentrate at the center (figure 4.11 (b)). The cost of increased bandwidth is also increasing antenna losses compared with the simulation.

4.4.2 Measurements on the Anechoic Chamber

Figures 4.12 and 4.12 show the the measured radiation pattern of the optimized size antenna for three different frequencies: 2.40, 2.45 and 2.50 GHz. Each plot was made with mentioned 2D setup, then the figure 4.12 represents the ZX plane and has the same polarization as the excitation (Co-polar direction), and figure 4.12 the ZY plane and azimuth angle φ is turn it 90° referred to excitation polarization (Cross-polar direction). As we can see both plots are almost equals, this behavior was expected from the simulation results, the reason is that this antenna has a symmetrical rotated linear polarization as we can see in figure 4.14, a 180° beam width between first nulls is achieved. The asymmetry around 270° is due to the fixing setup of the AUT in the axis rotor, there is an arm that holds the antenna in the (0,0,0) position as we can see in figure 4.10, this can be corrected by increasing the sampling resolution, this mean smaller steps of elevation angle ϑ to take samples.

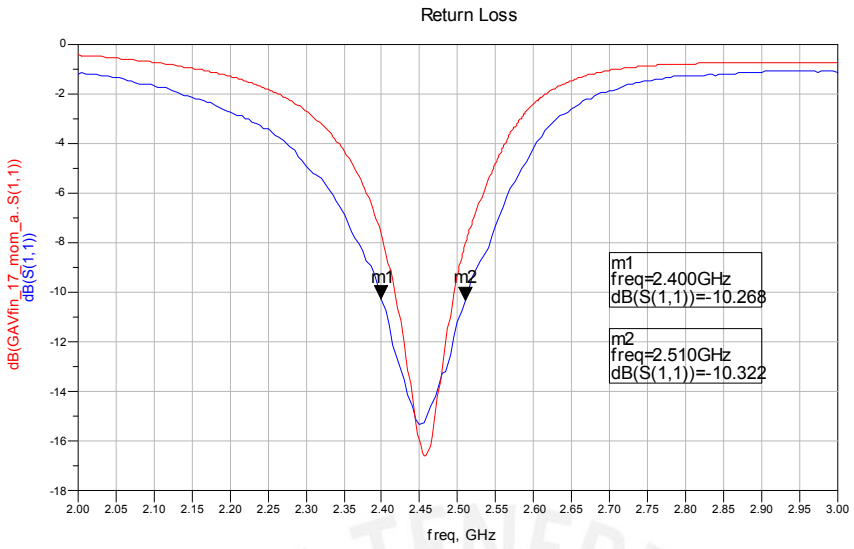

(a)

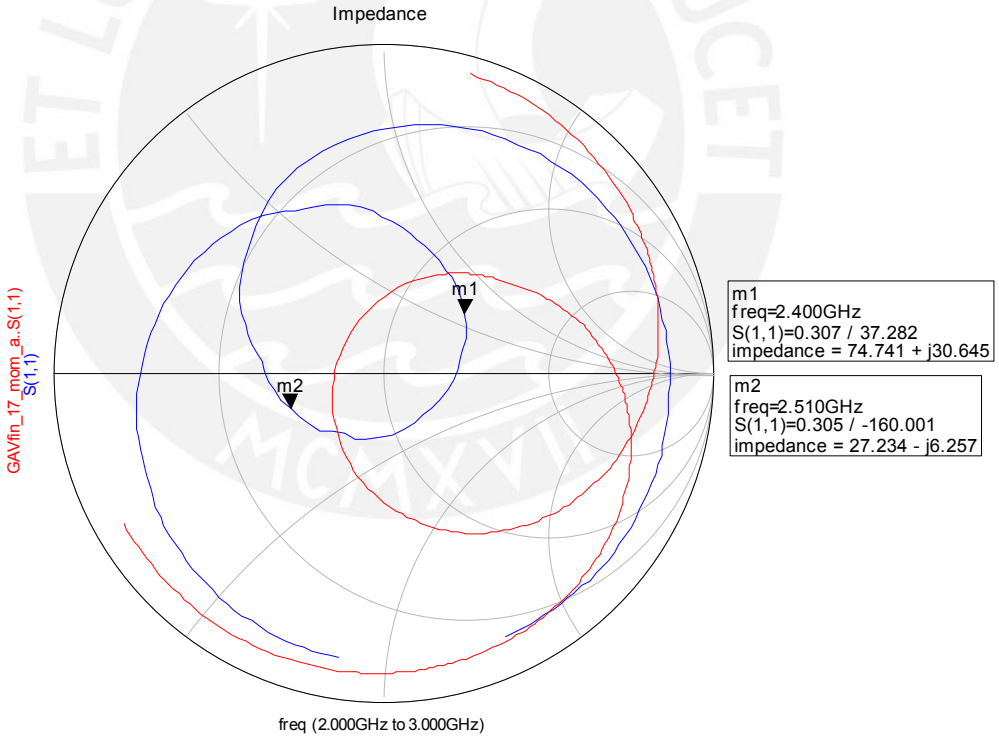

(b)

FIGURE 4.11: S11 parameters measured for the optimized size antenna in blue compared with the simulated results in red; (a) shows the return losses and (b) the impedance versus frequency. More than simulated bandwidth is achieved.

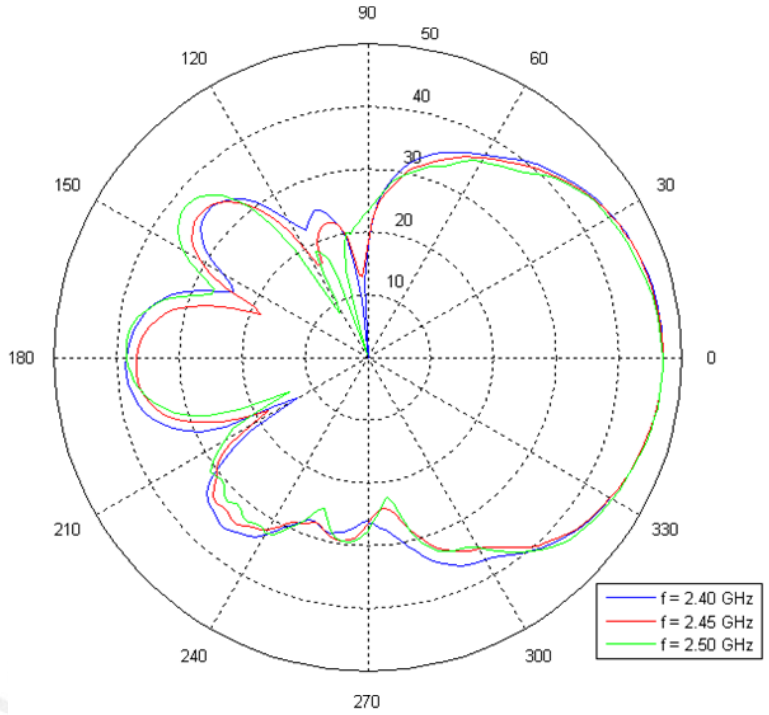

FIGURE 4.12: Radiation pattern in Co-polar Direction.

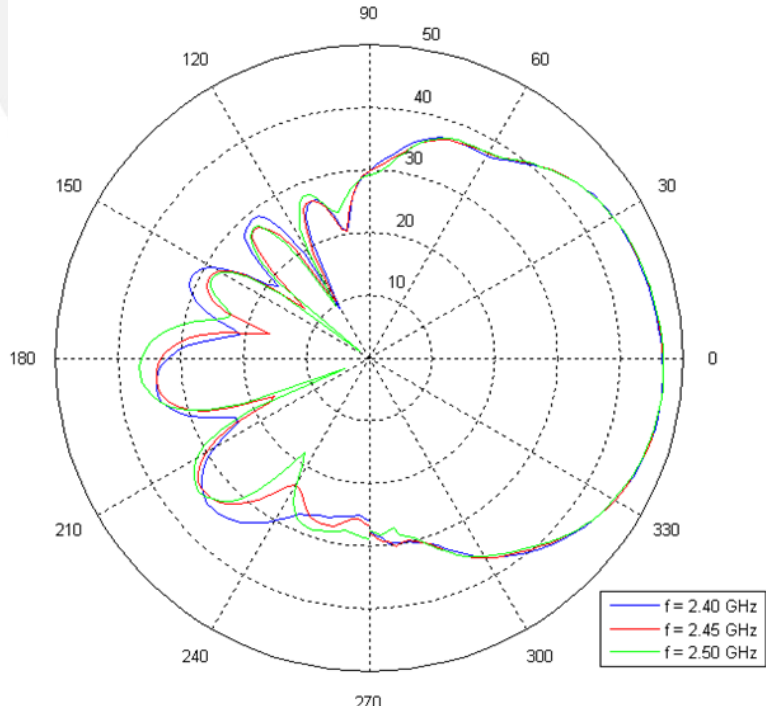

FIGURE 4.13: Radiation pattern in Cross-polar Direction.

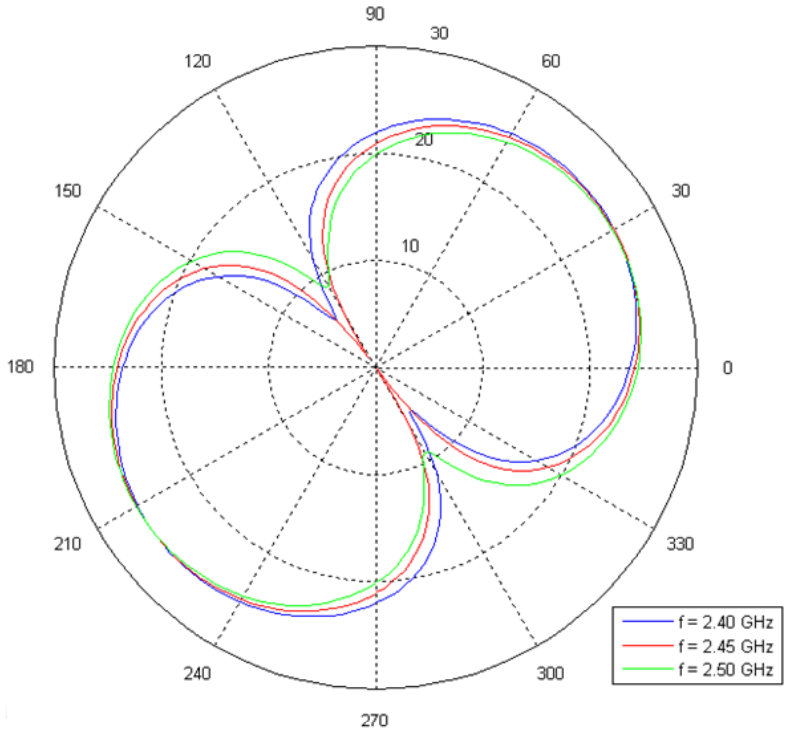

(a)

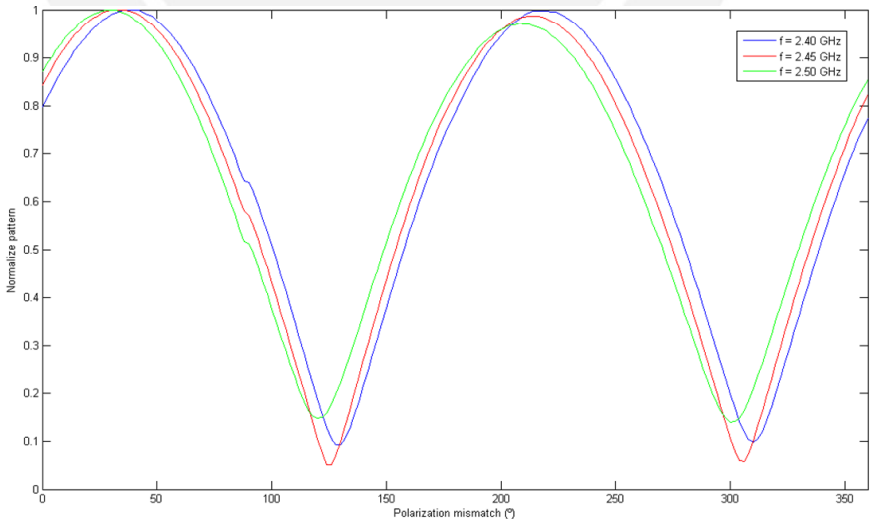

(b)

FIGURE 4.14: Polarization of the optimized size antenna.

	F = 2.40 GHz.	F = 2.45 GHz	F = 2.50 GHz
Directivity (dBi)	6.48	6.76	6.71
FB (dB)	8.44	10.37	8.55
Beamwidth(°) -3dB	71	69	72
Impedance Bandwidth	4.48%		
Polarization	Linear rotated 45(°)		

TABLE 4.1: Measures parameters from optimized size antenna

In figure 4.14 the polarization of the antenna is plotted for 2.40, 2.45 and 2.50 GHz. This data also comes from a 2D-measurement setup , figure shows the received power versus the azimuth angle of the antenna in polar plot at top (a) and cartesian plot at bottom (b).The behavior the same for the three frequencies; In (a) can seen clearly that there is a linear rotated polarization with the same rotated angle that the aperture coupled: 45 degrees, in figure (b) each trace is normalized to its maximum and shows clearly the nulls around 135 and 315(°). Table 4.1 shows a measured parameters resume of this antenna

4.5 Measurements of the Optimized Size and Polarization Bandwidth Antenna

4.5.1 S11 Parameters

Now we have an antenna with two ports to measure, each one will be analyzed separately; figures 4.15 and 4.16 shows the S11 parameters measured at port 1 and port 2 respectively, for the optimized size and bandwidth polarization antenna in blue in comparison with its S11 simulation in red. Return losses figures 4.15 (a) and 4.16 (a) show also a good matching at 2.45GHz., now the -10dB impedance bandwidth is 2.85%, now is achieved less bandwidth than in its simulation (3.07%), the loop in the smith chart for the measured antenna is concentrate at the center (figure 4.15 (b) and 4.16 (b)) but now also there is more expanded loops and discontinuities as a result of the interaction between more coupling elements (two U-shaped aperture coupled and two feed lines), this is the reason for the achieved bandwidth, in the simulation this was not a problem

because it was considered an infinite ground plane. the slightly reduction in impedance bandwidth of this design is strongly compensated with the duplication of polarization bandwidth

4.5.2 Measurements on the Anechoic Chamber

Figure 4.17 show the the measured radiation pattern of the optimized size and polarization bandwidth antenna that will be used in the integrated rectenna, figures show the E plane for each port; the measures also were made at three different frequencies: 2.40, 2.45 and 2.50 GHz. Each plot was made with mentioned 2D setup, then the figure 4.17 (a) represents the ZX plane and has the same polarization as the excitation (Co-polar direction) for port 1 while the port 2 is connected to a 50Ω load , and figure 4.17 (b) the ZY plane and azimuth angle φ is turn it 90° referred to excitation polarization from the last measure, this will be the Cross-polar direction for port 1 but Co-polar for port 2, now the measured is port 2 while port 1 is connected to a 50Ω load. As we can see the co-polar plane for port 1 (figure 4.17 (a)) is slightly higher than the co-polar plane for port 2, this could be due imperfections in the milled patch and in the aligning stacked layer process but in conclusion a dual linear polarization antenna now is achieved. A 210° beam width between first nulls is achieved and is greater than the previous antenna due to the straight apertures coupling position versus the rotated from the last one. The asymmetry around 270° in patterns radiation was corrected by increasing the resolution sampling. Figure 4.18 shows the directivity measures in a sweep of frequency per port from 2.25 GHz. to 2.55 GHz. 7.5 dB is achieved in general and in each port the tend, although slightly is a higher directivity for 2.45 GHz. this is consistent with the above co-polar plots when at 2.45 GHz. (red line) is achieved the maximum level for both ports. The polarization measures will be analyzed in the integrated rectenna measures due to we just need one output to analyze the polarization behavior from two ports and this will be the DC output. Table 4.2 shows a measured parameters resume of this antenna

4.6 Measurements of the One Branch Rectifier Circuit

The one branch rectifier as figure 3.30 was builded with the intention to measure its performance in matching and RF-DC conversion efficiency at three different input power: -20 dBm, -10 dBm and 0 dBm and with two kinds of input signals:(1) A single tone and (2) 802-11b modulated signal. Unfortunately when it was builded with the same component values tuned by simulation (table 3.7) the measures don't agree with its simulation results. Figures 4.19 and 4.20 show the return losses and RF-DC conversion

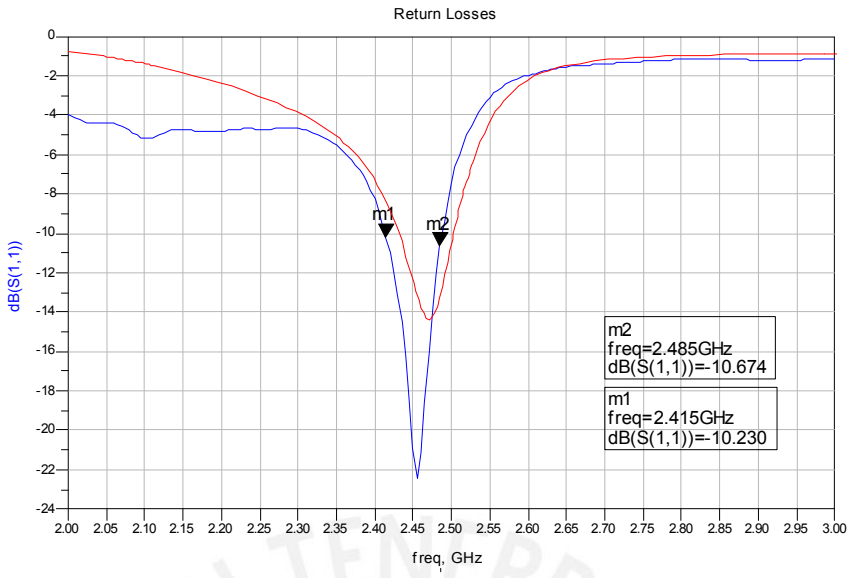

(a)

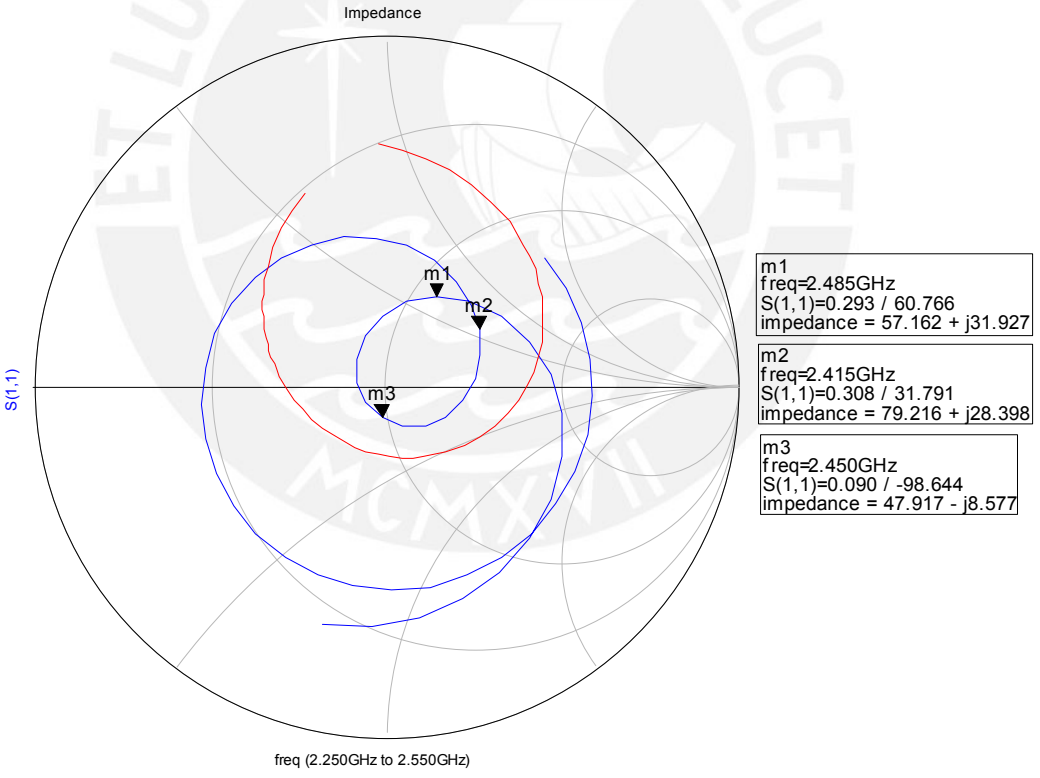

(b)

FIGURE 4.15: S11 parameters measured for the optimized size and polarization bandwidth antenna in blue compared with the simulated results in red, (a) shows the return losses and (b) the impedance versus frequency.

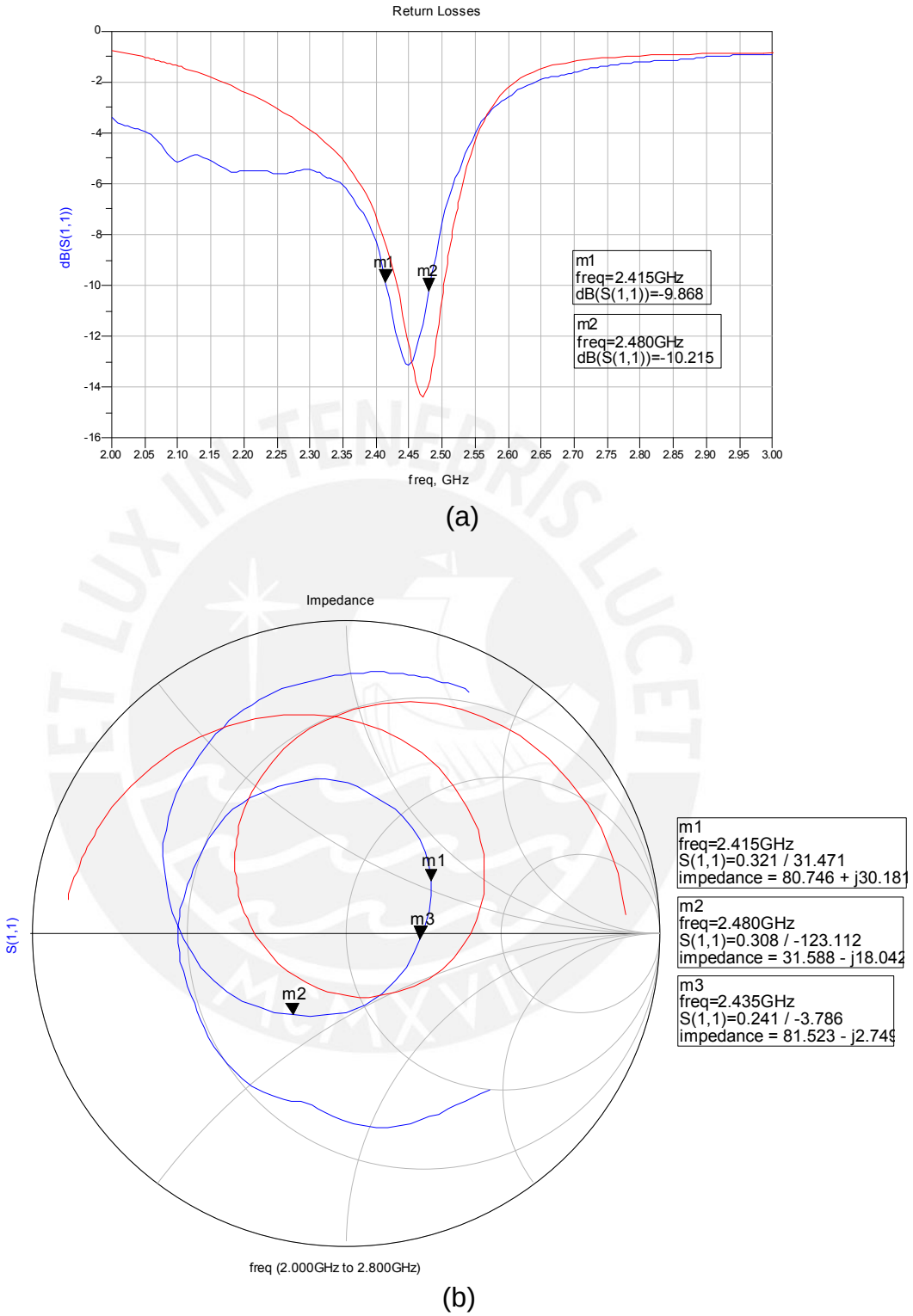

FIGURE 4.16: S11 parameters measured for the optimized size and polarization bandwidth antenna in blue compared with the simulated results in red, (a) shows the return losses and (b) the impedance versus frequency.

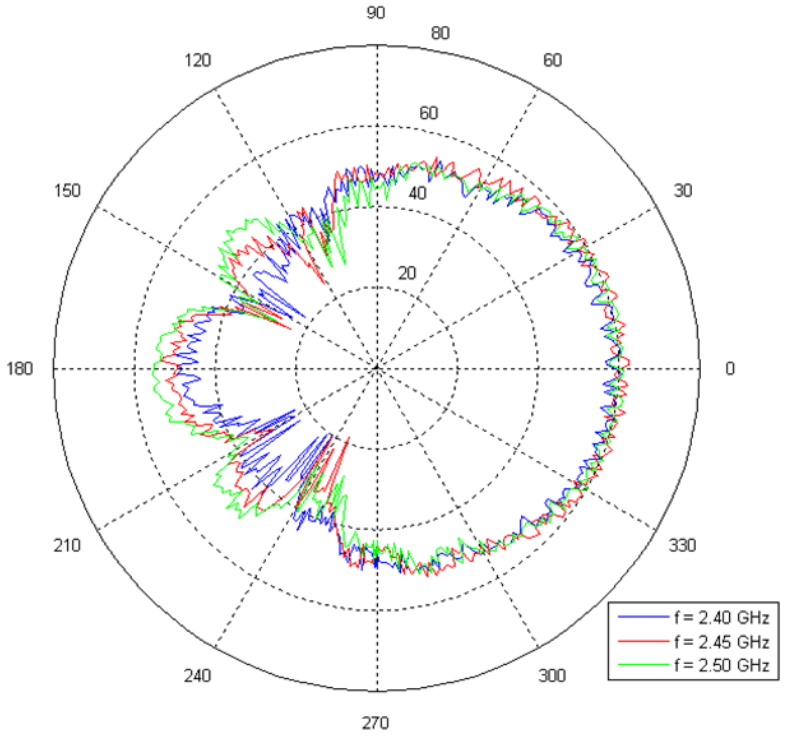

(a)

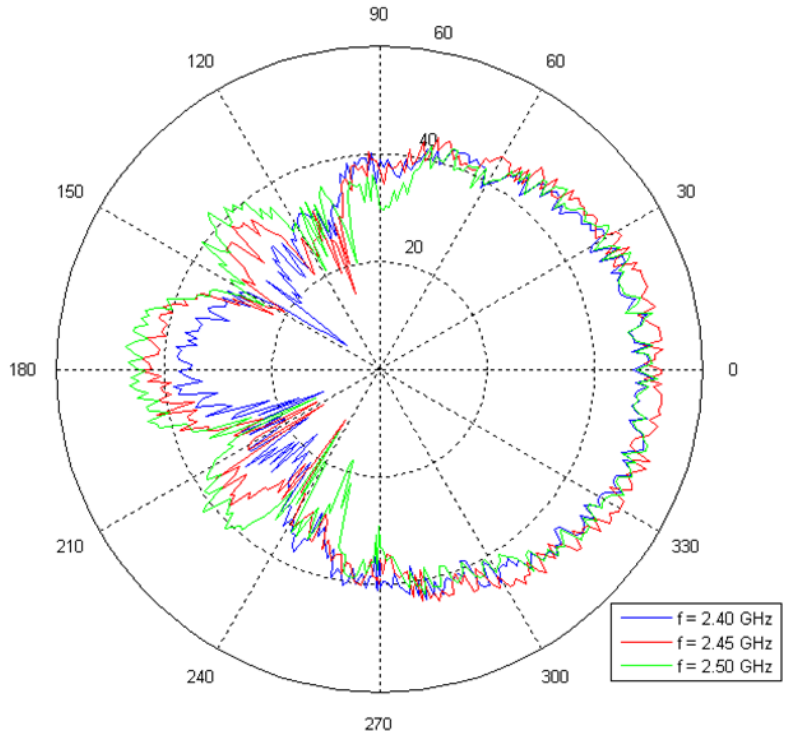

(b)

FIGURE 4.17: Radiation pattern in co-polar direction for ports 1 (a) and 2(b) for the optimized size and polarization bandwidth antenna.

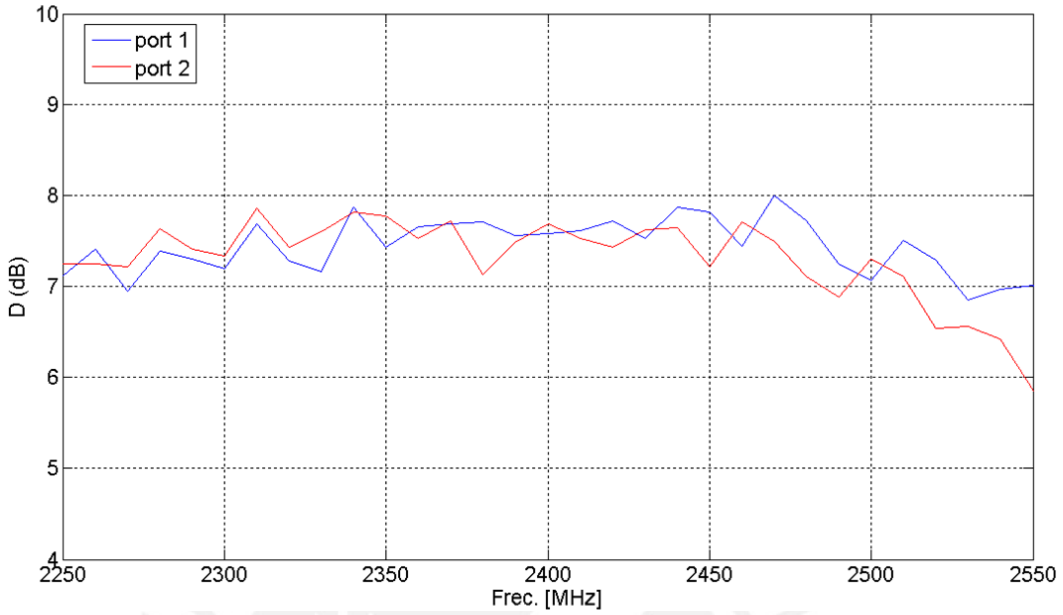

FIGURE 4.18: Directivity per port for the optimized size and polarization bandwidth antenna.

Layer	F = 2.40 GHz	F = 2.45 GHz.	F = 2.50 GHz.
Directivity (dBi)	7.68	7.89	7.71
FB (dB)	11.89	12.67	12.32
Beamwidth(°)	93	89	91
Impedance Bandwidth	2.85%		
Polarization	Dual Linear		

TABLE 4.2: Measures parameters from optimized size and polarization bandwidth antenna

Component	Simulation tuned	Empirical tuned
Inductor L1 Coilcraft	1.8nH	0.9nH
Inductor L2 Coilcraft	5.6nH	3.6nH

TABLE 4.3: Empirical tuning correction of Inductor values for a 2.45GHz. matching of the rectifier circuit

efficiency measures respectively for this first builded circuit . it can seen that is matched around 1.9 GHz. and no regard efficiency is achieved for 2.45GHz.Then was necessary to make the matching frequency higher, after an empirical tuning by trial and error process changing the inductors components (an small value works in a higher frequency) a 2.45 GHz. matching was achieved, this can be explain by the fact that the models of Coilcraft inductors used don't agree with its real performance, actually they works in a lower frequency. Table 4.4 shows the new inductors values compared with the previous ones. No comercial value exists for L1= 0.9nH due is very low, this is achieved by a shunt configuration of two 1.8nH inductors.

4.6.1 S11 Parameters for the Matched one Branch Rectifier

Figure 4.21 shows the S11 parameters measured at the 2.45 GHz. matched rectifier after the empirical tuning. Figure 4.21 (a) shows the return losses at three different input powers: -20 dBm in red, -10 dBm in blue and 0 dBm in purple, it can seen that the work frequency and also the -10 dB impedance bandwidth are proportional to the input power; bandwidths of 3.07% for -20dBm(2.40-2.475 GHz.), 3.25% for -10 dBm(2.42-2.5 GHz.) and 3.62% for o dBm (2.44-2.53 GHz.). In figure 4.21 (b) it can seen that the real an imaginary impedance's components increase with the input power; At -10 dBm (blue line) there is almost a perfect match, this is showed in return losses figure as very low reflection (-55 dB) at 2.46 GHz.

4.6.2 RF-DC Conversion Efficiency

One branch rectifier circuit was measured at two kinds of RF input signals, the setup configuration was introduced in section 4.3; figure 4.22 shows the results when a single tone is sweep from 2.40 to 2.50 GHz. in 0.01 GHz. steps was the input; the maximum efficiency achieved for the low input power -20 dBm is 13.9% at 2.43 GHz. the efficiency also increase with the input power and a maximum of 48.5% is achieved at 2.48 GHz. with an input power of 0 dBm. Table shows the efficiency achieved at 2412 MHz, 2442

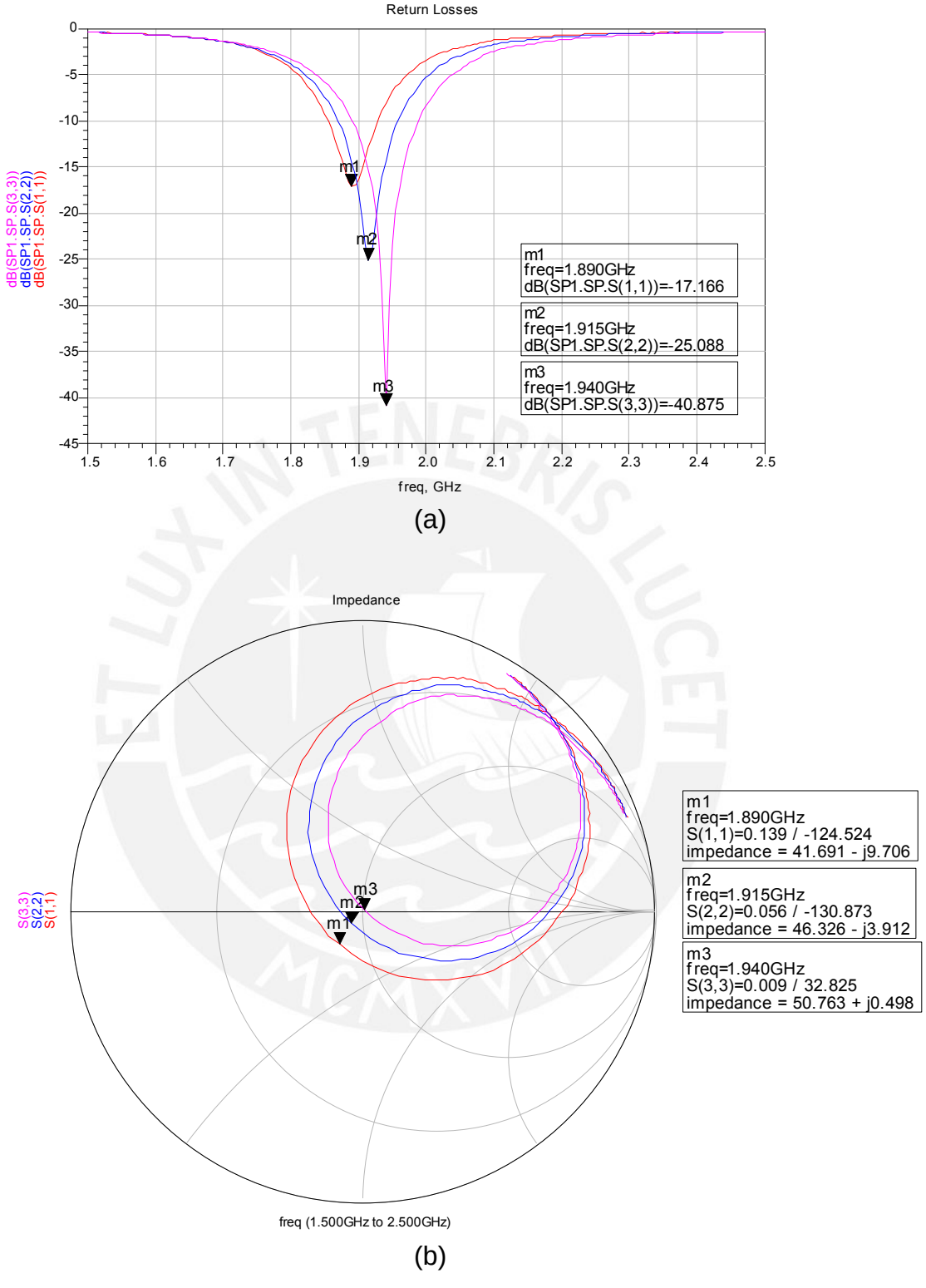

FIGURE 4.19: S11 parameters from one branch rectifier measured. At 1.9 GHz . matching is achieved and an empirical tuning was necessary to math at 2.45 GHz . (a) shows the return losses and (b) the impedance versus frequency both for -20 dBm (red), -10 dBm (blue) and 0 dBm (purple) of RF input power.

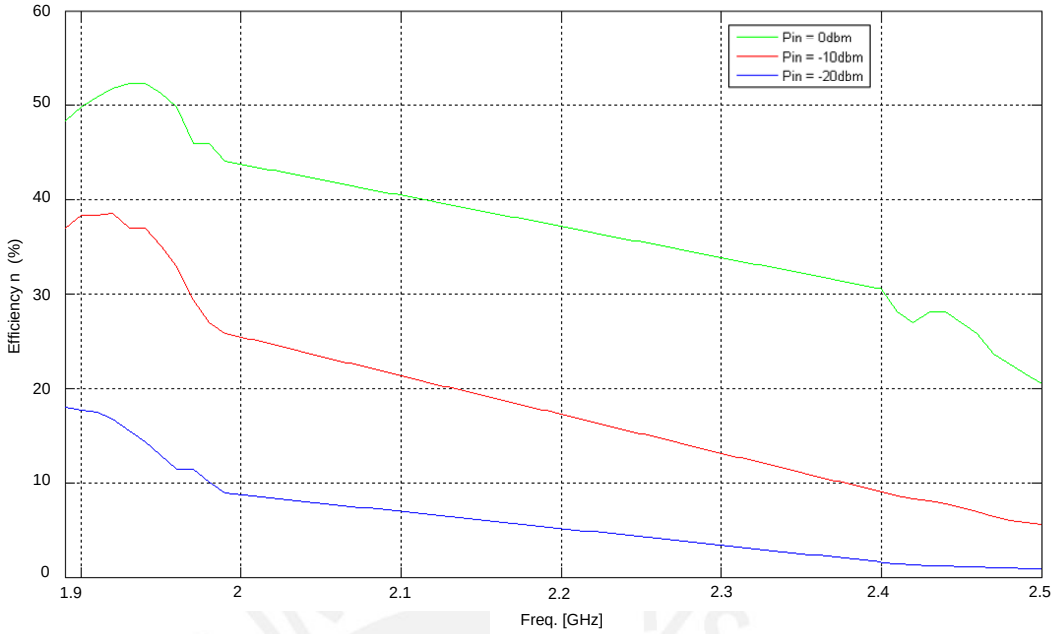

FIGURE 4.20: RF-DC conversion efficiency from one branch rectifier measured when no matching at 2.45 GHz. is achieved. The data from 1.9 to 2.4 GHz. was interpolated.

Component	2412 MHz.	2442 MHz.	2472 MHz.
-20 dBm	15.32%	17.56%	14.04%
-10 dBm	37.10%	40.08%	40.08%
0 dBm	44.13%	52.64%	55.67%

TABLE 4.4: Empirical tuning correction of Inductor values for 2.45GHz. matching at the rectifier circuit

MHz and 2472 MHz (see figure 4.8) when the RF input is a Wireless LAN signal from the IEEE 802.11b standard, this was a programable function of Agilent E4438C vector signal generator; its main characteristics are QPSK modulation, 22 MHz channels with 11 MHz of -3dBm bandwidth. This results show the possibility of using our rectenna in real applications on the 2.4 GHz. ISM band

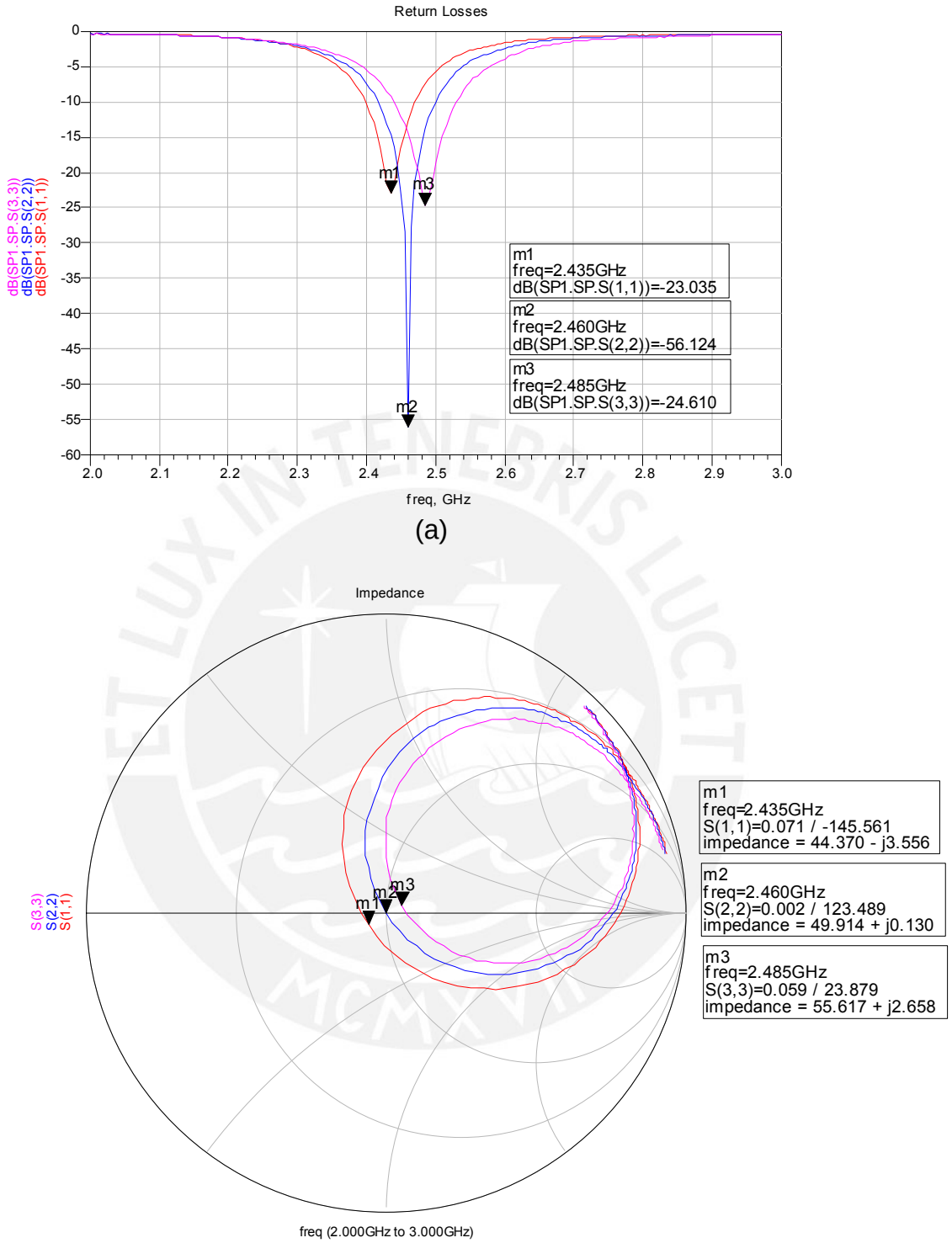

FIGURE 4.21: S11 parameters from one branch rectifier measured. At 2.45 GHz. matching is achieved after an empirical tuning. figure (a) shows the return losses and (b) the impedance versus frequency both for -20 dBm (red), -10 dBm (blue) and 0 dBm (purple) of RF input power.

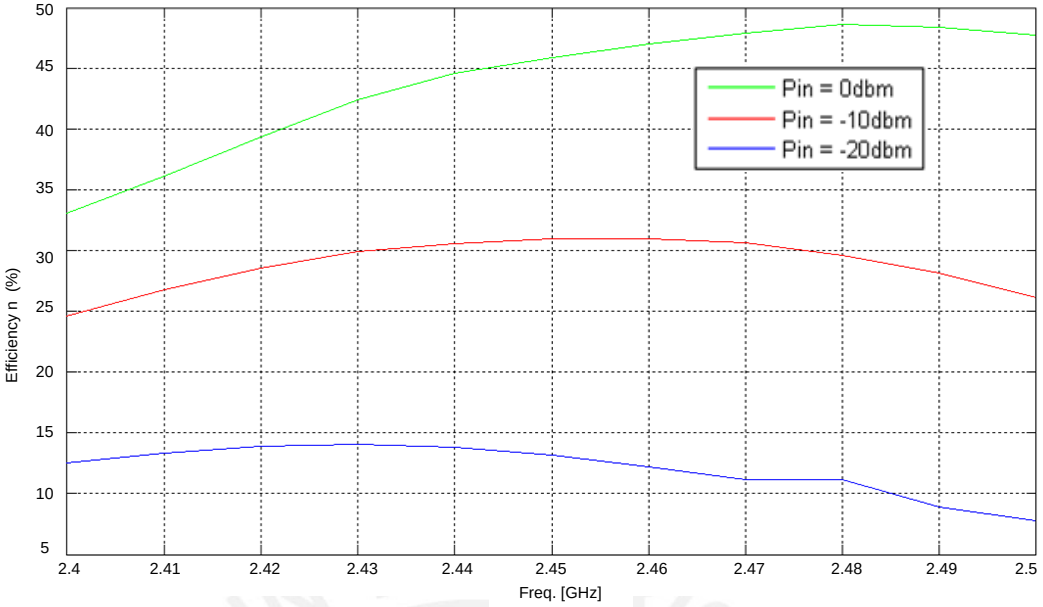

FIGURE 4.22: RF-DC conversion efficiency from one branch rectifier measured when matching at 2.45 GHz. is achieved.

4.7 Measurements of the Integrated Rectenna

4.7.1 Efficiency versus Incident Power

For this measurement the cables and the amplifier that are in the path between the sweeper and the transmission horn were calibrated from 0 dBm to 17 dBm sweeper output power. The sweeper output power, corrected by the calibration result, was then used to calculate the incident power of the rectenna, as setups mentioned in section 4.3 and equation 5.4. Figure 4.23 shows that the efficiency increases slowly but steadily with power proportionally at the incident power. The efficiency curve shows a steep increase first, then a leveling off and finally a slight decrease. The increase is a result of the exponential vi-curve of the diodes, whereas the decrease for high power levels is caused by two factors: the first is the RF voltage approach to the reverse breakdown voltage during the high impedance state of the diode. The second factor is the diode current as it approaches the saturation current of the diode during the low impedance state. Better results are achieved for 2.45 and 2.50 GHz. this can be explained by the RF-DC conversion efficiency of the rectifier circuit (section 4.6.1 and 4.6.2) where the frequency work, bandwidth and efficiency are proportional to the input power.Figure 4.24 shows the DC power achieved as a function of the incident power, also it can seen the better behavior for higher frequencies with almost no difference between 2.45 and 2.5 GHz.

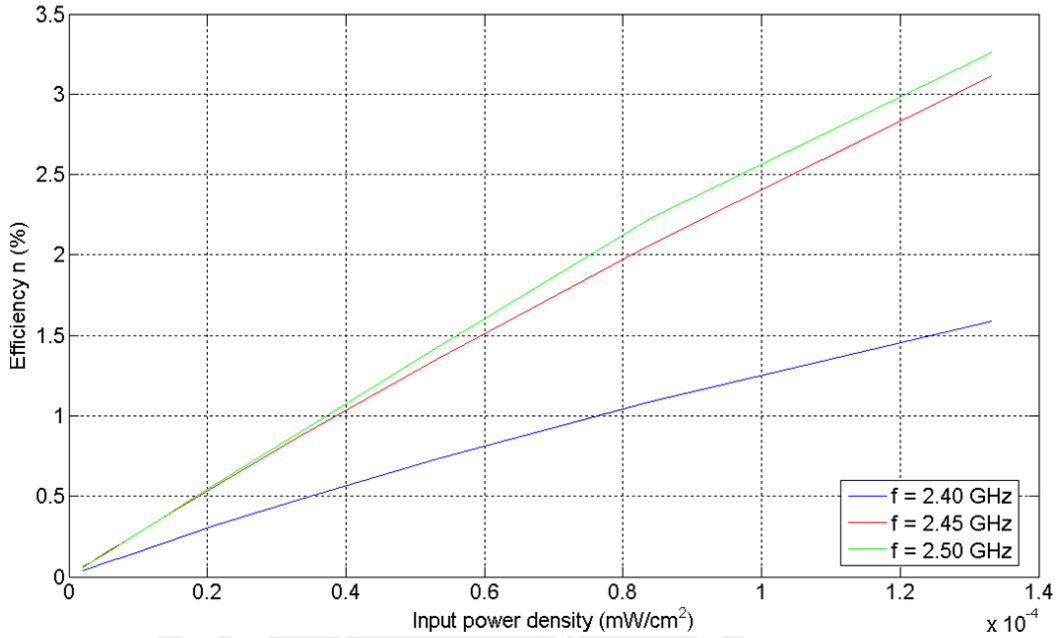

FIGURE 4.23: Efficiency versus incident power.

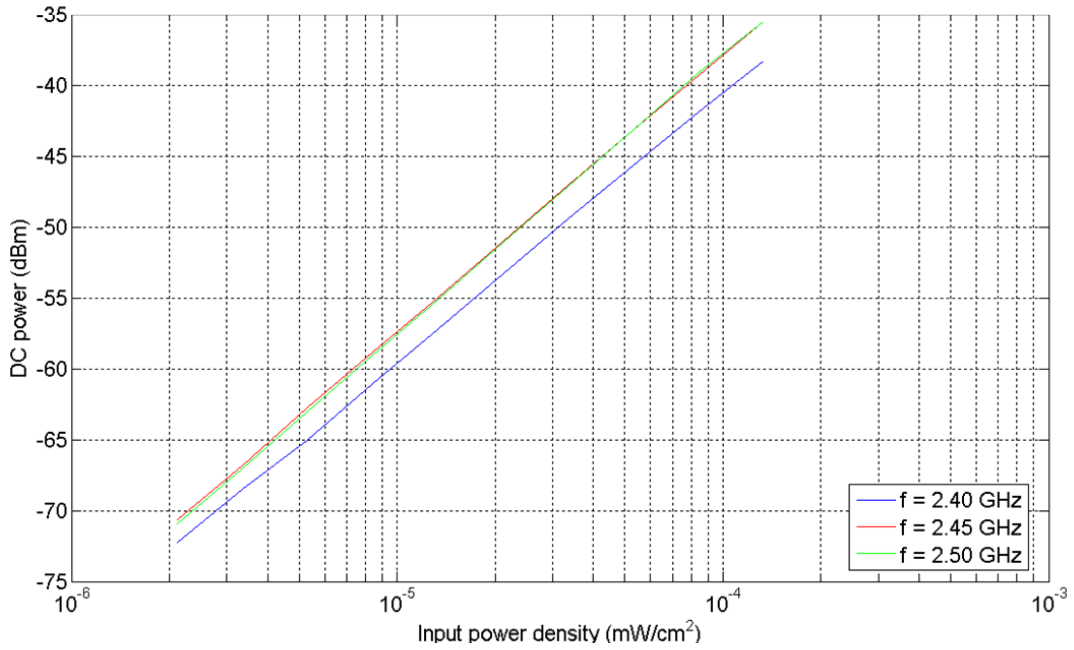

FIGURE 4.24: Output DC power versus incident power on the rectenna.

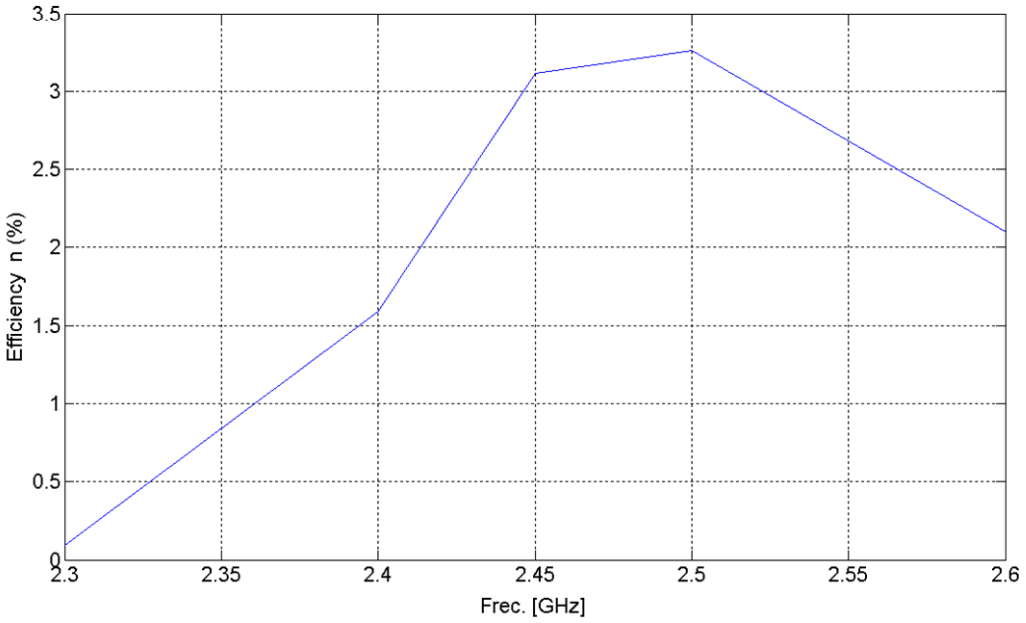

FIGURE 4.25: RF-DC conversion efficiency versus frequency for the rectenna.

Figure 4.25 shows that the overall efficiency is between 1.7 and 3.3 percent depending on the frequency, due mostly to the mismatch between two branch rectifiers and the antenna and to no good real performance for inductors models, avoiding predict its accurately behavior by simulation. It is important to mention here that calculating the received power needed to express efficiency is subject to an error on the order of 10% or more because the figure depends on the effective area of the antenna taken from the simulations. Since the DC power is measured directly, and the RF received power is over-estimated, the resulting conversion efficiency is under-estimate.

4.7.2 Polarization

In figure 4.26 the polarization of optimized size and polarization bandwidth antenna is plotted for 2.4, 2.45, and 2.5 GHz. The data comes from the mentioned 2D-polarization measurement. Figures show DC voltage achieved (mV) versus the azimuth angle of the rectenna. The distance between transmitter and rectenna was d = 3.63m and the load resistance R1 = 4kΩ. it can seen clearly that for our work frequencies the optimized antenna has a dual linearly polarization mutually perpendicular and overheads apparently this makes a circular shape. Figure 4.27 shows this polarization as function of polarization mismatch angle, a linear trend is observed (without nulls as figure 4.14).

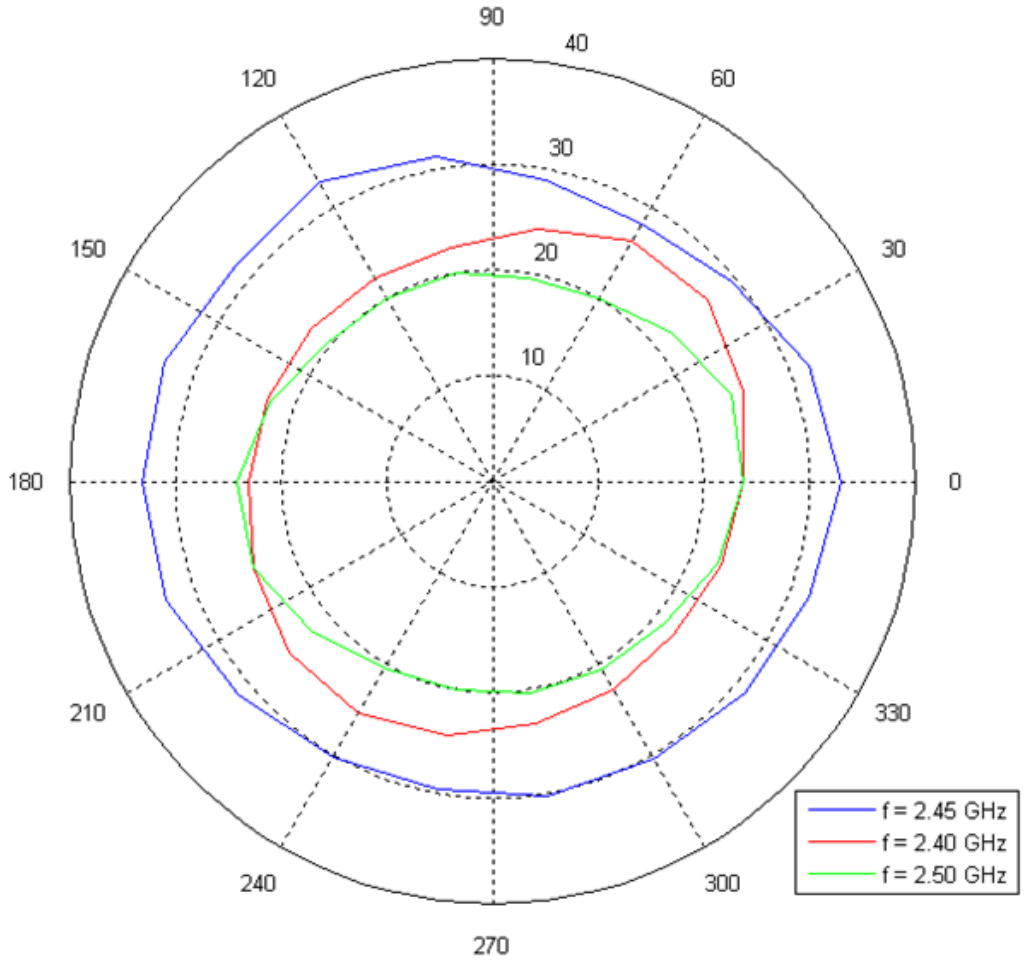

FIGURE 4.26: Polarization of the optimized size and polarization bandwidth antenna.

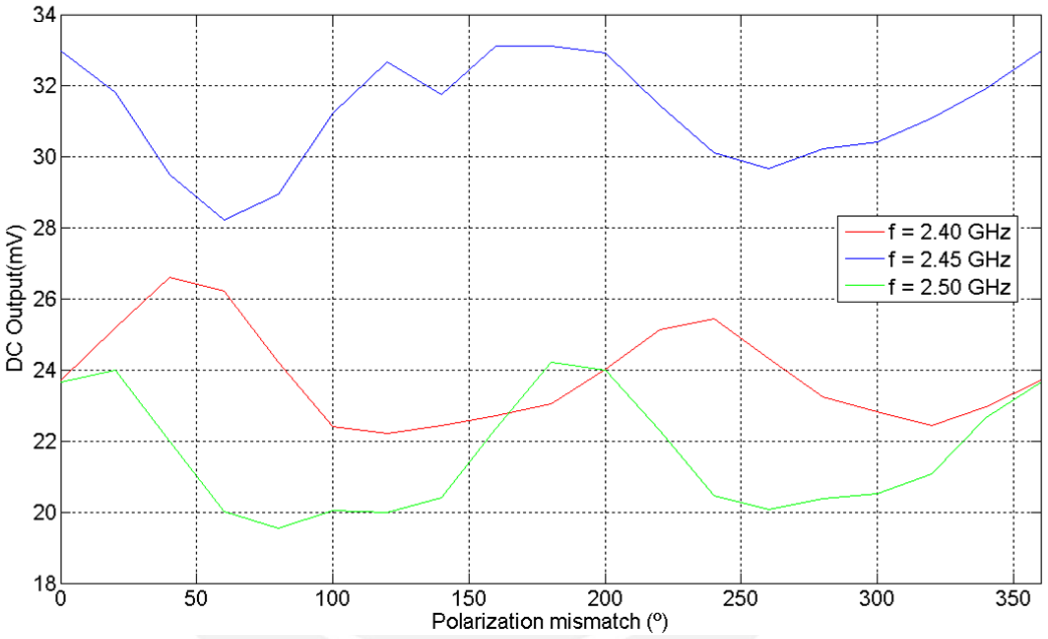

FIGURE 4.27: Polarization of the optimized size and polarization bandwidth antenna in cartesian plot

Chapter 5

Energy Storage and Management for Low-Power Applications

Figure 2.3 shows the more typical levels of ambient power densities in the microwave frequency range, with power levels that are too low for most continuous electronic functions. However, if this energy is stored over time efficiently, realistic functions can be performed in discrete time intervals. The ambient RF power levels vary by several orders of magnitude, implying a varying dc load to either match the output characteristics of the source with the load or to insert an intermediate dcdc converter with peak power tracking. Techniques and devices for efficient low-power dcdc conversion like presented as Maxim ICL 7662 inverter chip in the block "DC Power Processing" of figure 2.8 (98% efficiency) are need to be studied, examples of techniques are pulsewidth modulated (PWM) converters. Traditional PWM converters are likely to consume far too much power in the control circuitry and require large off-chip inductor(s) for low-frequency operation or as an alternative, switched-capacitor (SC) converters, these can provide high efficiency conversion at low power levels over a discrete range of conversion ratios determined by the circuit size and complexity [42].

Referring to the block diagram in figure 2.2, two options for energy storage include capacitors and micro-batteries. Capacitive energy storage is appropriate for applications where repeated functions of storing and utilizing small energy packets is performed, for prolonged operation or larger energy packets, energy densities up to four orders of magnitude higher can be achieved using micro-batteries. To illustrate the application of the rectenna energy source, we consider the ability to generate 10-μJ energy packets, which is sufficient for a 1-mW 10-μs ($10^{-2} - \mu$J) load operation. The energy packet size was selected arbitrarily but could be used, for example, for RF transmission of up to 10-kb data packets or simple sensory and signal processing functions. Over the range of

incident power densities under consideration (see figure 2.3) and assuming an rectenna of

$$A = A_{eff} = 25cm^2 \tag{5.1}$$

an estimate incident power levels of

$$P_{RFmin} = 250nW P_{RFmax} = 2.5mW, \tag{5.2}$$

Assuming a dcdc conversion efficiency of 90% and rectification efficiencies of

$$\eta(P_{RFmin}) = 1\% \eta(P_{RFmax}) = 20\% \tag{5.3}$$

an average dc power output is obtained as

$$P_{dcmin} = 2nW P_{dcmax} = 450\mu W. \tag{5.4}$$

The above estimated power levels can be recycled using this kind of a device. In another important application, batteryless sensors, this power is used to transmit power from this sensor. There are two possible scenarios, which are: (1) vary integration time to achieve fixed energy level and (2) fix integration time and vary energy packet level. Following approach (1), the system would be capable of fixed 10-μJ operation at discrete intervals varying from 1.4 h in the worst case to 20 ms in the best case. Thus, if a simple sensor required one energy packet to perform the sensory function and one packet to transmit data, it would be able to transmit new data around 20 times per second in the best case.

An example of the latter application is a manufacturing environment, where a large number of sensors occasionally transmit data such as stress, temperature, pressure, and light level. A large number of such sensors with no batteries that need replacing (or recycling) can be charged with a low-power transmitter. In such an indoor multipath propagation environment, the spatial distribution of polarization and power varies statistically. The results of this work show that it is possible to collect such energy by receiving and rectifying two orthogonal polarizations independently and adding the power upon rectification.

Chapter 6

Conclusion and Future Work

As a conclusion of this work there are two main aspects to mention. First this work shows that a rectenna can be simulated using harmonic balance simulation for the circuit by chosen properly model-library components, and electromagnetic simulators for the antenna part, being careful with the higher coupling sensibility between antenna and circuit. Second, the measured results presented indicate that rectennas might work as RF recyclers with an output power level enough to be efficiently stored and reused, in our case specifically working in 2.45 GHz. ISM band.

Further work would include devices that are able to collect and store energy from power levels that correspond to the rectenna output.Increase the frequency bandwidth of the antenna, achieved an arbitrarily polarized reception are other important tasks to do, it might be by multi frequency or broadband operation by changing the antenna's design, would be by stacking microstrip patches or a more complex designs as spiral antenna. Even if only insufficient amount of energy is scavenged from single rectenna, it is also possible to arrange multiple elements to receive more energy. Shrinking the size of the rectenna is another aspect, that requires more work. The frequency behavior might stay constant if the ε_r of the substrate increases with the decreasing size of the antenna. Furthermore, measurements of situations with more than one incident frequency, as they occur in real life, can be done. Two incident waves with different frequencies can interfere destructively as well as constructively. As a recommendation, in order to increase the RF-DC conversion efficiency; a carefully chose of components and build of rectifier circuit are vital.

Bibliography

[1] Nicolas Tesla. *Experiments with Alternate Current of High Potential and High Frequency*. McGraw, 1904.

[2] Nicolas Tesla. The transmission of electric energy without wires. *The thirteenth Anniversary Number of the Electrical World and Engineer*, 1904.

[3] William C. Brown. The history of power transmission by radio waves. *IEEE Trans. MTT*, 32(9):1230–1242, 1984.

[4] Peter Edward Glaser. Power from the sun, science. (162):857–886, 1968.

[5] N. Shinohara. Wireless power transmission for solar power satellite (spssecond draft). 2006. `http://www.sspi.gatech.edu/wptshinohara.pdf`.

[6] F-E. Litle J. O. McSpadden and A. Ignatiev. An in-space wireless energy transmission. *IECEC Energy Conversion Engineering Conf.*, 1996.

[7] H:K: Smith w. Epp, A.R: Khan. A compact dualpolarized 8.51 ghz. rectenna for high voltage (50v) actuator aplications. *IEEE Transactions on Microwave Theory and Techniques*, 2000.

[8] N. Kaya Y. Fujino. T. Ito, M. Fujita and T. Onadera. A driving test of a small dc motor with a rectenna array. *IEICE Trans. Commun.*, 1994.

[9] W. C. Brown. An experimental low power density rectena. *IEEE MIT-S Int. Microwave Symp*, 1991.

[10] J. O. McSpadden and K. Chang. A dual polarized circular patch rectifying antenna at 2.45 ghz. for microwave power conversion and detection. *IEEE Trans. MTT-S Digest*, pages 1749–1752, 1994.

[11] B. Strassner and K. Chang. A circulary polarized rectifying antenna array for wireless microwave power transmission. *IEEE MIT-S Int. Microwave Symp*, 2002.

[12] T. Yoo and K. Chang. Theoretical and experimental development of 10 and 35 ghz. rectenna. *IEEE Trans. MTT*, 40(6):1259–1266, 1992.

[13] William C. Brown. A microwaver powered, long duration, high altitude platform. *MTT- S International Microwave Symposium Digest*, 86(1):507–510, 1986.

[14] R. J. Gutmann and R. B. Gworek. Yagi-uda receiving elements in microwave power transmission system rectennas. *Journal of Microwave Power*, 14(4):313–320, 1979.

[15] N. Shinohara, S. Kunimi, T. Miura, H. Matsumoto, and T. Fujiwara. Open experiment of microwave power experiment with automatically target chasing system (japanese). *IEICE Trans. B-II*, J81-B-II(6):657–661, 1998.

[16] T. Ito, Y. Fujino, and M. Fujita. Fundamental experiment of a rectenna array for microwave power reception. *IEICE Trans. Commun.*, E-76-B(12):1508–1513, 1993.

[17] M. Fujita N. Kaya S. Kunimi M. Ishii N. Ogihata N. Kusaka Fujino, Y. and S. Ida. A dual polarization microwave power transmission system for microwave propelled airship experiment. *Proc. de ISAP'96*, 2:393–396, 1996.

[18] Y. Aoki M. Otsuka T. Idogaki Shibata, T. and T. Hattori. Microwave energy transmission system for microrobot. *IEICE-Trans. Electr.*, 80-c(2):303–308, 1997.

[19] Q. Xue Chin, C. H. K and C. H. Chan. Design of a 5.8-ghz. rectenna incorporating a new patch antenna. *IEEE Antenna and Wireless Propagation Lett.*, 4:175–178, 2005.

[20] J. A. Hagerty, N. D. Lopez, B. Popovic, and Z. Popovic. Broadband rectenna arrays for randomly polarized incident waves. *IEEE*, 2000.

[21] Y. Fujino and K. Ogimura. A rectangular parabola rectenna with elliptical beam for sps test satellite experiment. *Proc. of the Institute of Electronics*, Information and Communication Engineers(1–10):S29–S20, 2004.

[22] Alden A. and T. Ohno. Ingle foreplane high power rectenna. *Electronics Letters*, 21(11):1072–1073, 1992.

[23] Y. Fujino M. Fujita Saka, T. and N. Kaya. An experiment of a c band rectenna. *Proc. Of SPS'97*, 32(9):251–253, 1997.

[24] B. Strassner and K. Chang. 5.8-ghz. circularly polarized rectifying antenna for wireless microwave power transmission. *IEEE Trans. MTT*, 50(8):1870–1876, 2002.

[25] G. Akoun B. Essakhi L. Santandrea L. Pichon Leroy, P. and C. Guyot. An eficient global analysis of a rectenna using the combination of a full-wave model and a rational approximation. *Eur. Phys. J. Appl. Phys.*, (29):39–43, 2005.

[26] J. C. Lin. Radio frecuecny exposure and safety associated with base stations used for personal wireles communication. *IEEE Antennas Propagation Mag.*, 2002.

[27] Keisuke Tsukada Yoshihiro Kawahara and Tohru Asami. Feasibility and potential application of power scavenging from environmental rf signals. 2009.

[28] Zoya Popovic. Wireless powering for low-power distributed sensors. *Serbian Journal of Electrical Engineering*, 3(2):149–162, 2006.

[29] Yasutaka Takeda Hirohito Nishiyama, Yuichi Tokunaga. Method of power saving for sensor nodes. *Mitsubishi Denki Giho*, 80(9):14, 2006.

[30] Masateru Minami. Solar biscuit: Design of a battery-less wireless sensor network. *Proc. 7th International Symposium on RF MEMS and RF Microsystems (MEMSWAVE)*, 2006.

[31] Kai-Ping Yang and Kin-Lu Wong. Inclined-slot-coupled compact dual frequency microstrip antenna with cross-slot. *ELECTRONICS LETTERS 79th February*, 34 (9):321–322, 1998.

[32] VINCENT F. FUSCO S. EL-RABAIE and CARSON STEWART. Harmonic balance evaluation of nonlinear microwave circuits-a tutorial approach. *Transactions on Education*, 31(93):181–192, 1988.

[33] Constantine A. Blanis. Antena theory. *John Wiley and Sons, Ney York 2nd edition*, 1997.

[34] David Pozar. Microstrip antenna aperturecoupled to a microstripline. *ELECTRONICS LETTERS*, pages 49–50, 1985.

[35] David Pozar. A reciprocity method of analysis. for printed slot and slot-coupled microstrip antennas. *National Science Foundation, and by the General Electric Corporation, SyracuseN, y*, pages 1439–1443, 1986.

[36] David Pozar. A review of aperture coupled microstrip antennas: History, operation, development, and applications. *University of Massachusetts at Amherst*, 1996.

[37] PETER L. SuLLWAN and DANIEL H. SCHAUBERT. Analysis of an aperture coupled microstrip antenna. *University of Massachusetts at Amherst*, 1986.

[38] J. G. Macias Montero A. Akhnoukh L. C. N. de Vreede H. Yan, Student Member and J.N. Burghartz. An integration scheme for rf power harvesting. *WiComm Project, Delft University of Technology, Netherlands*, 2005.

[39] James O. McSpadden. Rectifing and oscillating integrated antennas. *PhD thesis, Texas AyM University*, 1998.

[40] Florian B. Helmbrecht. A broadband rectenna array for rf energy recycling. *Thesis*, 2002.

[41] Wireless Antennas ETS LINDGREN. Open boundary quadridge horn antenna (data sheet). `http://www.ets-lindgren.com/pdf/3164-05.pdf`.

[42] M. Makowski and D. Maksimovic. Performance limits of switched-capacitor dcdc converters. *IEEE Power Electronics Specialists*, 1995.